NASA Contractor Report 4223

A Cloud Model Simulation of Space Shuttle Exhaust Clouds in Different Atmospheric Conditions

C. Chen and J. A. Zak
ST Systems Corporation (STX)
Hampton, Virginia

Prepared for
George C. Marshall Space Flight Center
under Contract NAS8-36715

National Aeronautics and
Space Administration
Office of Management
Scientific and Technical
Information Division

1989

TABLE OF CONTENTS

LIST OF FIGURES

LIST OF TABLES

SECTION 1 - INTRODUCTION

Historical Perspective

The National Aeronautics and Space Administration (NASA) has been concerned with possible environmental impacts of the Space Shuttle since the early conceptual studies of the 1960's. The decision in 1972 to proceed with the Shuttle program was made with these potential impacts in mind and with enough information to formulate an environmental impact statement to comply with the National Environmental Policy Act of 1969. The first form of an environmental impact statement was published in Cohen [1974] and has undergone revisions several times since then [Potter, 1978].

The main impacts on the lower troposphere were anticipated for the most part. These are due to HCL produced by solid rocket booster exhausts during launch. A toxic cloud is generated at the launch tower from combinations of the combustion products from solid fueled and liquid fueled rocket engines together with water used for cooling and sound suppression which is atomized, vaporized and vented to the atmosphere. Subsequent properties of the cloud are determined to a large extent by the characteristics of the atmosphere in which it is contained. Uncertainties existed in the early analyses, and these were the subjects of a variety of research and measurement programs. Of primary concern was and continues to be the toxic effects of this cloud which is called the ground cloud, and the atmospheric properties influencing its behavior.

Early studies were concerned with the chemical composition of the ground cloud and, more importantly, the disposition of the nearly 23,000 kg of HCL produced in approximately the first 10 seconds after launch [Pellet, et al., 1983]. It was anticipated that the ground cloud would rise, due to its

buoyancy, stabilize, depending upon atmospheric properties, be transported by the wind, and, ultimately, decay from entrainment of dry air and natural diffusion.[1] The transport and diffusion process received much attention [Hwang and Pergament, 1976; Hwang and Mathis, 1977; Ybanez, 1985] and procedures for assessing and predicting HCL deposition were analyzed, developed and implemented [Stephens and Stewart, 1977; Boman, et al., 1985]. The basic thermodynamics and microphysics of the exhaust cloud together with inherent influences of the ambient atmosphere were difficult problems for which analytical solutions were elusive, expensive (in terms of model development and computer resources needed) and still in a research mode. However, the launch of STS-1 heightened the importance of cloud processes and environmental interaction as there was an underestimated acidic fallout observed as far as 7.4 km from the launch pad at the Kennedy Space Center. This observation prompted further study to define the production mechanisms, investigate other possible forms of weather modifications which could result from Shuttle exhaust products, and to conduct a field measurement program to further define the properties of the exhaust and fallout [Anderson and Keller, 1983]. A two-dimensional cloud model with more realistic treatment of the cloud rise problem was employed to try to bracket the acid precipitation event. While very preliminary, the model provided further evidence of trapping effects of strong inversions in the low levels of the atmosphere and to the possibility of natural cloud growth enhancement from Shuttle cloud interaction. The Anderson-Keller report covered the first 4 Shuttle launches and documented the observed effects of the ambient atmosphere on rise rate, cloud dimension, dissipation, and other properties such as liquid water content, hydrometeor

[1]This is a simplification of complicated cloud growth and environment interaction process but serves to describe visual, qualitative observations.

spectra, condensation nuclei, temperature, vertical velocity, ice nuclei and humidity in the cloud and surroundings. Among the conclusions were that deluge water spray, which was atomized by the hot rocket exhaust, was the controlling mechanism in the formation of the fallout drops, and that the exhaust cloud had sufficient buoyancy to lift drops (HCL) one millimeter in diameter for potential transport down wind. Range and azimuth for the fallout on a given day will depend almost exclusively on the low level atmospheric stability (temperature and moisture profile) and wind. It was recognized that further work was needed to confirm the preliminary 2-dimensional cloud model results and to better understand the atmospheric influences which governed cloud behavior. This is true not only because of the toxic cloud from routine launches, but as well as for future Galileo and Ulyses missions which will include nuclear-fueled power cells. Current areas of interest also include the meteorology of the West Coast and the reduced tolerance levels for Hydrozine. The latter demands increased precision in the toxic deposition assessment.

Purpose

The research in this report is a direct result of current concerns and needs to understand more fully atmospheric processes which govern the complex behavior of exhaust clouds.

From an analysis of the first 15 Shuttle launches, there are still unknowns about midfield (60 m to 1 km) impacts with regard to long term effects on the environment [Ybanez, 1985, pp 79-80]. Operational techniques for assessing the HCL deposition are compromises among simplicity, accuracy and timeliness. There are known deficiencies due to assumptions and simplifications in operational models of the cloud rise and diffusion

processes. This study, while containing simplifications and assumptions, more realistically treats these processes. The same timeliness constraints are not applied in this study. Also, sufficient computer power was available and operational pressures were absent. This study attempts to characterize the great variability from one ground cloud to another caused by from the dominant controlling influence of the environment. It will attempt to answer such questions as can a three-dimensional cloud model produce a cloud which realistically represents the asymmetrical Shuttle ground cloud? What are the effects of changing initial heat and moisture from rocket engines or exhaust vent configuration? Can the ground cloud be trapped in very low levels of the atmosphere where it can transport high concentrations of HCL and aluminum oxide considerable distance? Can the Shuttle trigger natural severe convection (thunderstorms)? What is the contribution of atmospheric wind shear on cloud integrity?

Procedure

A three-dimensional model of the atmospheric convection process was employed to simulate cloud growth, decay and movement from first principles of hydrodynamics and thermodynamics. The cloud model was modified to accept initial heat and moisture conditions from rocket exhaust and launch platform configurations. Model grid, domain, and initial conditions were optimized for efficiency from a computer resource standpoint and also for match of detailed observed cloud properties in known atmospheric conditions with exhaust clouds produced by the model. The use of the three-dimensional model reflects the highly asymmetric nature of most observed rocket exhaust ground clouds.

The best observed-model match was obtained for four different Shuttle launch conditions. Case studies were then run with the same rocket exhaust

initialization but different atmospheric conditions representing very unstable, moderately unstable, wind shear and stable environments where the latter also contained a strong observed low-level inversion. Details of the initialization procedure, a description of the model itself, results of photogrammetry of actual launch clouds, the ground truth comparisons for establishing model credibility, and results of the simulations are discussed in subsequent sections.

SECTION 2 - THE NUMERICAL CLOUD MODEL

The model used for this applied research is a state-of-the-science cloud model which has been employed in the past to study nuclear fire storms, tornadic thunderstorms, microbursts, aircraft accidents and the atmospheric boundary layer. The model is called the Terminal Area Simulation System (TASS). It is thoroughly documented in NASA CR 4046, April 1987 [Proctor, 1987]; and its verification is documented in NASA CR 4047, April 1987 [Proctor, 1987].

General Properties

The model utilizes a nonhydrostatic, compressible and unsteady set of governing equations which are solved on a three-dimensional staggered grid. The model divides water into six bulk categories. Each are governed by a prognostic equation. The six categories are 1) water vapor, 2) ice crystals, 3) cloud droplets, 4) rain, 5) snow, and 6) hail/graupel. The former three categories represent nonprecipitating forms of water, while the latter three represent precipitating forms of water. The hail/graupel category may consist of either hail or graupel. All three phases of water (i.e., vapor, liquid, and solid) are included. The numerous microphysical interactions that result in exchanges of water between the six categories are summarized in Table 1. These are parameterized in the model. For treating turbulent mixing the model adopts the subgrid closure approach. Scales of turbulence larger than the assumed grid size are simulated explicitly within the flow field. Scales of turbulence less than the grid size are parameterized from a closure approximation. The subgrid closure model currently in use is a conventional, first-order, diagnostic approximation. TASS also incorporates surface

Table 1. Cloud Microphysical Interactions

- Autoconversion of cloud water into rain
- Accretion of cloud water by rain
- Condensation of water vapor
- Evaporation of cloud water and rain
- Spontaneous freezing of supercooled cloud water and rain
- Initialization of cloud ice
- Accretion of cloud water by cloud ice
- Autoconversion of snow into hail
- Deposition and sublimation by hail, snow, and cloud ice
- Accretion by hail of cloud water, cloud ice, rain, and snow
- Initiation of hail due to the collection by supercooled rain of cloud ice and snow
- Melting of cloud ice, snow, and hail
- Shedding of unfrozen water during wet hail growth
- Shedding of water from melting snow and hail
- Conversion of cloud ice into snow
- Accretion by snow of cloud water, cloud ice, and rain
- Evaporation from melting snow and hail

stresses which are dependent upon stratification, ground roughness and local winds. Numerical stability and conservation in the solution of the governing equations relies on an appropriate choice of numerics and boundary conditions. The model uses quadratic-conservative space differencing and incorporates a modified Orlanski radiation boundary scheme. Application of the radiation boundary condition to the open lateral boundaries allows the outward propagation of waves with minimal reflection. Also, the procedure for applying the radiation boundary conditions is free of domain-wide mass trends. Other features of the model are 1) the option of a vertical grid-size stretching, 2) movable mesh with time varying translation speed, 3) a numerical filter and sponge applied below the top boundary, and 4) specification of an initial environment from a sounding that is either observed or predicted from a regional model simulation. The model is initialized by a temperature and moisture perturbation which in this application includes the actual heat and moisture from the rocket exhaust and launch system. Input is the vertical profile of temperature, moisture, and wind at the time and location of the launch. This atmospheric sounding, as it is called, can also be predicted from another model. Output from the TASS model includes three-dimensional fields of wind velocity, particulates, rain, snow, hail, cloud water, temperature, and pressure. Forward and backward trajectories and model domain averages for selected variables are also output. Any variable can be shown in vertical or horizontal cross section.

SECTION 3 - MODEL INITIALIZATION FOR A SIMULATED SHUTTLE LAUNCH

Launch Platform

The launch platform for the Space Shuttle is unique and has an effect on the way rocket engine exhaust products are vented to the atmosphere. Water spray used for cooling and sound suppression also impacts the important contribution to ground cloud liquid and vapor content. The platform shown in Figure 1 is for the Kennedy Space Center launch complex 39A. It is representative of 39B as well. The separation of the exhaust gases through trenches is significant for this modelling effort. Both solid rocket motors are vented into the trench which points to the north (shown in Figure 1). Main engines are vented to the south. During a launch, about 680 kl of liquid water are sprayed into the exhaust ducts and lower tower areas [Ybanez, 1985 p. 37]. This is in addition to water from the combustion process and afterburning. Part of this water runs off the pad as liquid, part becomes vapor from the intense heat and part is atomized by the turbulent exhaust forces.

The force of the exhausts also produces a considerable horizontal spread of the components as shown in the picture of STS-1 a few seconds after launch (Fig. 2). The amount of water contributing to the ground cloud in the form of liquid (atomized) and vapor must be estimated but consistent with the total mass of water available (less runoff). The three parts of the ground cloud merge into an irregular cloud mass in the first minute after launch.

Launch Parameterization Approach

There are assumed to be a column part and ground part to the near surface heat and moisture perturbations at launch. The column part, corresponding to

Figure 1. Kennedy Space Center Launch Complex 39A.

Figure 2. STS-1 a few seconds after liftoff.

rising rockets, is allowed to tilt as the vehicle changes pitch in the early part of the flight. The ground portion of mass and energy contains the amounts for the first 7.5 seconds due to the vehicle begin very near the surface. There are three parts to this ground portion: a center and two sides. These correspond to a split trench for directing exhaust products as shown in Figure 2. The mass and energy distributions are shown in Figures 3 and 4 respectively for this configuration.

The vapor temperature, and smoke perturbation are

i). Northern trench

$$\Delta r_{VN} = (m_{Deluge})\ W_{NE} + M_v\ W_{NM}\ \exp(-(y-y_1)/\ell)/(\rho_o\ \Delta z \Delta x \ell) \qquad (1)$$

$$\Delta\theta_N = 7.5\ \frac{A\theta}{c_p}\ W'_{NE}\ \exp(-(y-y_1)/\ell)/(\rho_o\ \Delta z \Delta x \ell)$$

$$\Delta r_{aN} = 7.5\ A_a W_{NM}\ \exp(-(y-y_1)/\ell)/(\rho_o\ \Delta z \Delta x \ell)$$

ii). Southern trench

$$\Delta r_{VS} = (m_{Deluge})\ W_{SE} + M_v W_{SM}\ \exp((y-y_2)/\ell)/(\rho_o\ \Delta z \Delta x \ell) \qquad (2)$$

$$\Delta\theta_s = 0$$

$$\Delta r_{as} = 7.5\ A_a\ W_{SM}\ \exp((y-y_2)/\ell)/(\rho_o\ \Delta z \Delta x \ell)$$

iii). Center piece

$$\Delta r_{VC} = (m_{Deluge}\ W_{CE} + M_v\ W_{CM})\ \exp(-((x-x_o)^2 \qquad (3)$$

$$+ (y-y_o)^2)/\ell^2)/(\rho_o\ \Delta z \ell^2 \pi)$$

$$\Delta\theta_c = 7.5\ \frac{A\theta}{c_p}\ W'_{CE}\ \exp(-((x-x_o)^2$$

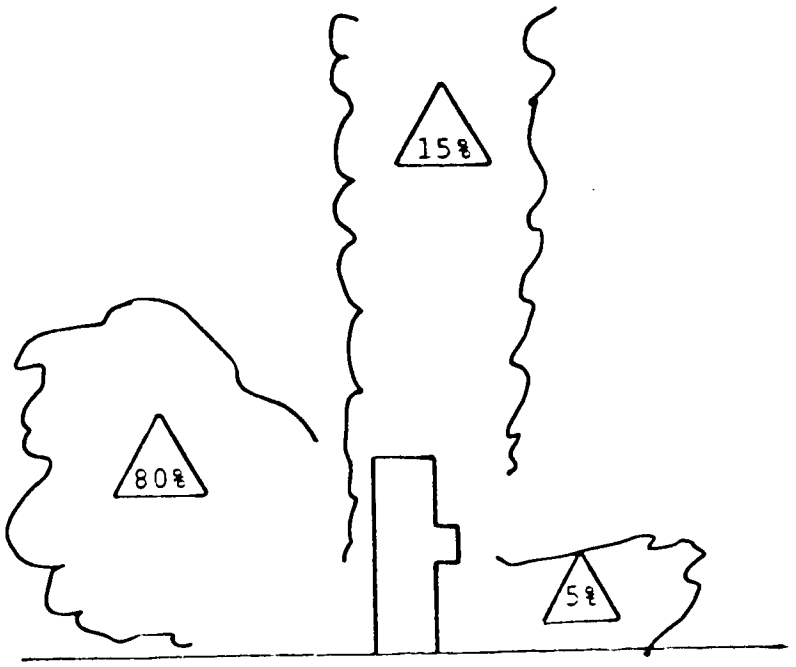

Figure 3. Assumed mass distribution of exhaust cloud in the first 7.5 seconds.

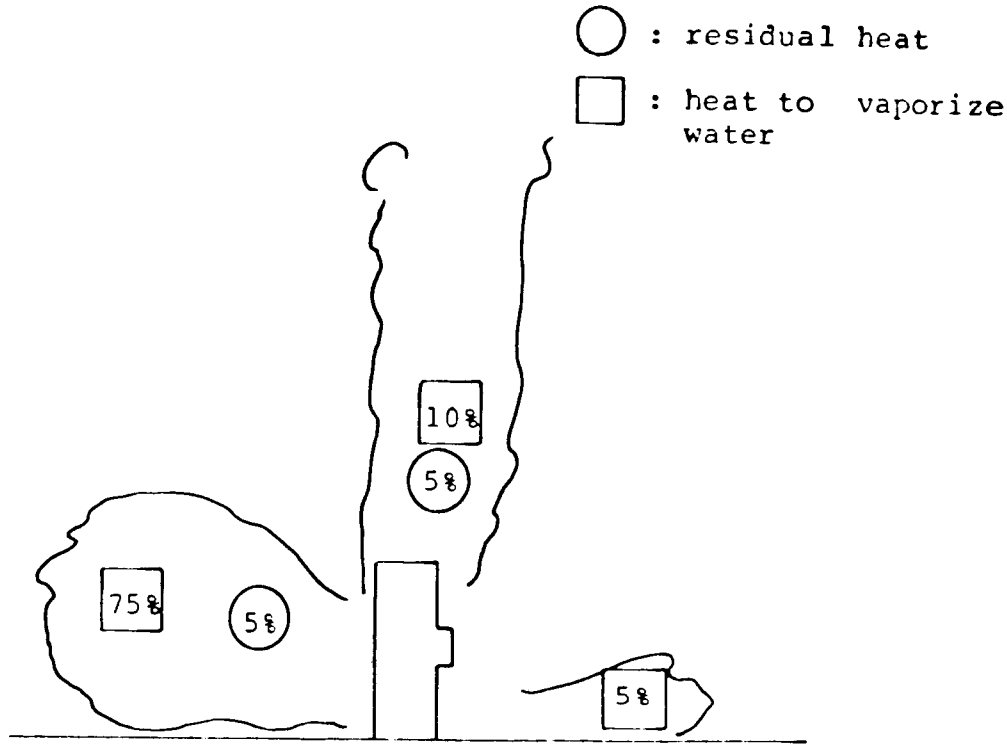

Figure 4. Assumed energy distribution of exhaust cloud in the first 7.5 seconds.

$$+ (y-y_o)^2)/\ell^2)/(\rho_o \Delta z \ell^2 \pi)$$

$$\Delta r_{ac} = 7.5 A_a W_{CM} \exp(-((x-x_o)^2 + (y-y_o)^2/\ell^2)/(\rho_o \Delta z \ell^2 \pi)$$

where ℓ is given as 200 m which is the e-folding distance in the y direction. The mass of evaporated deluge water is $m_{Deluge} = 7.5 A_\theta L_v (W_{NE} + W_{CE} + W_{SE})$. The location of the trenches is Y_1 and Y_1. $M_v = 7.5 A_v$ is the mass of water vapor from the rocket engines. W_{NE}, W_{SE}, W_{CE}, W_{NM}, W_{SM}, W_{CM}, W'_{NE}, W'_{CE} are the weighting functions per Figures 3 and 4 as follows: the weighting function for heat to evaporate water, (W_{NE}, W_{SE}, W_{CE}) = (0.75. 0.05, 0.1); and the weighting function for mass, (W_{NM}, W_{SM}, W_{CM}) = (0.80, 0.05, 0.15); and the weighting function for residual heat, (W'_{NE}, W'_{CE}) = (0.05, 0.05). The grid spacing in the vertical is Δz, and Δx is the east-west spacing. ρ_o is the dry air density. A_θ, A_v A_a are the heat, vapor and smoke output rate from rocket motors. L_{ev} is the latent heat of evaporation.

As shown in eqs. (1) and (2), the evaporated deluge water is spread in y direction only for the North and South trench. The maximum release of water vapor is at the two sides of the launch pad. In addition, it is easy to show that the volume integration of moisture perturbation is equal to $m_{Deluge} + M_v$.

For the column cloud initialization (after 7.5 seconds), the perturbation of smoke, moisture and heat due to the exhaust from the rocket motors is simulated in the model from the surface to the top of the model along the flight path according to the following:

$$\Delta r_a(z) = A_a \exp(-((x-x_o)^2 + (y-y_o)^2/\ell^2)$$
$$(t(z) - t(z-\Delta z))/(\rho_o \Delta z \ell^2 \pi)$$

$$\Delta r_v(z) = A_v \exp(-((x-x_o)^2 + (y-y_o)^2/\ell^2) \quad (4)$$
$$(t(z) - t(z-\Delta z))/(\rho_o \Delta z \ell^2 \pi)$$

$$\Delta\theta(z) = \frac{A_\theta}{c_p} \exp(-((x-x_o)^2 + (y-y_o)^2)/\ell^2) \quad (5)$$
$$(t(z) - t(z-\Delta z))/(\rho_o \Delta z \ell^2 \pi)$$

where

$A_a = 3.26 \times 10^3$ kg/s, $A_v = 5.01 \times 10^3$ kg/s, $A_0 = 11.8 \times 10^{11}$J/S, and (x_o, y_o) is the coordinate of the launch pad. The term t(z) is the time in seconds after lift-off for the vehicle to reach altitude z, and C_p is the specific heat. According to eqs. (4) and (5), the perturbation of moisture and heat is distributed exponentially in x and y directions. Moreover, the volume integration of eqs. (4) and (5) shows that the perturbation of heat and moisture is consistent with its output rate from the rocket motors.

The initial momentum imparted to the ground cloud was only considered in the separation of the exhaust channels at the surface. The initial thrust forces the cloud considerable distance from the platform. This is reflected in the model by spreading the initial values for heat and moisture several grid points in the N-S direction at the surface.

The initialization for the one case of a simulated TITAN explosion was different. For this case, approximate values of heat and moisture were obtained from the Air Force Engineering and Services Center (Hass and Prince, 1982), but this amount of solid fuel burn is still an area of active investigation. These values were added in one lump sum at a location centered

about 200 m (one grid point) above the launch pad. Exponential functions were used to spread the perturbation in horizontal and vertical directions.

This initial perturbation is given as:

$$\Delta\theta(z) = \frac{B_\theta}{cp} \exp(-((x-x_o)^2 + (y-y_o)^2/\ell^2) \exp(-z/\ell) / (\rho_o \ell^3 \pi)$$

$$\Delta r_v(z) = B_v \exp(-((x-x_o)^2 + (y-y_o)^2) /\ell^2) \exp(-z/\ell) / (\rho_o \ell^3 \pi)$$

$$\Delta r_a(z) = B_a \exp(-((x-x_o)^2 + (y-y_o)^2)/\ell^2) \exp(-z/\ell) / (\rho_o \ell^3 \pi)$$

where B_θ, B_v and B_a are the amount of heat, vapor and smoke released by the explosion. The heat output rate for the TITAN rocket is assumed to be 5.7×10^9 J/S. During the explosion, the rocket fuel is burned for 240 S. Thus, B is given as $5.7 \times 10^9 \times 240$ J. The amount of vapor and smoke released are B_v = 14713 Kg, B_a = 63736 Kg.

Sensitivity to Initialization Schemes

The TASS model and most other cloud models available today usually are initialized with a near spherical heat impulse of 5 to $10^{o}C$ near the surface to represent solar heating in the natural environment. This impulse is the trigger to begin the convection process. During initial stages of this research, different types of initializations were tried in order to investigate the sensitivity of the model cloud to those initial impulses in identical atmospheric conditions (the same upper air soundings).

Results for both a $5^{o}C$ and $10^{o}C$ truncated cylindrical thermal impulse of radius 400m and height 1000m were compared for cloud bases, tops, vertical motion, and liquid water. The differences were less than 10% in all parameters at 4 minutes for the mission 41D atmosphere (1242 GMT 3/30/84) and 51A atmosphere (1215 GMT 11/8/84). For example, vertical velocity for 51A changed only 0.2 ms^{-1}, whereas the change between vertical velocity due to the atmosphere between 41D and 51A was nearly 200% (7.4 ms^{-1} for 41D compared to 2.5 ms^{-1} for 51A).

This illustrates the dominant influence of the atmosphere. There is one notable exception, however, in that the thermal perturbations for the mission 41D atmosphere produced a model cloud which continued to rise beyond 8 minutes. This was not observed for the photographed cloud. The actual heat and moisture from the Shuttle exhaust system which was used for all case study results discussed in this report produced the observed result of height stabilization and erosion from entrainment after 8 minutes.

SECTION 4. GROUND TRUTH

Photogrammetry

Photogrammetric calculations were made for the evolution of the height, base and width of the Shuttle ground clouds photographed on 16 mm film for three launches. These were Mission 41C (April 6, 1984), Mission 41D (Aug. 30, 1984) and Mission 51A (Nov. 8, 1984). Details of this work are documented in NASA CR 4103 [13]. The results are presented here to serve as the ground truth for the numerical model.

Results for Mission 41C

The calculated cloud top and base are shown for UCS 6 and UCS 9 films in Figure (5). Measurement from these camera views showed the altitude of the cloud top to reach a peak of 2200 m 4 minutes after launch. This is followed by a rapid decline to 1700 m by 6 minutes. The top remained at approximately 1700 m until the cloud began to dissipate after 9 minutes. The base of the cloud rose steadily after one minute and approached an asymptote of 1000 m at 10 minutes. The altitudes calculated from the two different camera views agreed to within 160 m for the cloud top and to within 110 m for the base.

The calculated maximum cloud widths near the top and the average widths from UCS 6, UCS 9, and UCS 2 (Fig. 6) show the cloud to be quite asymmetrical. After 6 minutes, the cloud appeared to be much wider in the North-South direction (UCS 6) than in the East-West direction (UCS 2, 9). The maximum width near the top as measured from UCS 6 increased almost linearly with time to 2500 m at 10 minutes. The maximum width that measured from UCS 2 reached a peak of 1800 m at 7 minutes and subsequently decreased. The maximum width from the UCS 9 view peaked at 1500 m at 4 minutes and remained between

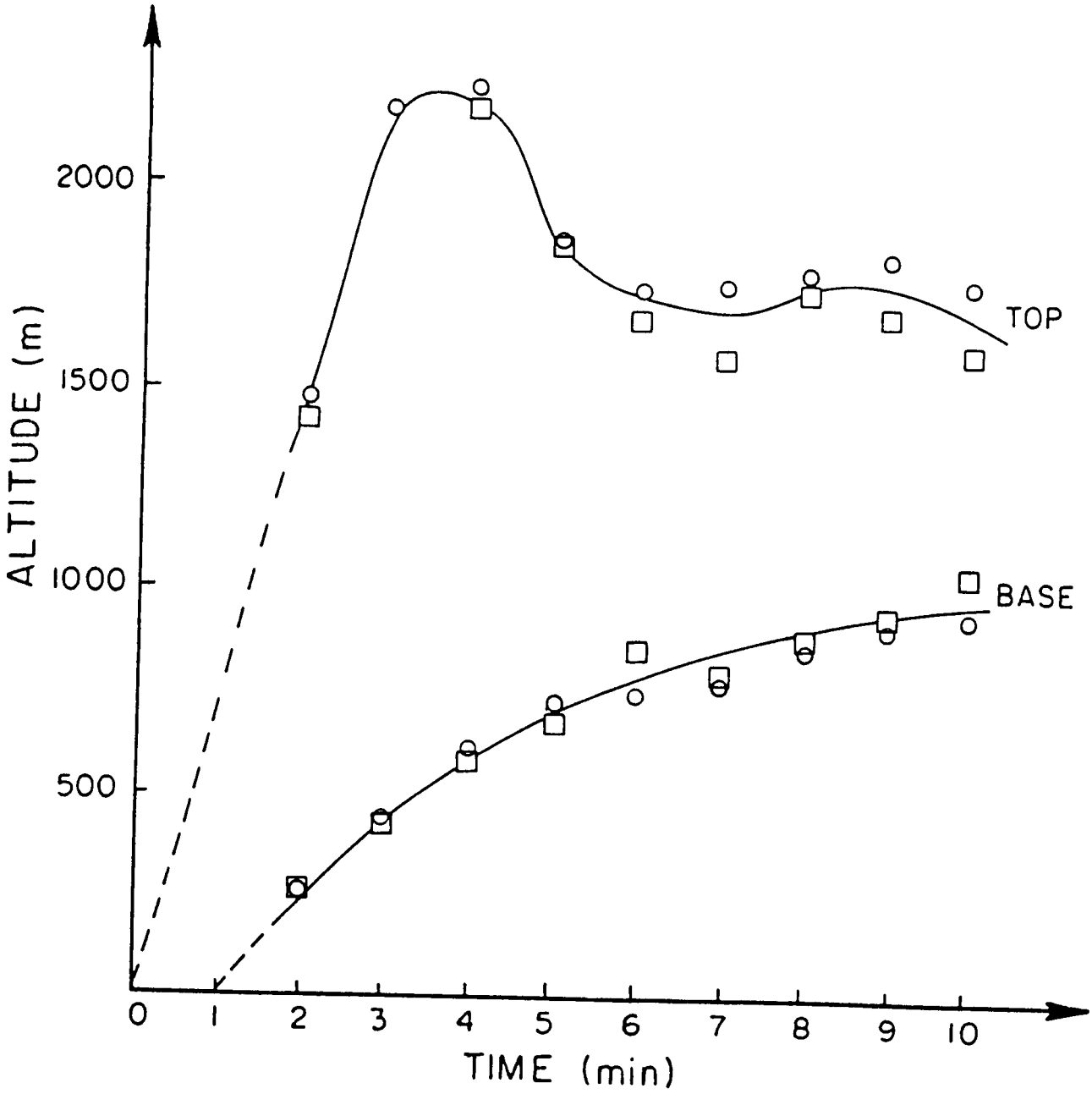

Figure 5. Altitude of the top and base of the Shuttle exhaust cloud versus time for Mission 41C. Circles are for UCS-6 camera looking east, squares for UCS-9 looking south.

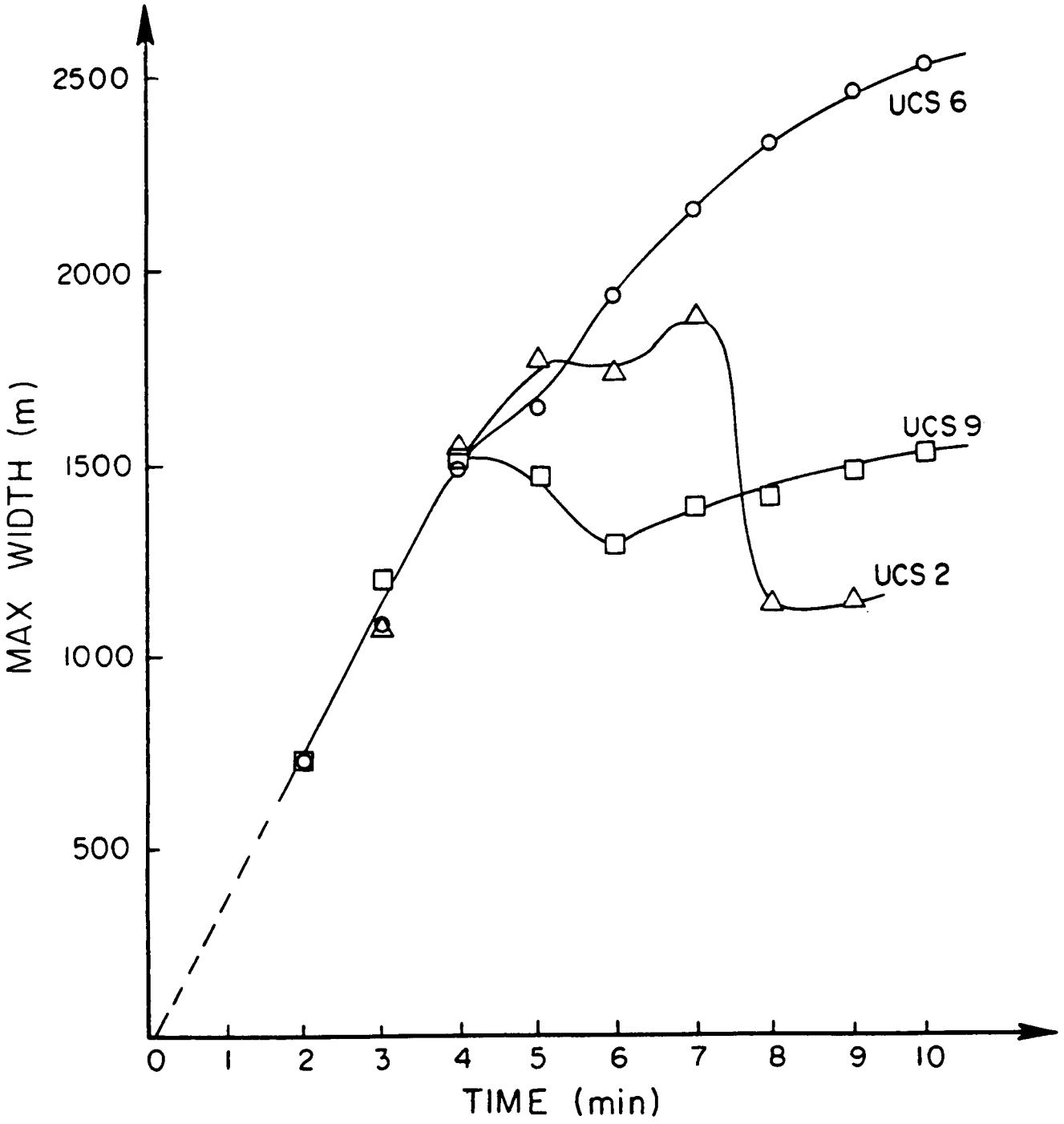

Figure 6. Maximum widths (at top) of Shuttle exhaust cloud versus time for Mission 41C.

1300 m and 1500 m afterwards. Figure (6) indicates that the cloud's orientation may have shifted between 6 and 9 minutes as a result of a change in wind directions. Figure (7) shows the average width measured from UCS 6 after 6 minutes to be about 800 m greater than the stable 1200 m width measured from both the UCS 2 and UCS 9 views.

Results for Mission 41D

The cloud top and base for Mission 41D were calculated from UCS 6 and UCS 9 films and are shown in Figure (8). Measurements from these camera views showed the altitude of the cloud top to reach a peak of 3500 m at 5 minutes followed by a gradual decline to 3000 m at 10 minutes. In general, the cloud top for Mission 41D rose to a much higher altitude and remained there for a longer time than that of Mission 41C. Like that of Mission 41C, however, the base of the cloud for 41D rose steadily after 1 minute and reached 1000 m at 10 minutes. The altitudes calculated from the two different camera views agreed to within 190 m for the cloud top and to within 100 m for the base. The cloud base was difficult to estimate for most of the tracings because of its nonuniformity.

The maximum widths (near the cloud top) and the average widths are shown in Figure 9. The calculated maximum cloud widths from UCS 6 and UCS 9 show the cloud to be quite asymmetrical near the top. For this launch, the cloud was up to 700 m wider in the East-West direction (UCS 9) than in the North-South direction (UCS 6) between 4 and 7 minutes. At the other times, however, the view-to-view width difference was less than 200 m. The maximum width near the top measured from both UCS 6 and UCS 9 rose asymptotically towards 1200 m at 10 minutes.

The volume was estimated for the ground cloud at 5 minutes after

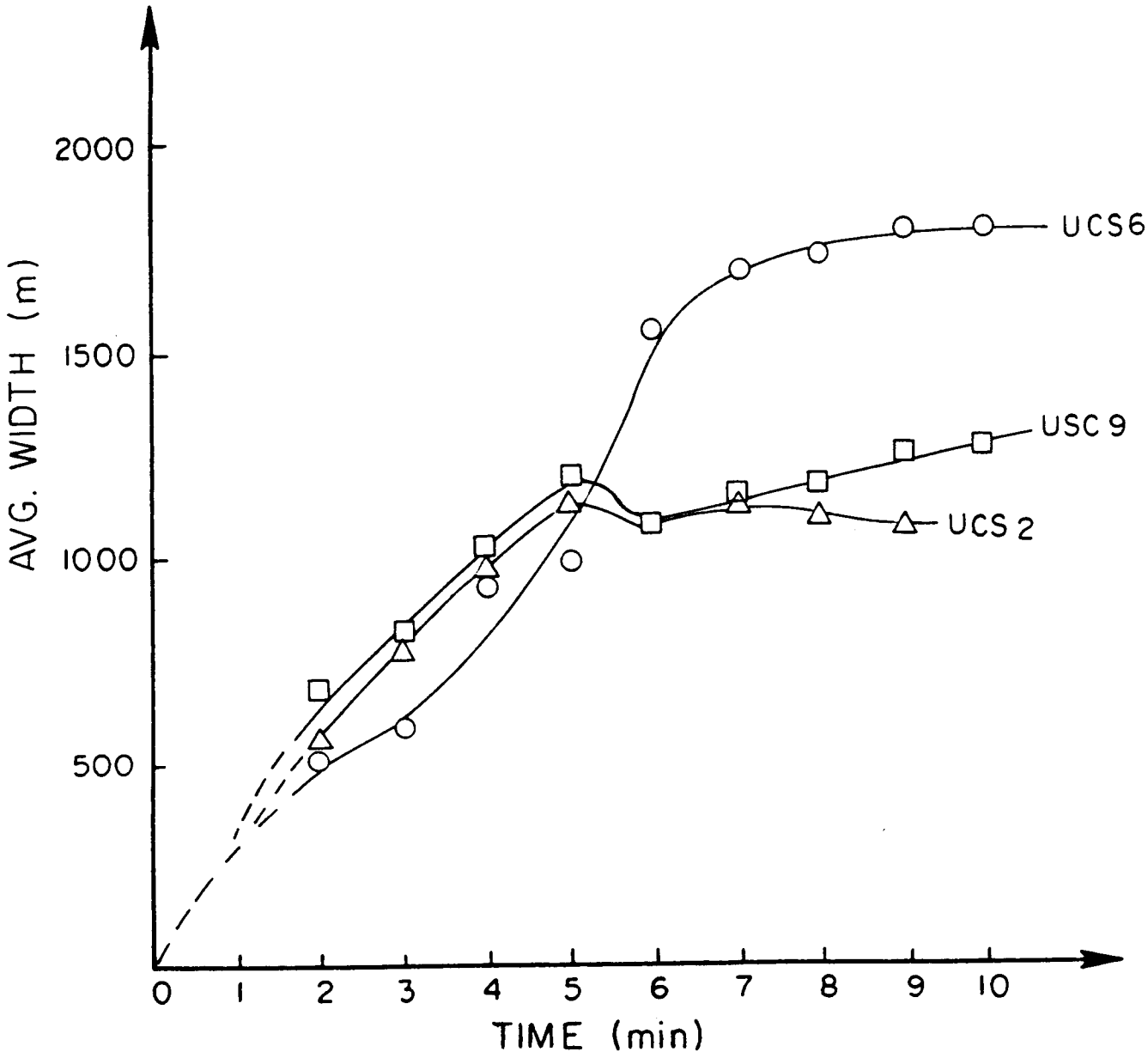

Figure 7. Average widths of Shuttle exhaust cloud versus time for Mission 41C.

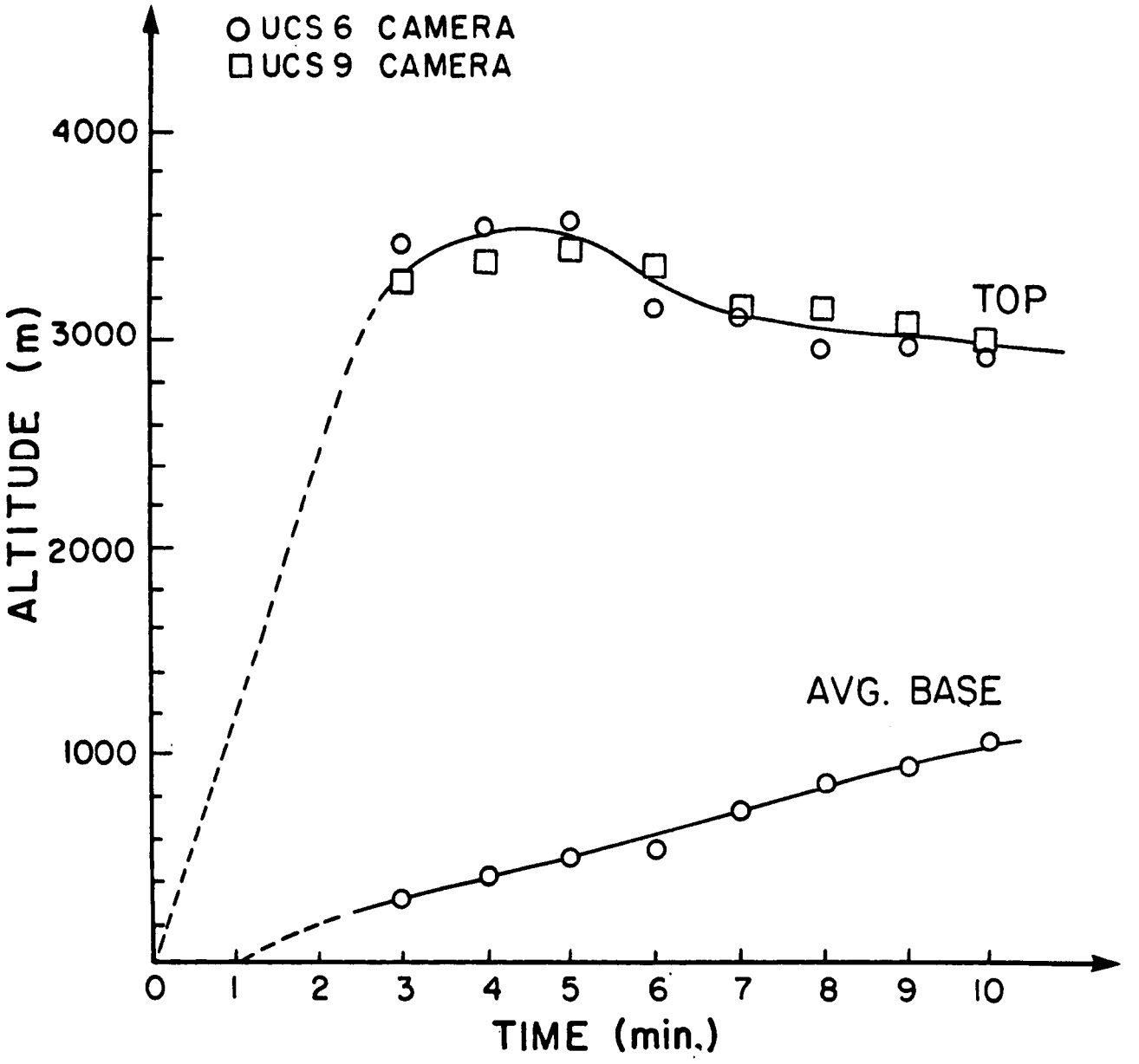

Figure 8. Altitude of the top and base of Shuttle exhaust cloud versus time for Mission 41D.

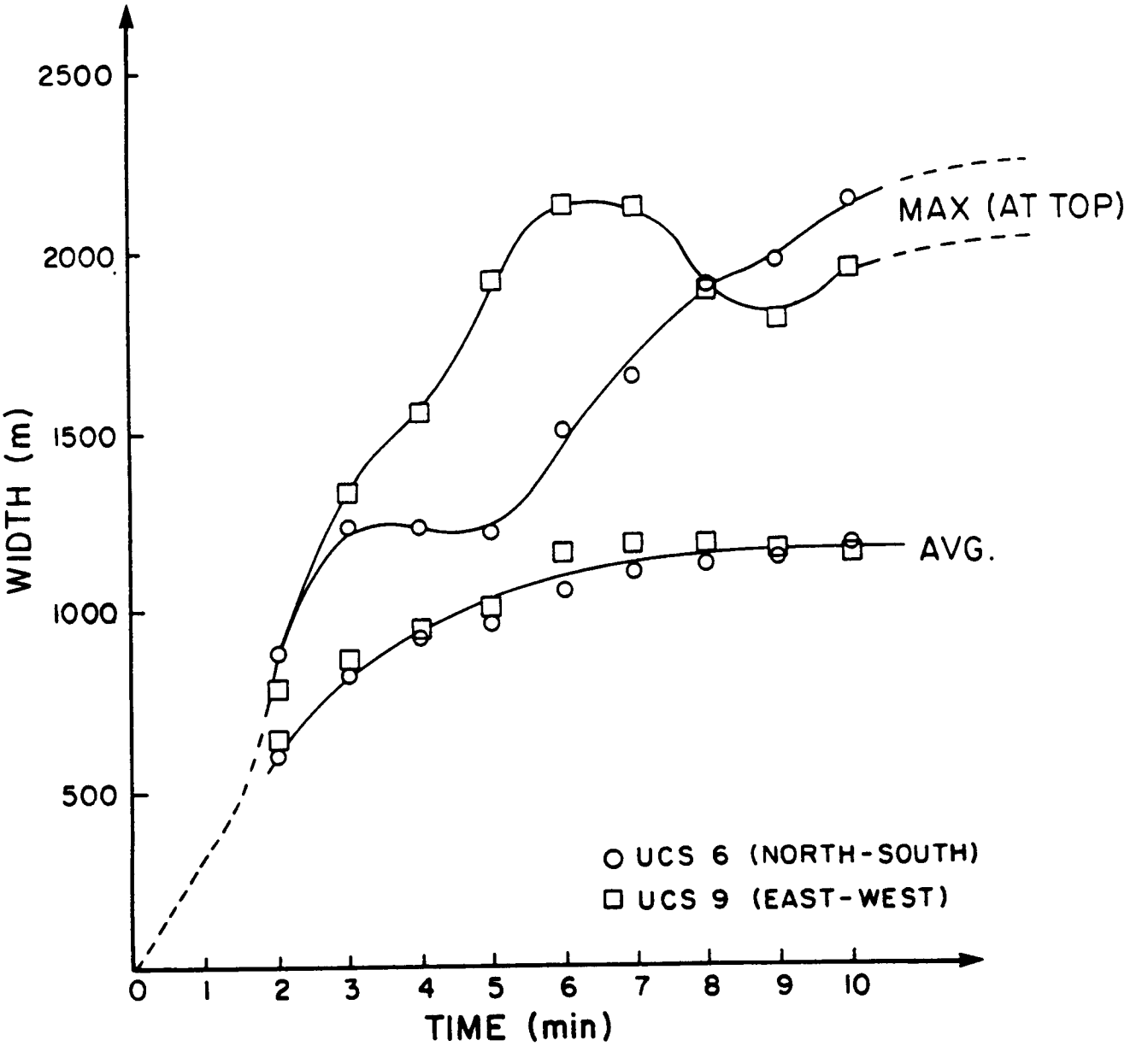

Figure 9. Average widths and maximum widths (at top) of Shuttle exhaust cloud versus time for Mission 41D.

10. The altitude of the cloud top was estimated to reach a peak of about 2400 m at 4 minutes since the cloud extended above the camera's view. After 5 minutes, the cloud top fell rapidly to 1800 m by 8 minutes. The cloud base, similar to those of the other launches, rose steadily after one minute and reached about 900 m at 8 minutes. By 8 minutes after launch, the cloud had spread out considerably and moved too close to the camera site to be entirely contained within picture frames.

The average and maximum cloud widths for Mission 51A are shown in Figure 11. The calculated maximum cloud width from UCS 6 reached a peak of 1700 m at 6 minutes, but was difficult to estimate afterwards. The average width was calculated from UCS 6 and estimated from UCS 2 based on what was visible beneath the environmental cloud cover. The UCS 2 calculations showed the average width to be up to 700 m wider than that from UCS 6. However, since the cloud shape was diagnonal from top to bottom in the UCS 6 view, the average width was measured diagnonally across the cloud (perpendicular to its sides) in order to provide a more accurate width that could be used in a rough volume estimate. As a result, the UCS 6 width may have been considerably less than that which was measured horizontally (because of the limited visibility of the cloud) from the UCS 2 view.

Aircraft Data

Some data were available from aircraft measurement programs conducted during the first few Shuttle missions. Details of the aircraft instrumentation and measurement techniques are available in Anderson and Keller [1983]. STS-3 was launched on March 22, 1982 at 1600 GMT. A National Oceanic and Atmospheric Administration (NOAA) WP-3D Orion made in-situ cloud microphysical measurements. Of primary interest for comparing TASS model

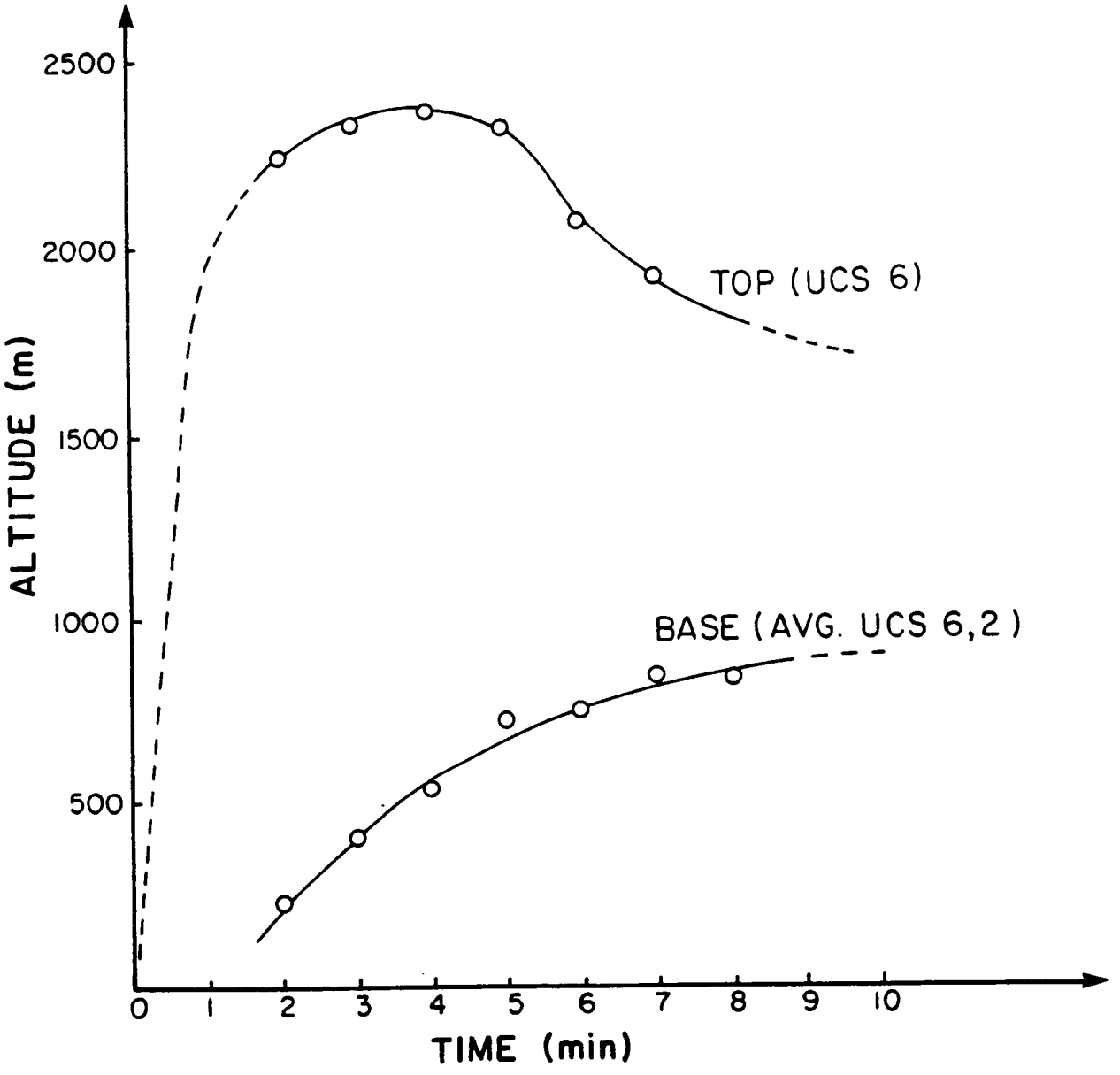

Figure 10. Altitude of top and base of Shuttle exhaust cloud versus time for Mission 51A.

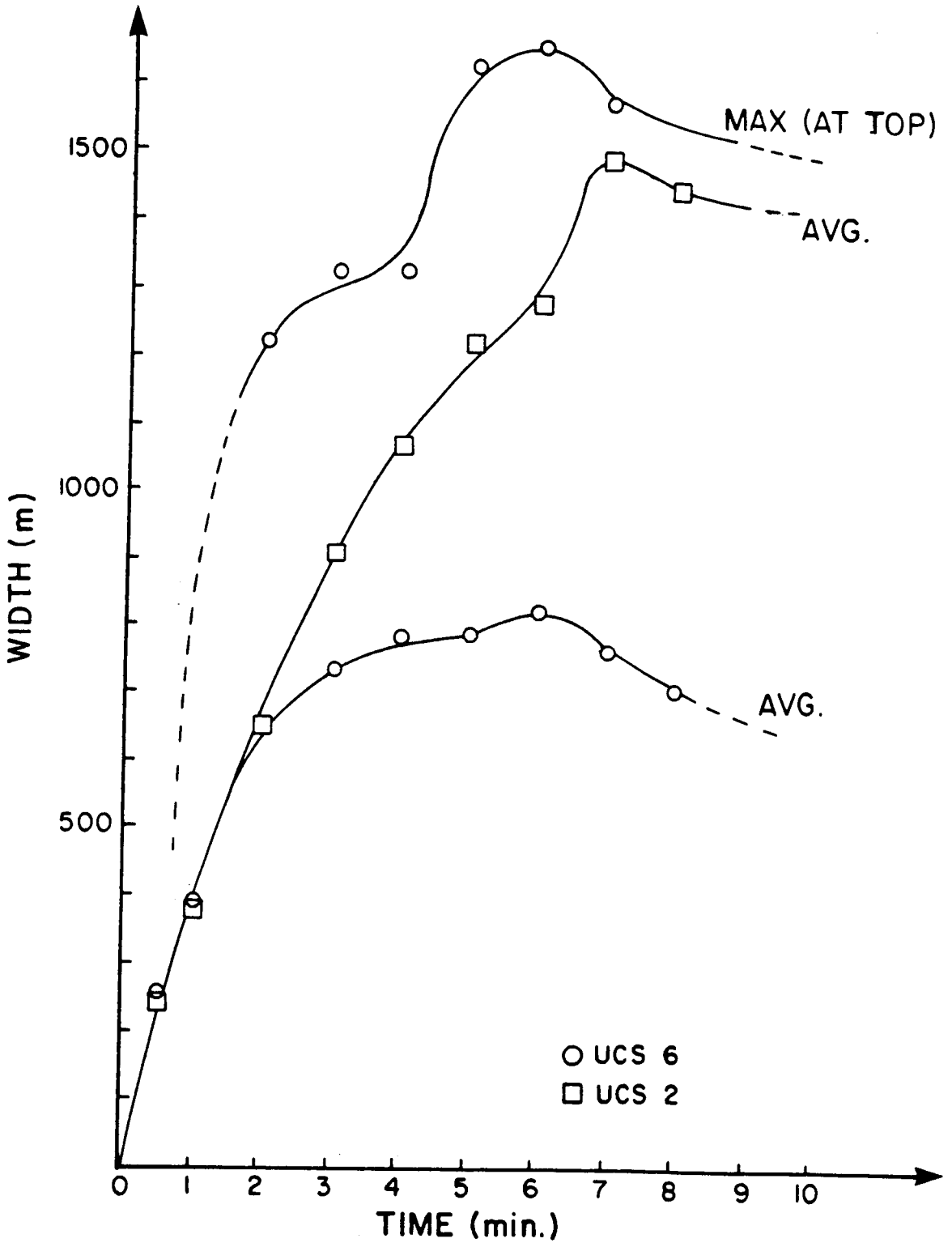

Figure 11. Average widths and maximum widths (at top) of Shuttle exhaust cloud versus time for Mission 51A.

results are the cloud liquid water content, and in cloud vertical velocity. The first cloud penetration was made at 700 m about 4 minutes after launch. There were others at 7 and 9 minutes as well. Results of the aircraft measurements are summarized in Table 2.

In general this cloud contained very little cloud water (0.3 g kg^{-1}), and the max vertical motion field was about 4 m sec^{-1} which is sufficient to support mm size drops.

Model-Truth Comparison

The purpose of the photogrammetry and aircraft data discussion above was to establish a data base for observed Shuttle ground cloud characteristics in known atmospheric conditions. This data base is compared to results from model simulations in order to establish the degree to which the model can simulate observed features of the ground cloud.

Limitations in Ground Truth

First we should point out that there are several difficulties in comparing the complicated structures of a 3-dimensional, rapidly varying, asymmetrical cloud with model results. One difficulty is that any two-dimensional view captures the asymmetry only in the plane of observation at the time of the observation. Similarly, a cross section through the model cloud produces quantitative results for that specific cross section slice and time. There are numerous other such slices for that time which would present different results and the higher the asymmetry, the more the variation in cross section properties. There is no guarantee that a particular cross section through the modeled cloud or measurements from a selected path through an observed cloud will provide the maximum value of a particular parameter at

Table 2. Summary of STS-3 Insitu

Aircraft Measurements

Time after launch (min)	Aircraft Altitude (m)	Maximum liquid water content (g kg^{-1})	Maximum vertical velocity (m sec^{-1})
4	700	0.3	4.0
7	990	0.3	4.0
9	800	0.2	4.2

the given time (or short time interval in the case of an aircraft measurement). Finally, there could be differences in averaging techniques, degree of subjectively in the choice of parameters to compare and especially in what constitutes the visible cloud (smoke or water).

Nevertheless, a degree of confidence can and will be established for the basic characteristics of cloud top base, width, volume, liquid water content and vertical velocity for all cases where measurements or observations existed. As mentioned before, the environment plays the dominant role in all properties of the ground cloud so that for every comparison, the atmosphere presented to the model as represented by the sounding is the same atmosphere in which the observed cloud grew. There is one exception in that neither the spatial variations nor time change in the 10 minutes or so of the comparisons were available to the model.

Cloud Parameters

Table 3 summarizes model results and observations for cloud parameters. For all cases the agreement in maximum cloud top for liquid water clouds or smoke field for dry environments is very good.

Cloud top comparisons were made using the model liquid water content threshold of 0.01 g kg^{-1}. Cloud bases in the photogrammetry results did not count the small low hanging piece of cloud which seemed to originate from the north trench. The model calculations included all points in the domain. Therefore, much of the discrepancy in cloud bases is due to these differences in averaging.

The cloud volume was computed from the model cloud domain for case 41D at 5 minutes after launch. The value of 1.4×10^9 m^3 is lower than the photogrammetry estimates of about 3.0×10^9 m^3 because the latter included

Table 3. Comparisons of Observed Clouds with Model Clouds

	Parameter Observed/Model					
Shuttle Mission	Time After Launch	Maximum Top (km)	Average Base (km)	Average Width (km)	Average Max.* Liq. Water (g/Kg)	Average Vertical Velocity (m/s)
	3 min	2.2/-	0.3/-	0.7/-	-/-	-/-
41C	6 min/7 min	1.7/1.6	0.7/1.2	1/1/0.7	-/0.3	-/0.5
	9 min	1.8/1.4	0.8/1.2	1/3/0.5	-/0.2	-/0.4
	3 min	3.3/2.8	0.4/0.1	0.7/1.6	-/0.6	-/8.5
41D	6 min	3.3/3.2	0.5/0.1	1.1/1.7	-/0.7	-/3.5
	9 min	3.0/3.2	0.8/0.7	1.2/1.7	-/1.0	-/2.4
	3 min	2.2/2.4	0.4/1.3	0.8/1.6	-/0.4	-/5.3
51A	6 min	2.0/2.4	0.7/1.3	1.0/2.0	-/0.7	-/3.1
	9 min	1.7/-	0.7/-	0.9/-	-/-	-/-
	4 min	1.0/1.4	0.2/0.1	1.2/1.4	0.3/0.4	0.7/3.2
STS-3	7 min	1.2/1.4	0.4/0.7	1.9/1.4	0.3/0.4	0.6/0.6
	9 min	1.2/1.2	0.4/0.7	2.0/1.1	0.2/0.2	0.6/0.1

*The Max. liquid water and vertical velocity for model results is the highest value of the horizontal cloud domain average computed from 200 m thick horizontal "pancakes".

both smoke and liquid water whereas the former included only liquid cloud water. Smoke volume was calculated from horizontal averages for pancakes within the model domain and found to be about 5×10^9 m^3. Observed liquid water content in the cloud was only available for STS-3. Here, agreement with model results is excellent. Model results for the other cases are all reasonable based on the available atmospheric moisture and degree of low level stability.

The model is also able to reproduce some of the convective bubbling observed in cloud rise. After the first minute both the model and observations indicate a merging of the different surface elements into an irregular but contiguous cloud mass. Thereafter, the part of the cloud originating in the region about 1 to 2 km appears to rise to its maximum altitude in the first 4 to 5 minutes. Model simulations show this feature as well but about one minute slower. The main bubble appears to include the heat and moisture from the exhaust accumulation near the ground. It rises more slowly but can be seen in the video tapes and film. It accounts for the slight rise at the 8 minute point in overall cloud tops from the photogrammetry results for 41C and 41D. In the case of 51A, it was too difficult to observe the main bubble rising through a significant natural stratocumulus cloud layer. The model also develops this main bubble but again the timing is about a minute slower than observed.

Cloud width is very difficult to compare due to high asymmetry and whether or not you measure smoke or cloud water. The model is able to reproduce much of the observed asymmetry and for clouds with significant liquid water such as 41D, agreement in widths is excellent.

Vertical motion observations are only available for STS-3 within the cloud and agreement with model results is reasonable considering the

differences in obtaining the numbers for comparison. In Table 3 the vertical velocity is the computed average at 1 second intervals from plots in Anderson and Keller (1983) at fixed altitudes and duration of cloud penetration. For model results a horizontal domain average is calculated, then the maximum for any horizontal pancake is shown. The maximum model value of 4 m/s from an xz cross section occurred at 4 min after launch (initialization). This compares well with the maximum observed value of 4 m/s during the first penetration.

Some of the above characteristics are discussed in the context of atmospheric influences during the case studies presented in the next section.

Model Limitations

As in any numerical simulation there are assumptions necessary to deal with the complexities of the natural environment, techniques needed to treat the artificial boundary processes and discretization imposed by the model, and practical limitations, all of which affect the results. No model is ever perfect, and the only valid test of model performance is the extensive comparison of model results with true atmospheric processes. This study has devoted considerable time to the verification process as discussed in the preceding section. For a detailed discussion of the assumptions in the modelling process and numerical techniques, see Proctor [1987].

One of the compromises necessary to reduce computer costs was the model resolution or spacing between grid points. The choice of 200 m (300 m for the unstable cases) was necessary in order to preserve detail, reduce computer run time and therefore increase the number of simulations possible within a fixed computer budget. The computer used in these simulations was the Langley Research Center VPS-32. It is a modification of a CYBER 205 which is a vector processing machine capable of 100 million operations per second. Computer

costs were directly proportional to the number of grid points at which numerical solutions were required. If the grid spacing is cut in half, the number of grid points increases by $2^3 = 8$. For our domain of 6 km x 6 km x 5.6 km, the number of grid points would change from 25,200 for a 200 meter resolution to 201,600 for a 100 m resolution or 8 times the cost. Also, the time step would need to be reduced, further increasing run time. Considerable detail was reproduced in model cloud structure and reasonable comparisons with observed clouds were obtained using the 200 m resolution and the run time was reasonably low. Therefore, 200 m was selected to be the optimum choice. There is no reason other than computer costs to limit model resolution.

Resolution is important because the model treats atmospheric processes explicitly only at wavelengths greater than the grid spacing. Parameterizations are used for smaller scales. While the parameterization process is generally accepted in numerical models, and even though they are carefully selected to best represent atmospheric processes, they are still approximations. The rocket exhaust cloud is a turbulent entitity so that small scale processes are active. The total effect of model resolution can not be quantified but there are affects on turbulent eddy mixing, entrainment of dry air affecting cloud dissipation and possibly in the speed of the model's reaction to the initial impulse. Comparative runs at 200 and 300 m resolution indicate a small reduction in the 300 m simulated cloud water and weaker vertical velocity.

Other choices were made from a project cost standpoint. There was no precipitation scavenging in the model but this should only affect the near field droplet depletion as no natural cloud precipitation developed. Also there was no gravitational settling allowed for the smoke tracer. The latter affects model cloud appearance and the base of the ground cloud computed from

the domain averaged smoke. This is discussed in conjunction with case study results. Finally, there is no chemical treatment for HCL which is contained in rather large quantities in both liquid and gaseous forms.

SECTION 5. CASE STUDIES

Once the model with initialization for Shuttle exhaust characteristics was tested and verified with atmospheric soundings from documented Shuttle launches, then different atmospheric soundings were used corresponding to different weather regimes. Of particular interest from a toxic deposition standpoint were two situations: a very unstable atmosphere in which cloud growth was anticipated to be more vigorous, and a very stable atmosphere which contained a strong low-level inversion (temperature increase with height) below which the ground cloud might be trapped. Wind shear was also of interest. A summary of all case studies discussed in this report is contained in Table 4. Even though some of these cases were used to document model performance, they contain important atmospheric features and will serve as case studies also to help illustrate the significant atmospheric influence on ground cloud properties and behavior.

Unstable Atmospheres

CASE 41D. This sounding shown in Figure 12 contains a very moist, potentially unstable region below 2.5 km. The winds were light with maximum speed about 5 m sec^{-1} below 3 km. The wind direction shifts from the southeast to west at about 500 m. Any parcel of air[2] with an upward velocity (such as in the Shuttle ground cloud) would reach saturation quickly from adiabatic cooling due to the high moisture content of the atmosphere in the dynamic cloud growth region (below 2.5 km). Additional heat would be released

[2]The parcel theory for the convective process is an oversimplification to the complex interactions between many scales of motion in the turbulent exhaust cloud and environment but it is useful for explaining some of the features observed.

Table 4. Summary of Case Studies Used for Model Simulations

Case	Resolution	Simulation Time	Sounding
41D	200 m	9	KSC 1242 GMT 3/30/84
51A	200 m	9	KSC 1215 GMT 11/8/84
41C	200 m	9	KSC 1358 GMT 4/6/84
STS3	200 m	9	KSC 1600 GMT 3/22/82
INV	200 m	6	Vandenberg 1200 GMT 6/24/87
TITAN	200 m	6	Vandenberg 1315 GMT 4/18/86
UNS	300 m	6	KSC 0115 GMT 8/30/83
MASS	300 m	9	KSC MASS Sounding 0300 GMT 8/30/83
UNS41D	200/300 m	12	Modified 41D Sounding, Remove Inversion
MOS41D	300 m	9	Modified 41D Sounding Remove Inversion Add Moisture
UNSDB	200 m	6	KSC 0115 GMT 08/30/83 Double Initialization

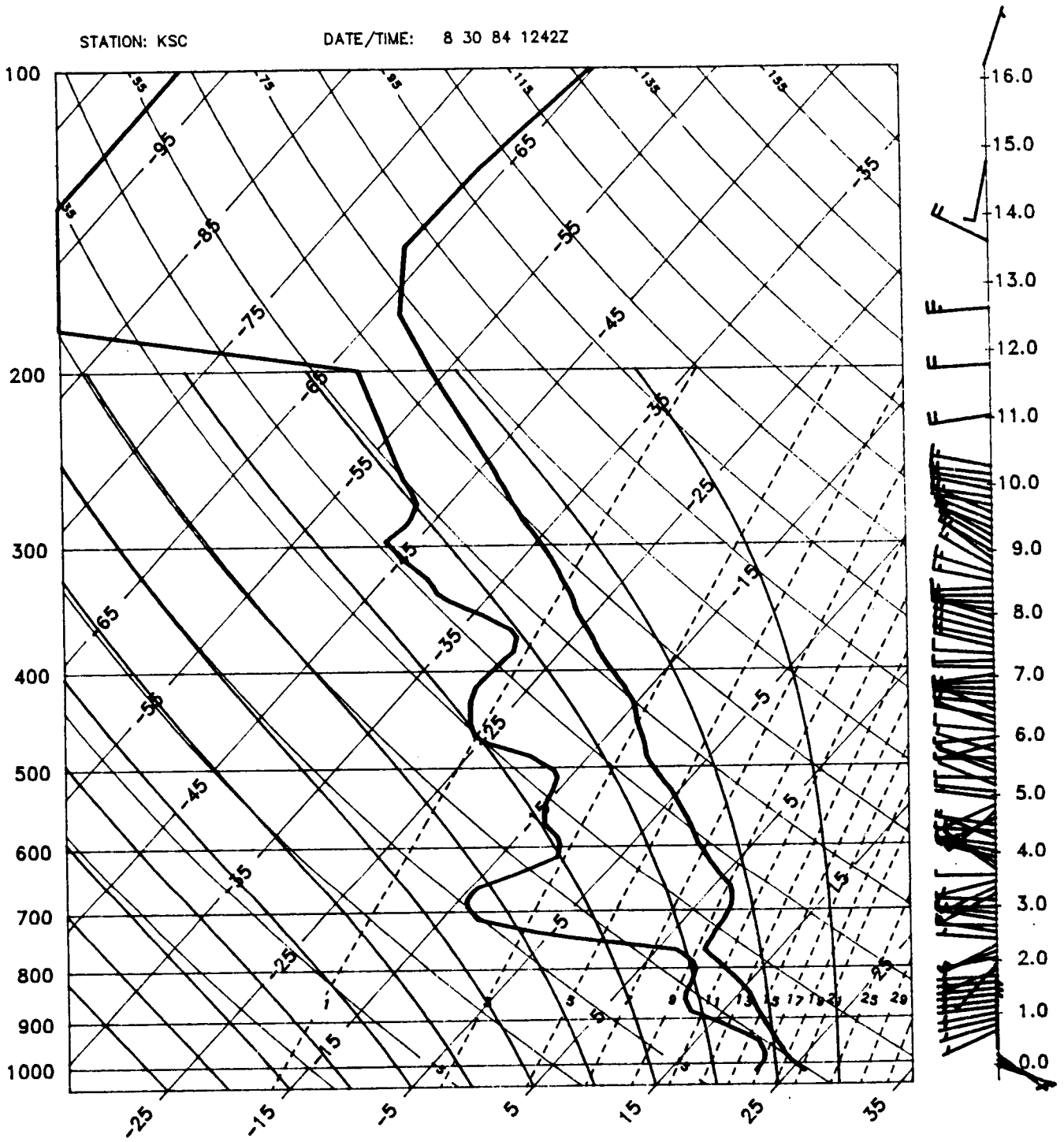

Figure 12. Upper-air soundings for Mission 41D, August 30, 1984 1242 GMT.

from the condensation process which would add buoyancy to the already buoyant ground cloud. This process would continue in the 41D atmosphere until cloud parcels reach about 3.0 km where their temperature would be the same as the environment. The isothermal layer between 2.2 and 3.2 km and pronounced dryness in this region should provide an effective cap to the rise of the ground cloud.

We have the luxury in this case of observing the behavior of the actual ground cloud for this launch from 16 mm films (and video tapes) taken from three different ground-based camera sites. Digitized film frames for 1, 3, 5 and 7 minutes after launch looking east from camera site UCS-6 are shown in Figure 13. In addition a trace of the cloud outline at 3 and 5 minutes after launch is shown in Figure 14. The trace was made by projecting a 16 mm image onto a paper screen.

The complex, asymmetrical, shape can be seen as the cloud rises in a series of convective bubbles. The first bubble appears to originate within the first minute from the part of the column cloud between about 1700 to 2500 m. It reaches its maximum altitude in 3 to 4 minutes then descends. The next bubble, which appears to be the largest, originates from the region below about 1500 m. It rises more slowly reaching its maximum altitude in 7 to 8 minutes. This maximum altitude is slightly lower than the first bubble and its decay is slower. The corresponding time-height plot of cloud top and cloud base determined by photogrammetry was shown in Figure 8 looking east (UCS-6) and south-southwest (UCS-9).

The next five Figures are model results for the same atmospheric sounding. Figure 15 is a perspective plot of cloud liquid water generated by the condensation, droplet-growth process at 3, 5, 7, and 9 minutes after initialization (simulated launch). The minimum threshold for contouring is

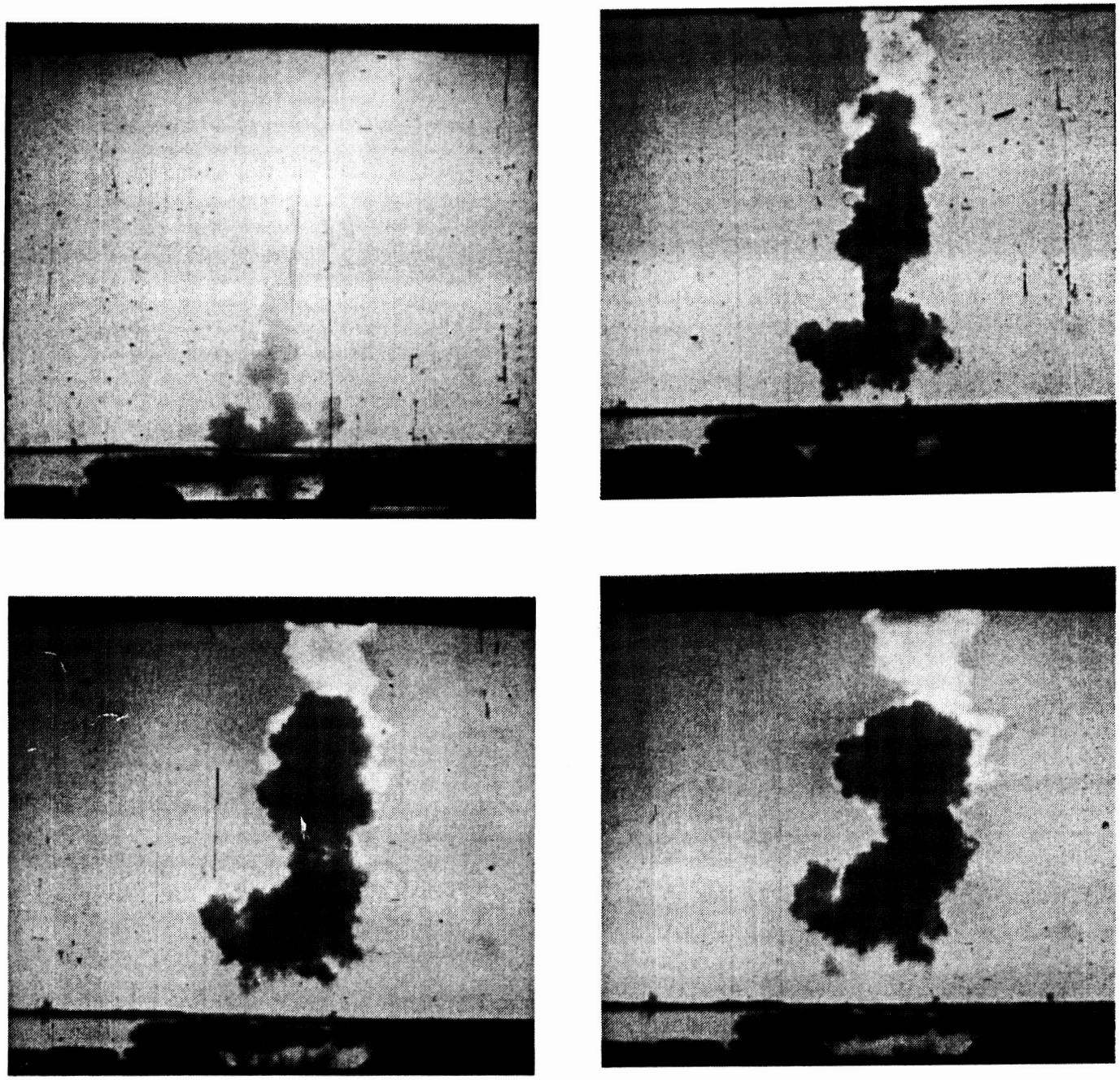

Figure 13. Photographs of digitization of 16mm film for the Shuttle Mission 41D ground cloud looking east at one minute (top left), 3 minutes (top right), 5 minutes (bottom left), and 7 minutes (bottom right) after launch.

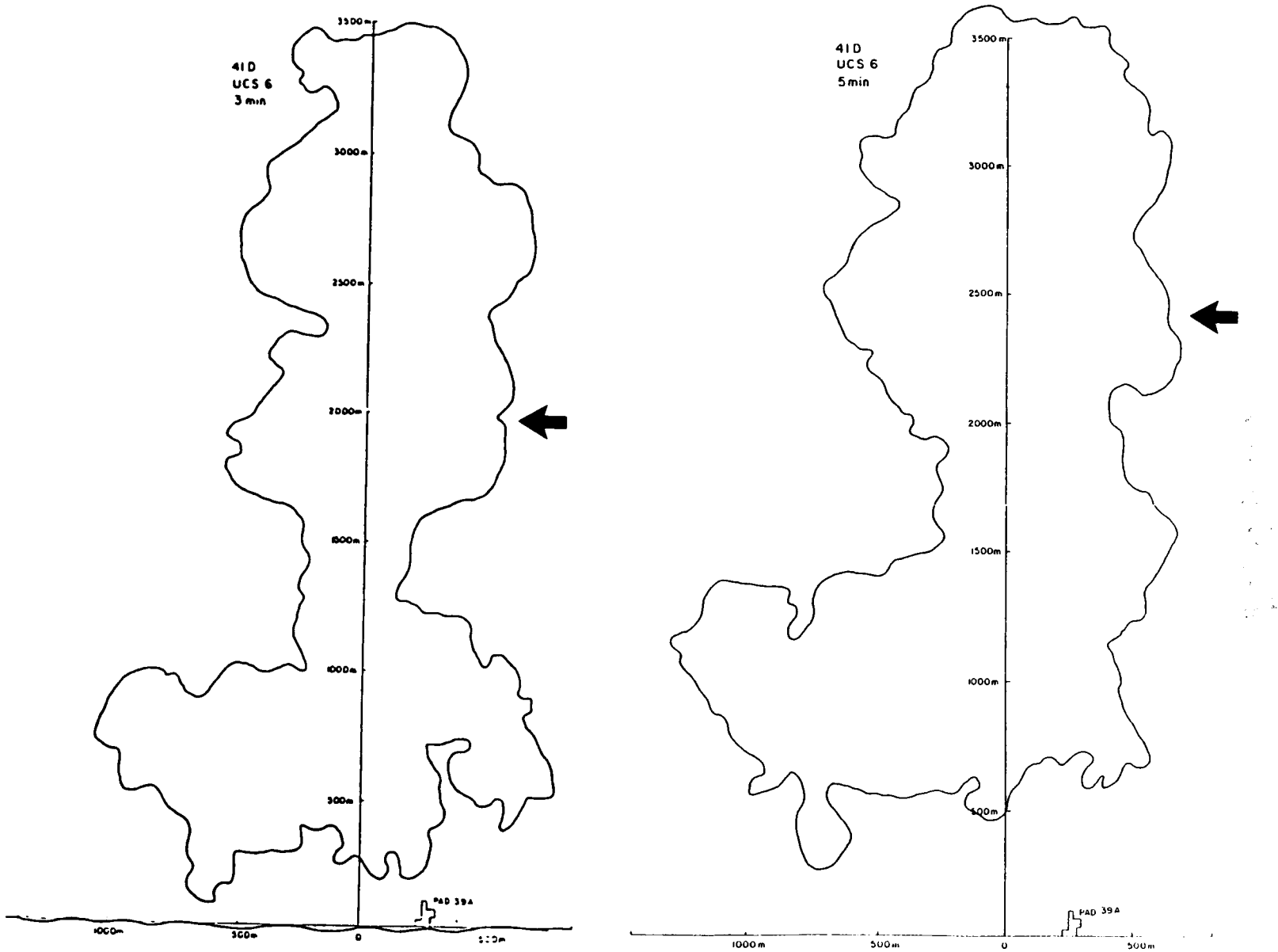

Figure 14. Trace of the observed Mission 41D cloud outline at 3 minutes (left) and 5 minutes (right) after launch looking east.

Figure 15. Perspective view of model cloud water (liquid) at 3, 5, 7, and 9 minutes after initialization for Mission 41D looking east.

0.01 g kg^{-1}. The tick marks on the axis represent 1000 m intervals. From this view looking toward the east (comparable with Figure 13), the convective bubbling can be identified. At 5 minutes into the simulation the column portion of the model generated cloud reaches its maximum altitude, 3200 m, then descends to about 3100 m at 7 minutes. Thereafter, another bubble rises again and stabilizes at about 9 minutes.

The lower part of the simulated cloud system arises from the north trench. It differs somewhat in shape from the photographs (Figure 13); however, the orientation and evolution pattern are in good agreement. This lower portion of the cloud appears to be dominated in both reality and model simulation by the near neutrally buoyant northern portion which is produced by both solid rocket booster exhaust gases mixed with significant water for cooling and acoustic wave suppression. The model smoke field is shown in Figure 16 looking east. The same 0.01 g kg^{-1} threshold for the smoke mixing ratio is used for display. In the model simulation even after 7 minutes the smoke field is still hanging near the surface. This is due to the fact that the model smoke field was being used primarily as a tracer of cloud dynamics. Smoke was given no mass (therefore, no gravitational settling is allowed) and not allowed to participate in the microphysical processes. The small lateral displacement of the smoke indicates the weak dispersion from the light winds in the lower part of the atmosphere.

The high asymmetry of the water cloud is shown qualitatively from the perspective plot looking toward the south (Fig. 17). The ascent and descent of convective elements can again be seen along with the tilt of the upper part toward the east consistent with the winds at that altitude. Note that the convective turrets at the top change location with time. The perspective view looking toward the northeast (Figs. 18, 19) confirms the convective bubbling

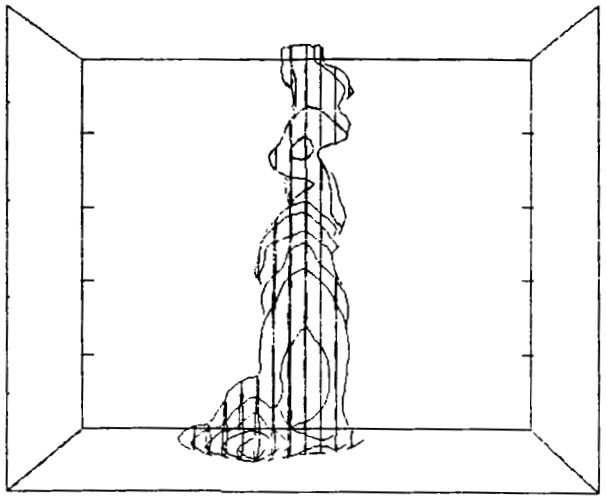

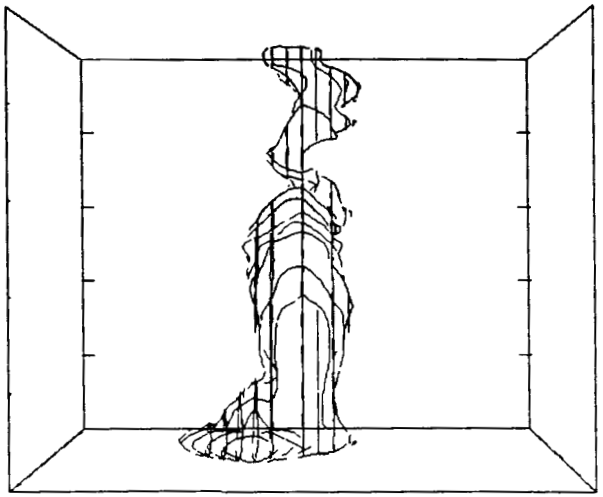

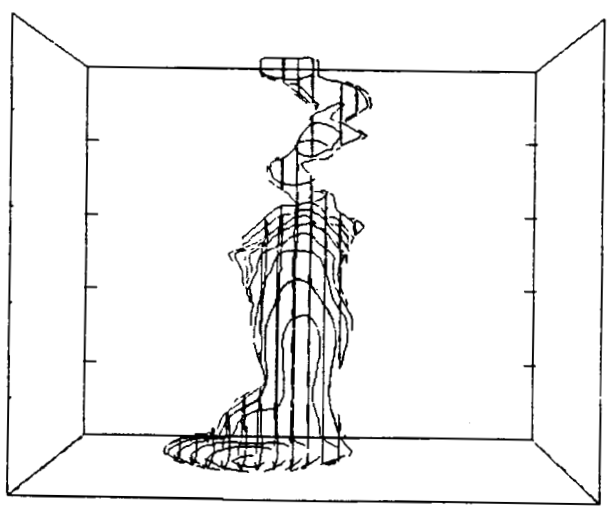

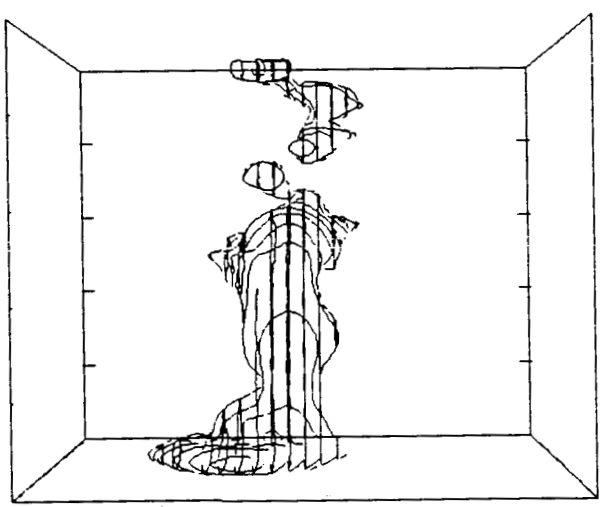

Figure 16. Perspective view of model smoke at 3, 5, 7, and 9 minutes after initialization for Mission 41D looking east.

Figure 17. Perspective view of model cloud water at 3, 5, 7, and 9 minutes after initialization for Mission 41D looking south.

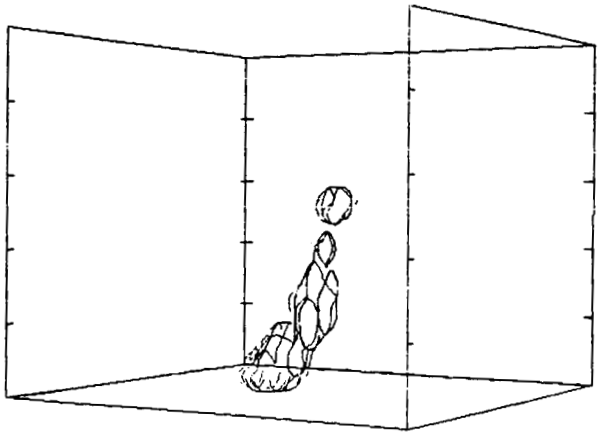

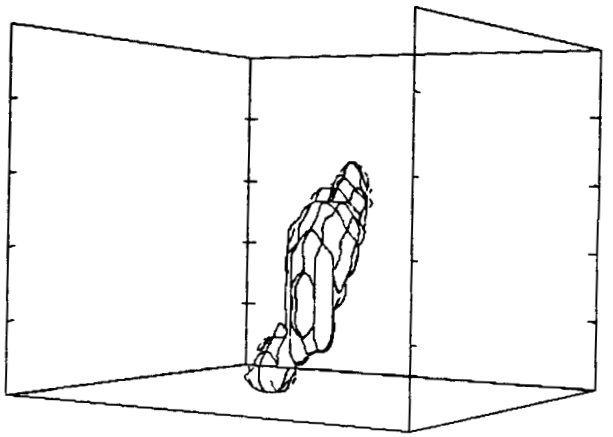

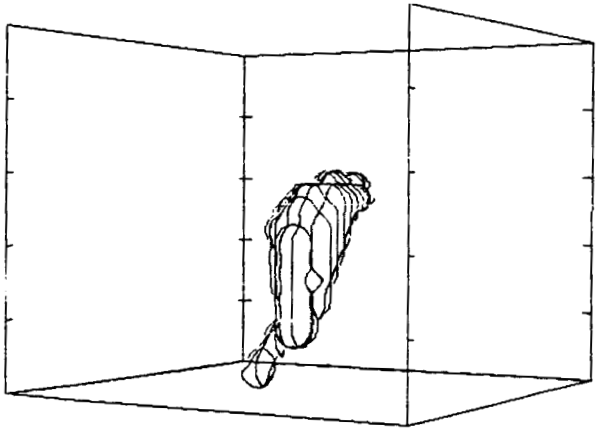

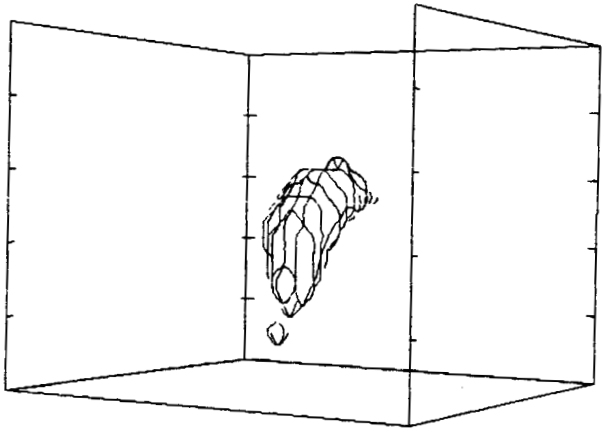

Figure 18. Perspective view of model cloud water at 3, 5, 7, and 9 minutes after initialization for Mission 41D looking northeast.

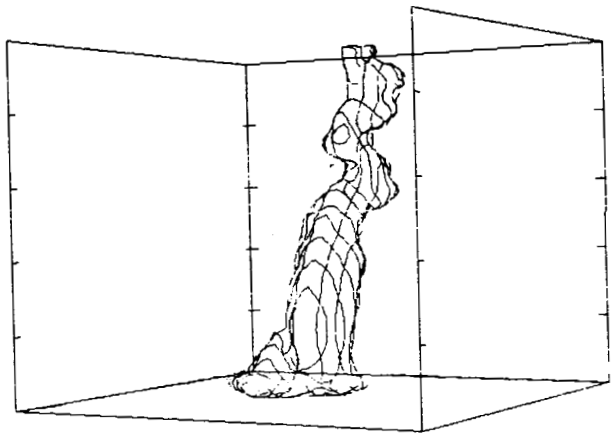

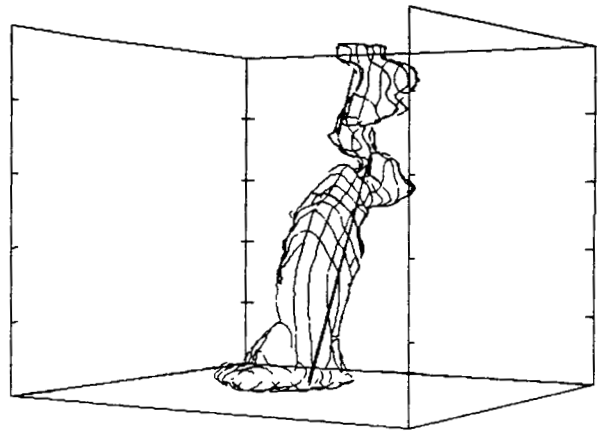

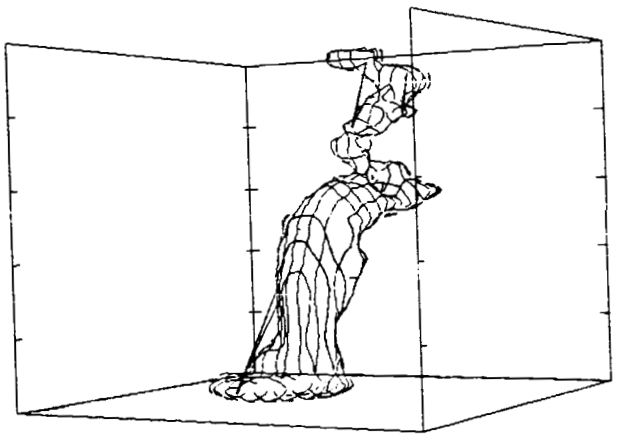

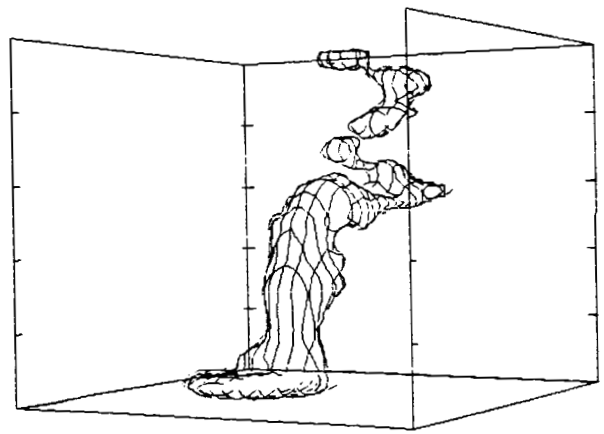

Figure 19. Perspective view of model smoke at 3, 5, 7, and 9 minutes after initialization for Mission 41D looking northeast.

and the eastern tilt as indicated by observations.

The evolution of the cloud top and width from model results compared to observations is shown in Figures 20 and 21, respectively. The convective bubbles in the model cloud are about a minute slower than observed. The observed cloud top from the column portion of the Shuttle exhaust system reaches its maximum in 4 minutes whereas the model indicates the maximum in about 5 minutes. The main convective bubble in video tapes appears to reach its maximum altitude in the 7 to 8 minute time period compared to the model bubble at about 9 minutes. It appears that the model needs a little longer to adjust to the large heat and moisture impulse presented at the beginning of the simulation.

The computed cloud width shown in Figure 21 is in good agreement with observations. The average width ranges between 1 and 2 km depending on orientation. In general the cloud is wider in the east-west direction both from observations and model results. This is most likely due to the wind shear and eastward tilt of the top portion of the ground cloud.

Other properties of the cloud can be shown quantitatively in vertical cross sections. It should be noted, however, that due to the high asymmetry, each cross section will be different. There is no guarantee of capturing the mathematical maximum for any property in any selected cross section. Figures 22 to 26 show arbitrary slices through the 3-dimensional model in the yz or xz planes. Figure 22 shows the yz cross section of vertical velocity (w) for 3, 5, 7, and 9 minutes. The strongest vertical motion of 8 m sec^{-1} occurs at five minutes while the region within the cloud where vertical motion is strongest continues to rise in altitude to about 2.5 km at 9 minutes. The eastward tilt of the top part of the cloud channel is shown in Figure 23 along

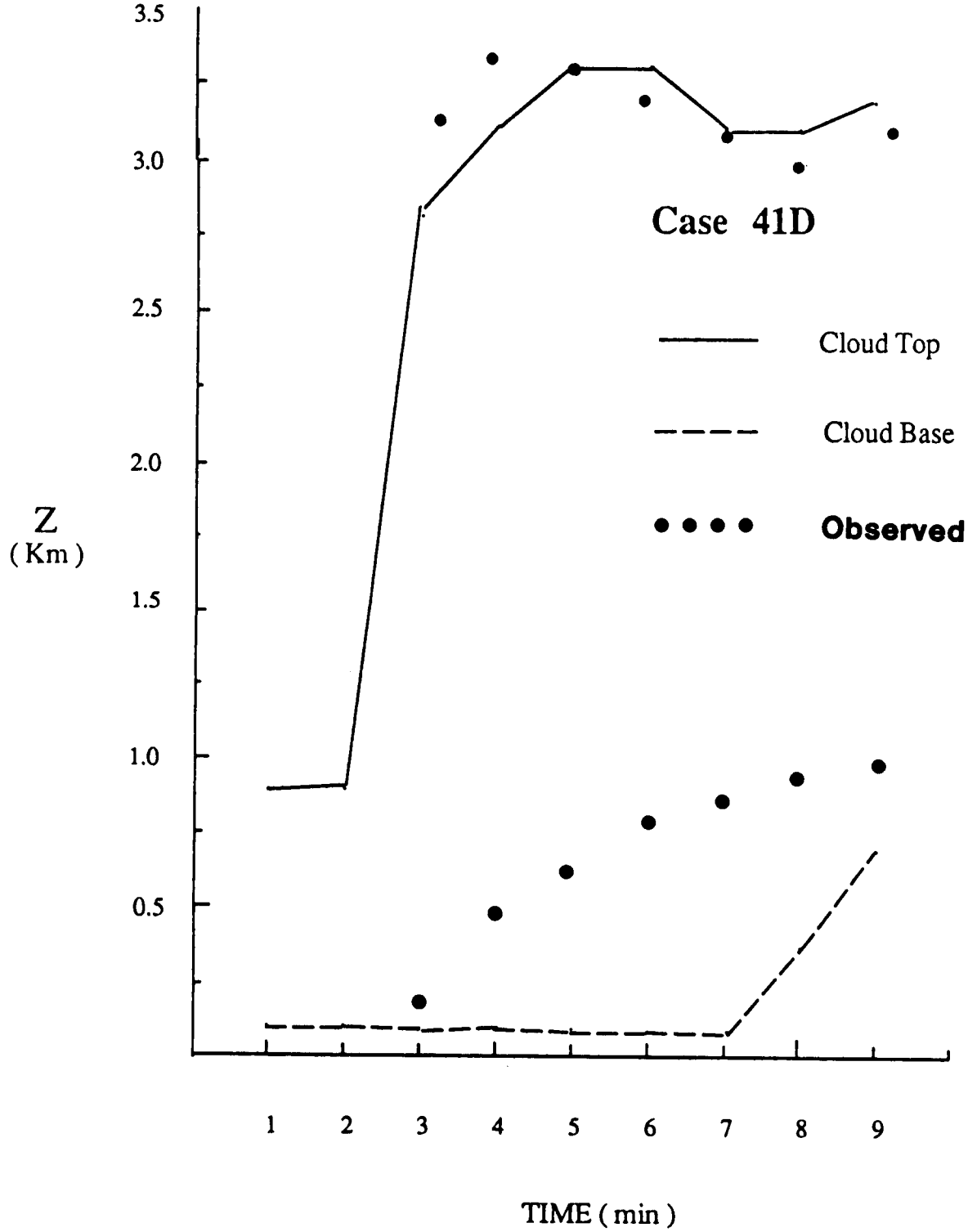

Figure 20. Comparison of model results and observations for the evolution of cloud top and base for Mission 41D.

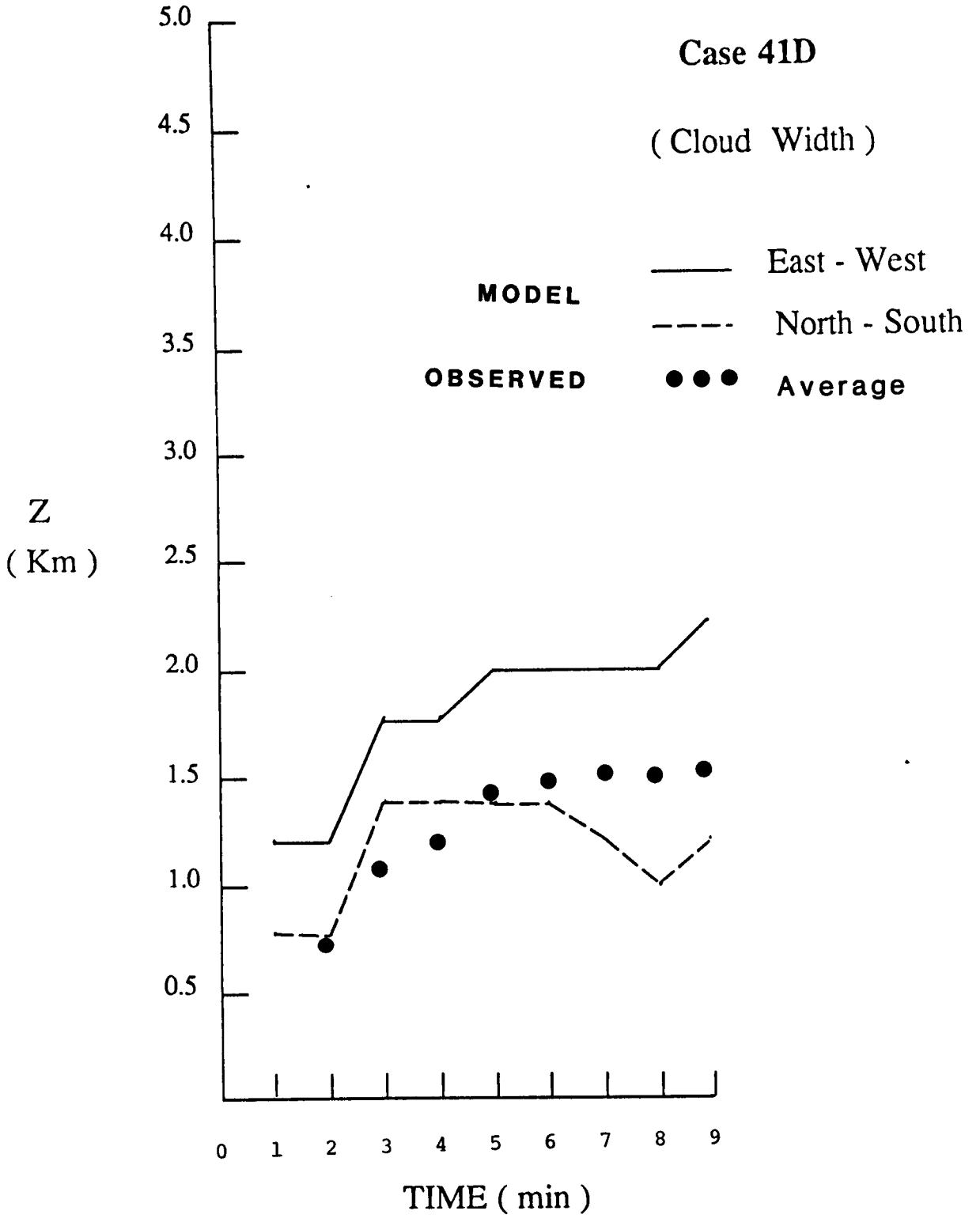

Figure 21. Comparison of model results and observations for the evolution of cloud width for Mission 41D.

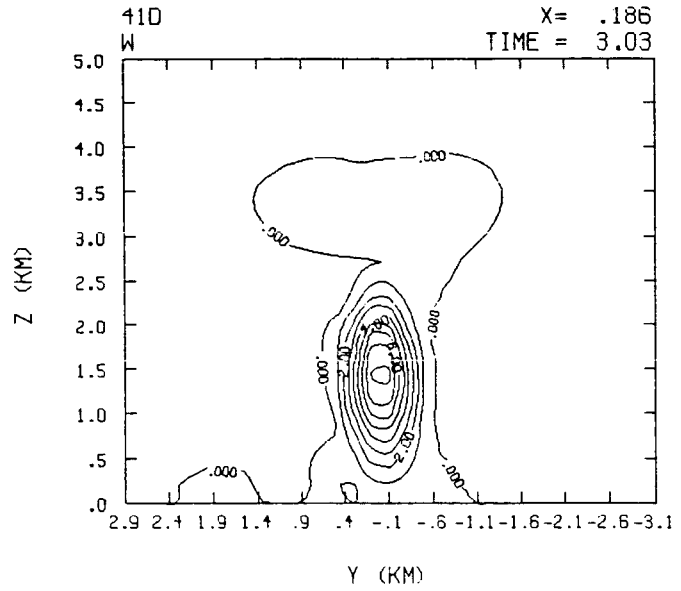

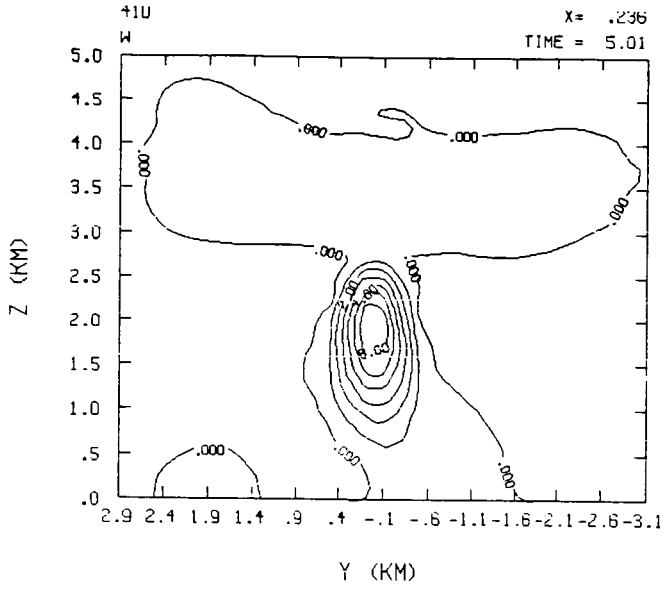

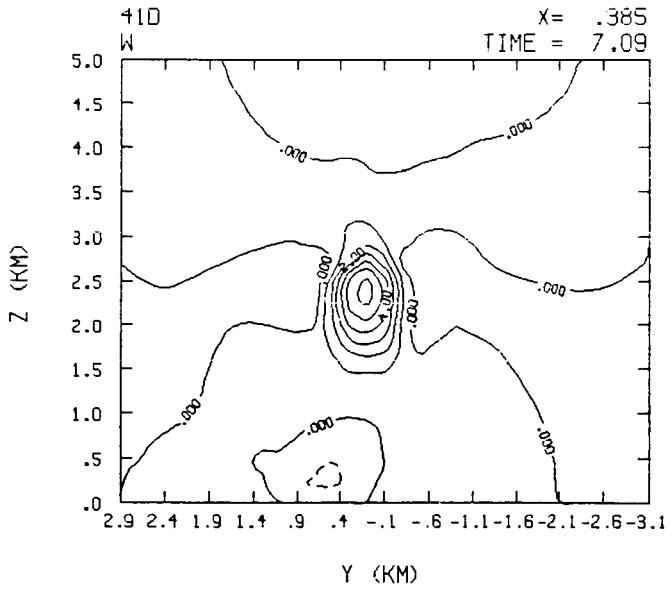

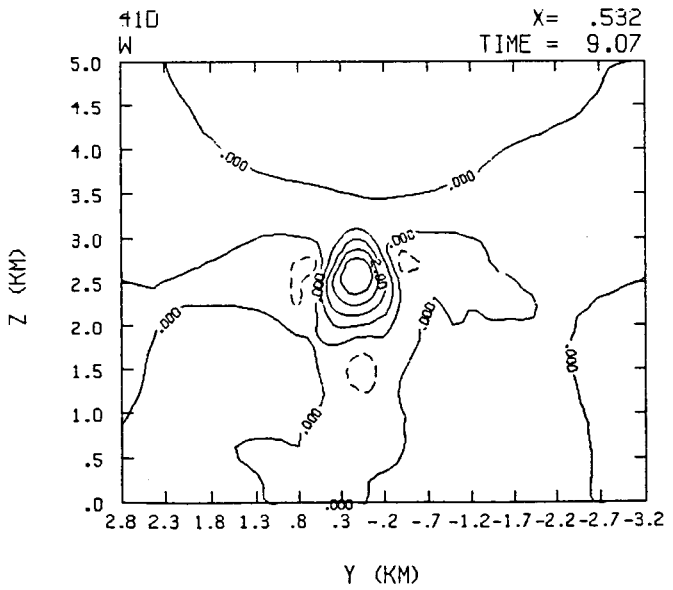

Figure 22. YZ cross section of vertical velocity for 3, 5, 7, and 9 minutes after model initialization for Mission 41D.

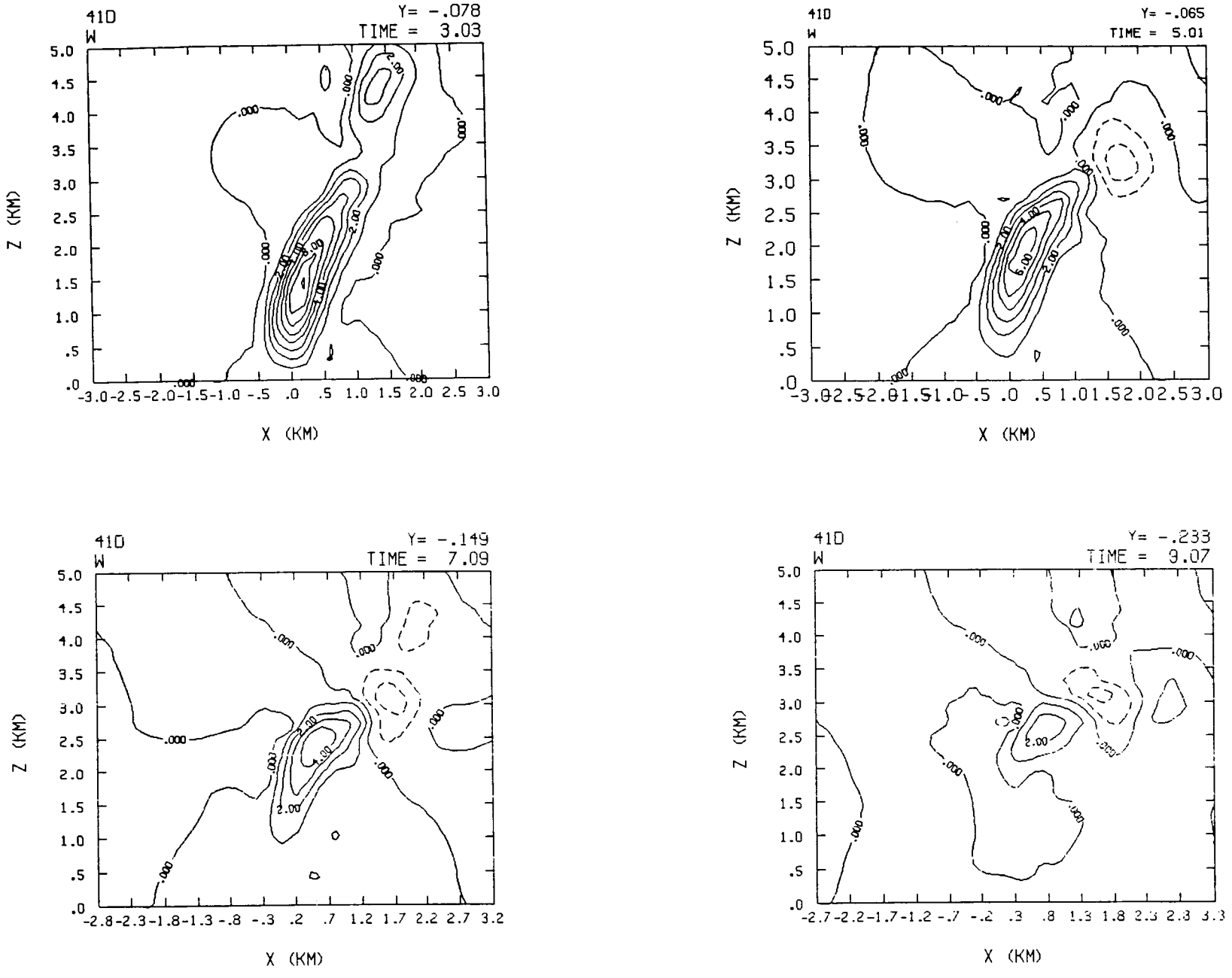

Figure 23. XZ cross section of vertical velocity for 3, 5, 7, and 9 minutes after model initialization for Mission 41D.

with the apparent break up of the vertical motion core at 9 minutes. However, the latter could also mean that we have not sliced through the main channel due to its high asymmetry. It is interesting, to note that the integrity of the vertical motion core seems to be higher in the yz cross section (Fig. 22) representing a slice in the north-south plane. Slices along the same azimuths as in Figures 22 and 23 are shown in Figures 24 and 25 for liquid water contours. The maximum value near the cloud top of 1.04 g kg^{-1} is shown at 9 min. The smoke field is shown in xz cross section in Figure 26. The high concentration near the ground is an artifact of the smoke having no mass or scavenging in the model. Notice how the concentration aloft is spread to the east in response to the atmospheric winds.

The change in height of average vertical motion, smoke, and liquid water are shown in Figure 27. Averages were computed for horizontal pancakes 200 m thick, and the vertical axis is divided by the maximum model cloud altitude, in this case 3.2 km. This is a convenient way of comparing relative maxima in these parameters for different cases. At nine minutes the average maximum liquid cloud water is near the top of the cloud whereas vertical motion peaks about 3/4 of the distance to the cloud top. The evolution of cloud volume in the model determined both from cloud water and smoke integrated through the model domain is shown in Figure 28. Cloud volumes were calculated from model results for these horizontal pancakes. The smoke volume continues to increase which is due in part to the way smoke was not allowed to deposit on the surface or be cleansed by liquid. The cloud volume computed from liquid water reaches a maximum at six minutes despite continued spreading at the top.

Figure 29 shows the results for the 9 minute time period. Both the smoke field and cloud water output are shown to have nearly the same shapes in vertical variation indicating that the dispersion of smoke or any aerosol

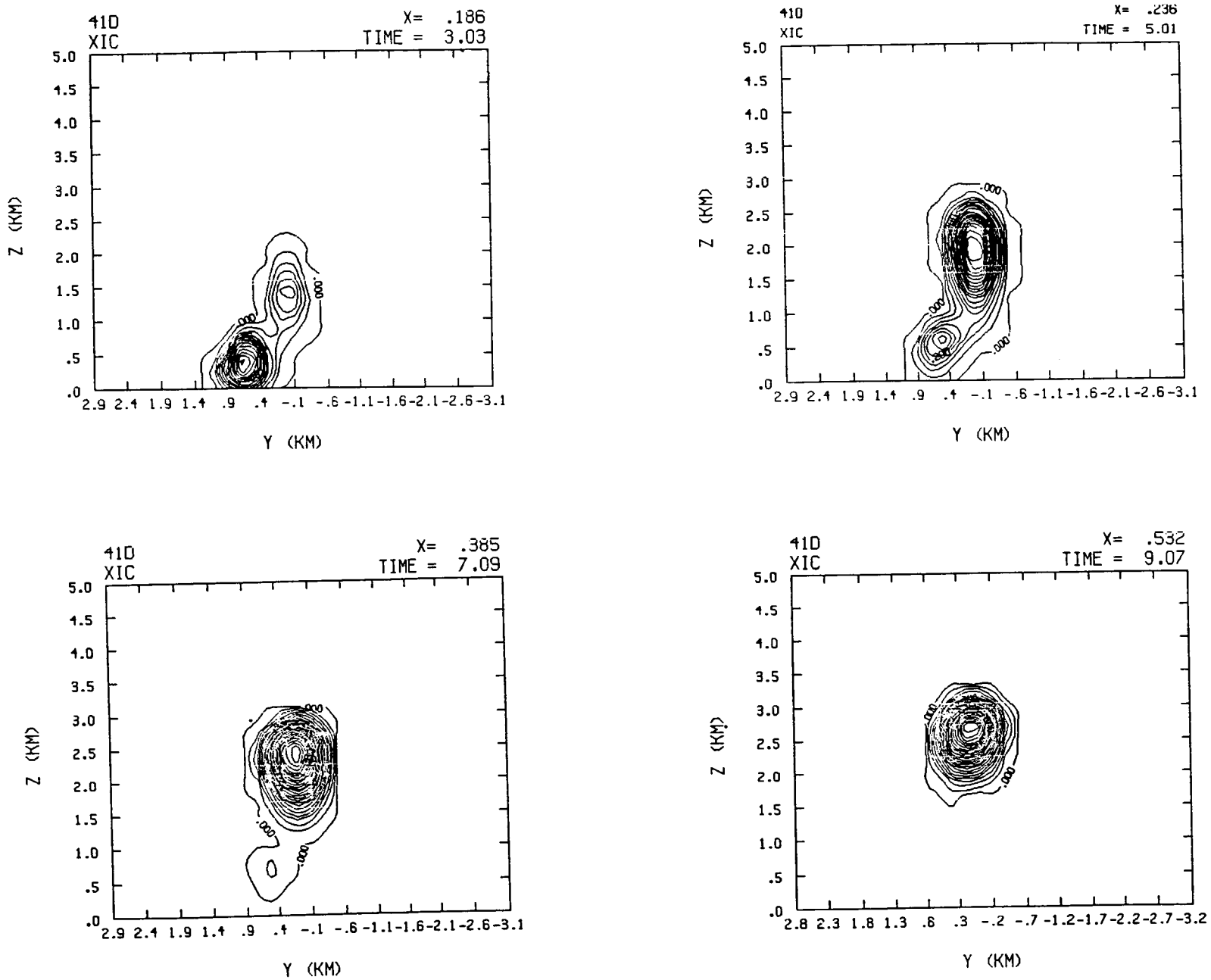

Figure 24. YZ cross section of liquid cloud water for 3, 5, 7, and 9 minutes after model initialization for Mission 41D.

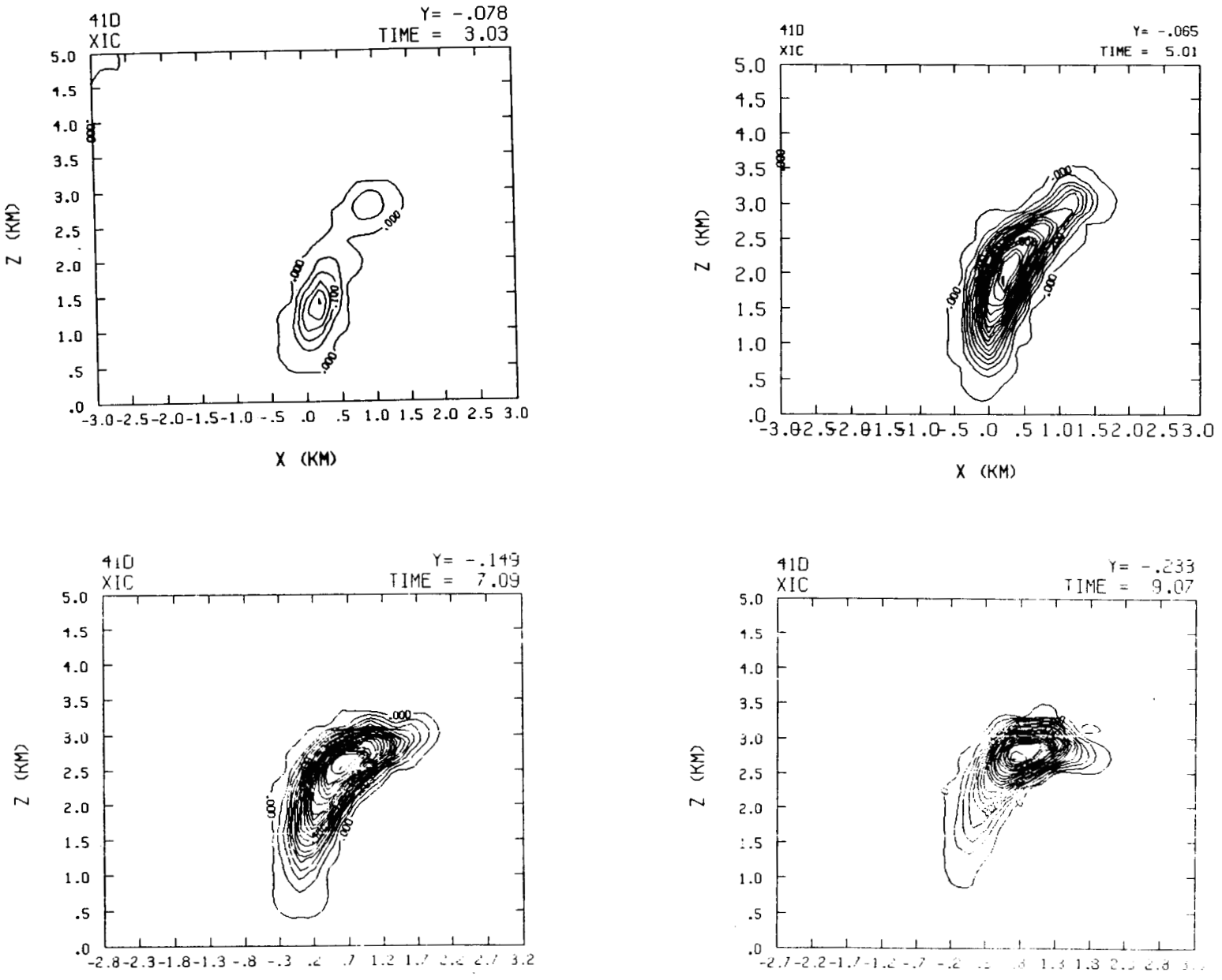

Figure 25. XZ cross section of liquid cloud water for 3, 5, 7 and 9 minutes after model initialization for Mission 41D.

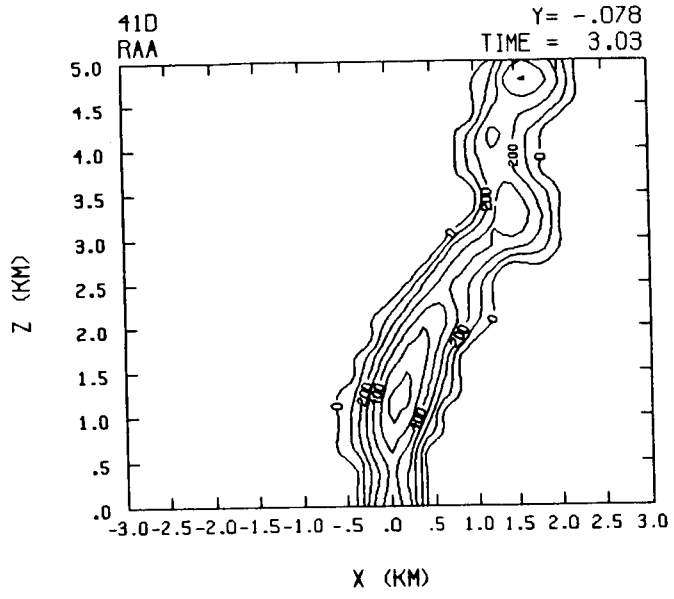

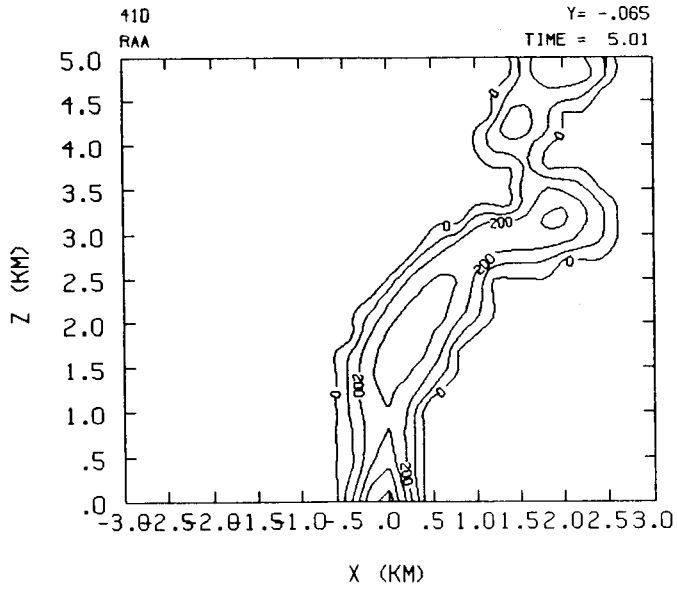

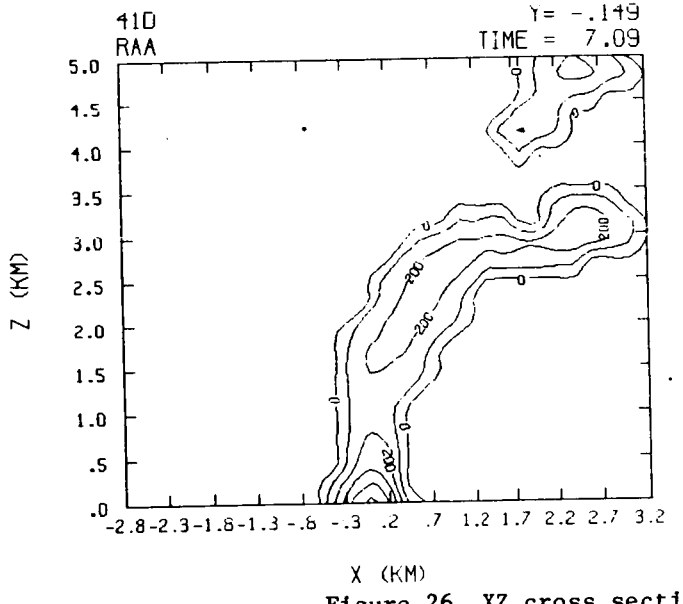

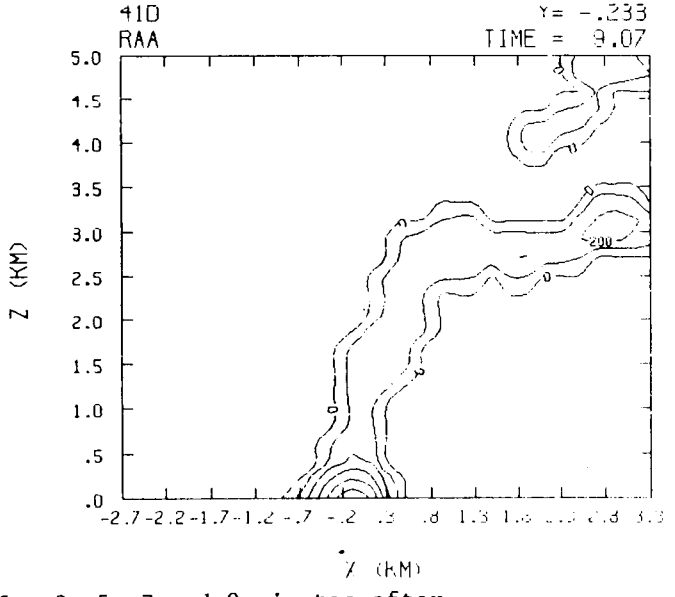

Figure 26. XZ cross section of smoke for 3, 5, 7 and 9 minutes after model initialization for Mission 41D.

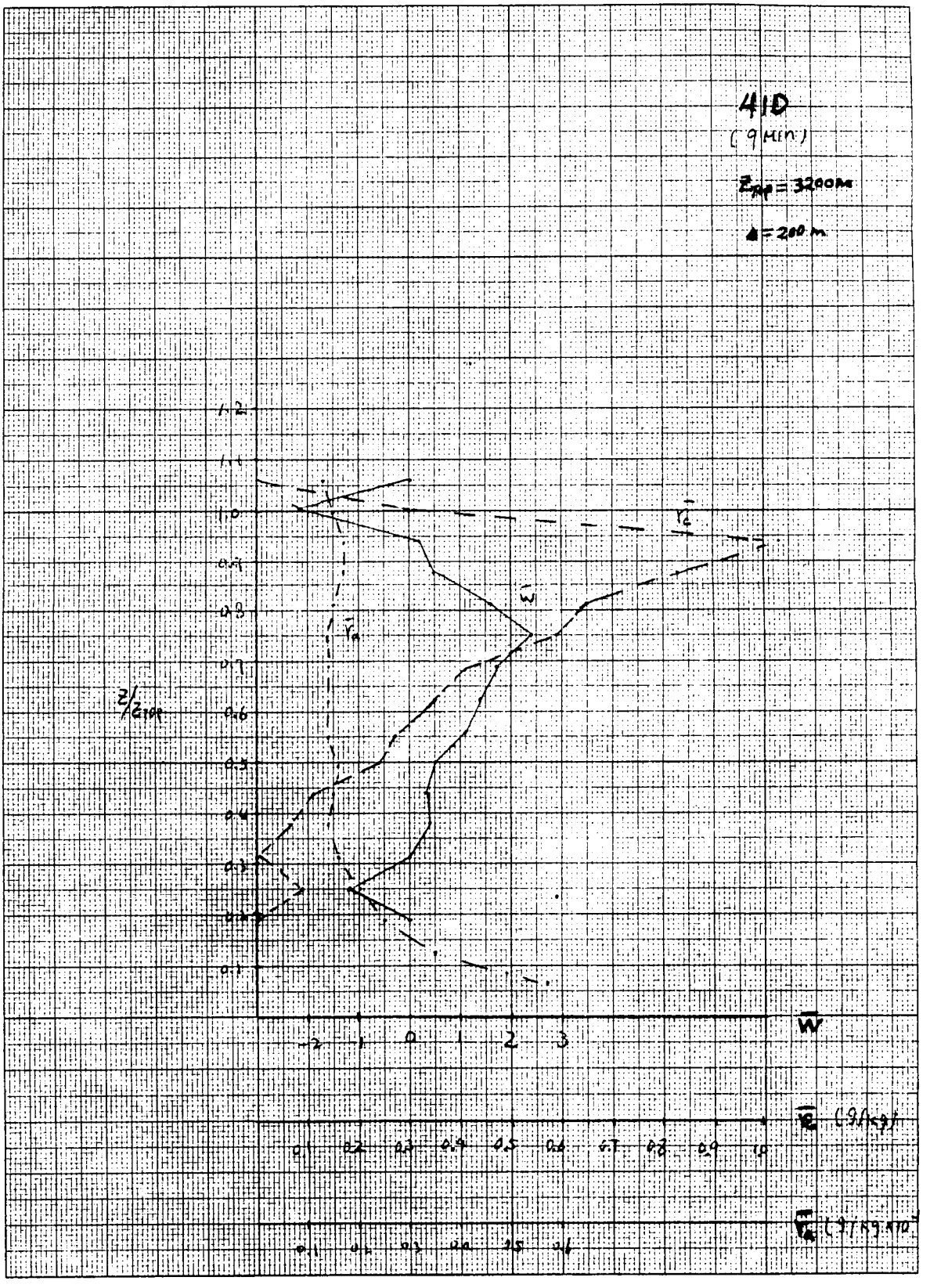

Figure 27.

ORIGINAL PAGE IS
OF POOR QUALITY

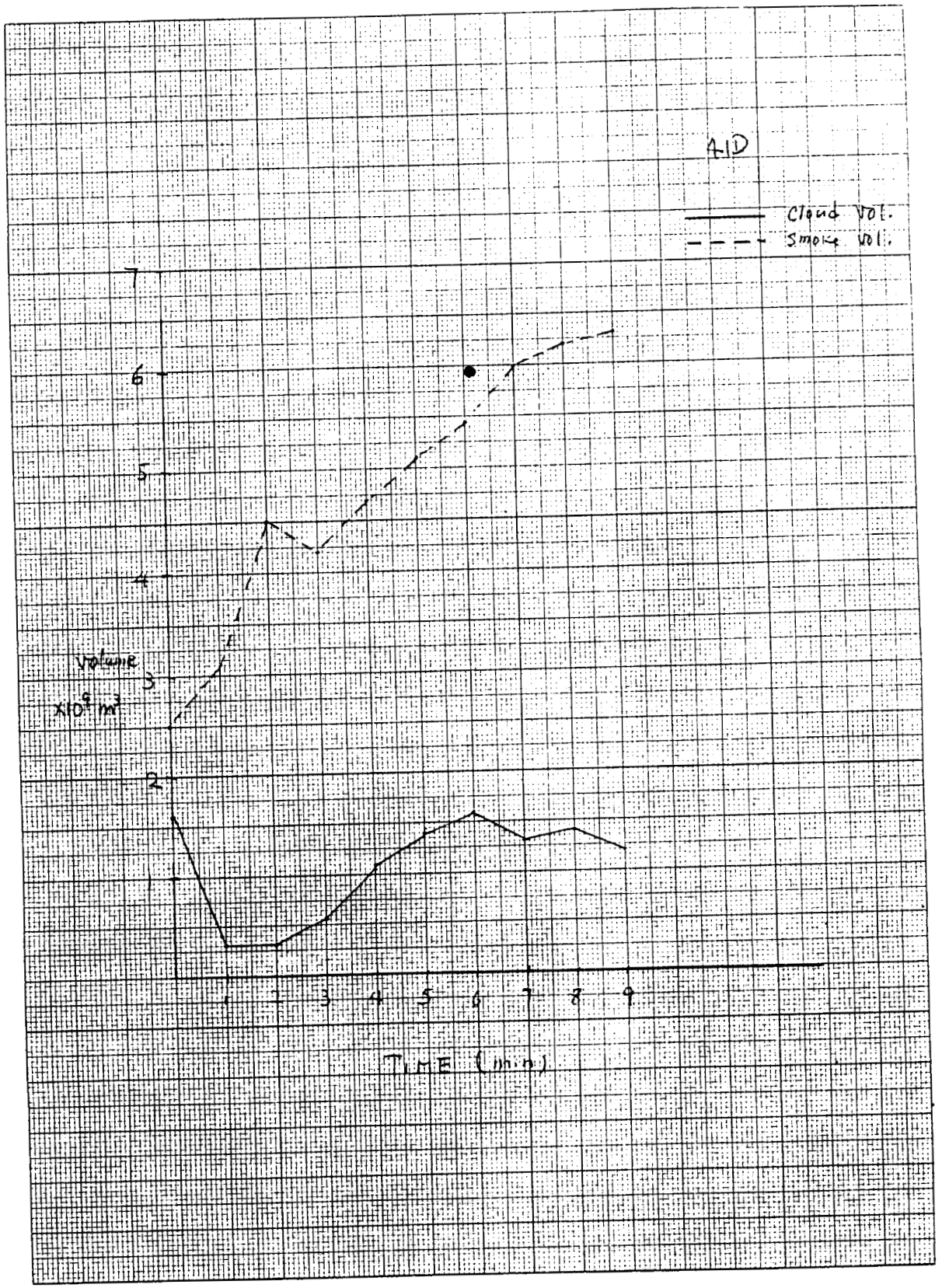

Figure 28.

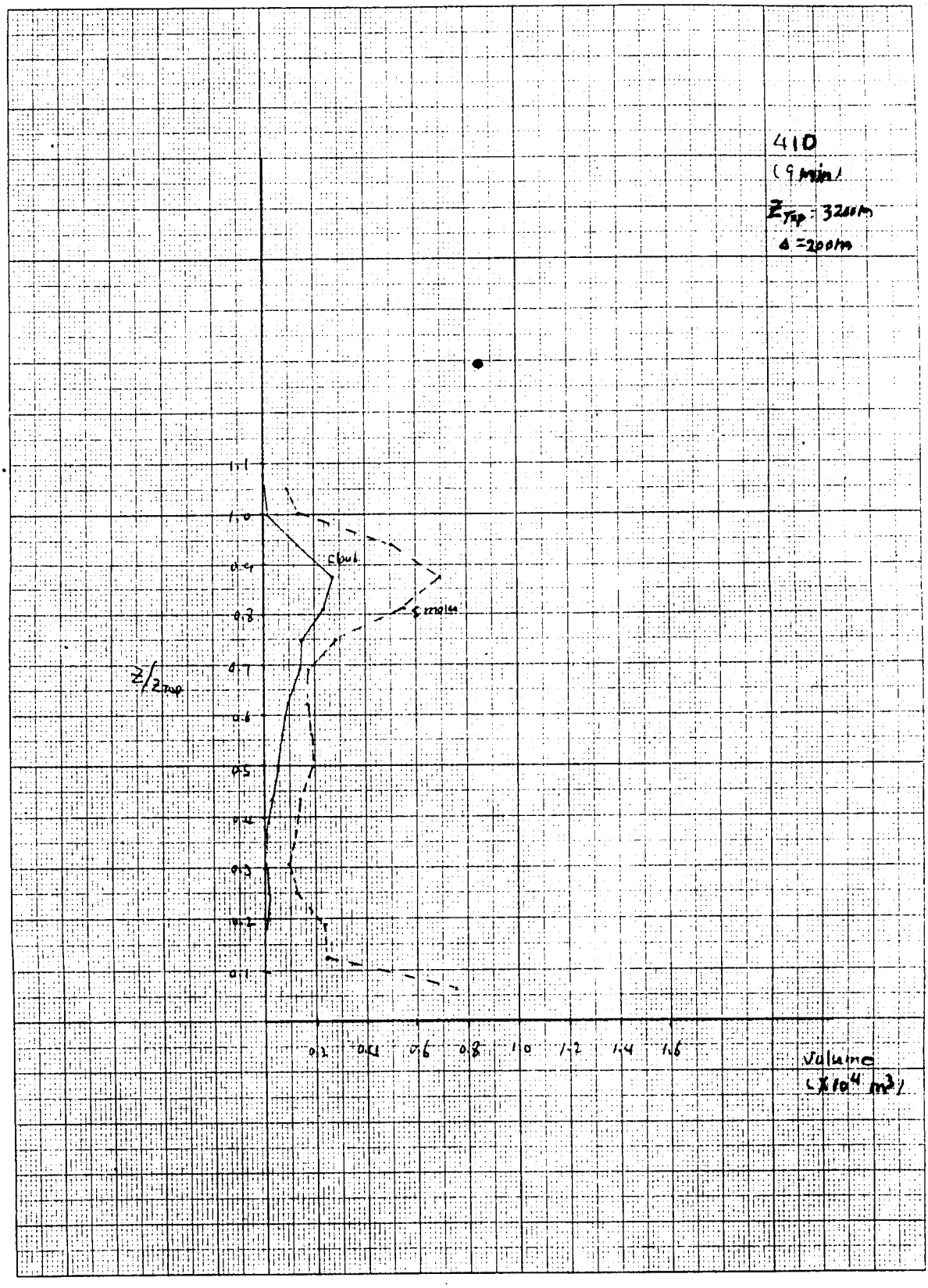

Figure 29.

(massless) tracer should be closely related to the convective cloud process. Similar vertical profiles of liquid water (Fig. 30) and smoke (Fig. 31) are shown for 3, 5, 7 and 9 minutes.

From this case it appears that the convective cloud system generated by the Shuttle exhaust rose from its own buoyancy and that from the condensation process in a moist unstable atmosphere. The vertical motion and liquid water content of the simulated cloud are consistent with values for a small natural cloud. Very little rain water was observed in this model cloud due to the convective process, and cloud growth ceased after 8 minutes (observed) and 9 minutes in the model. The cloud appears to grow from a series of convective impulses similar to plume rise theory but in a highly asymmetric fashion and with significant three-dimensional structure evident even in the rather coarse 200 m grid.

CASE UNS41D

The original case 41D contained a potentially unstable and moist atmospheric layer below 3 km and produced a substantial convective cloud which grew only to a little above this inversion altitude. Its vertical development was assumed to be capped by the inversion. Therefore, we modified the 41D sounding to substantially reduce the thermal inversion at the top (Fig. 32). The expectation was that cloud buoyancy would carry it higher into the troposphere. Such was not the case. After a nine minute simulation, the cloud rose to about the same height as unmodified case 41D. Figure 33 shows the vertical distributions of cloud water, smoke, and vertical velocity at 9 minutes into this simulation. There is less cloud water but stronger vertical velocity at the top of the cloud layer than in unmodified 41D. These results are consistent with a more rigorous entrainment process at the top of the

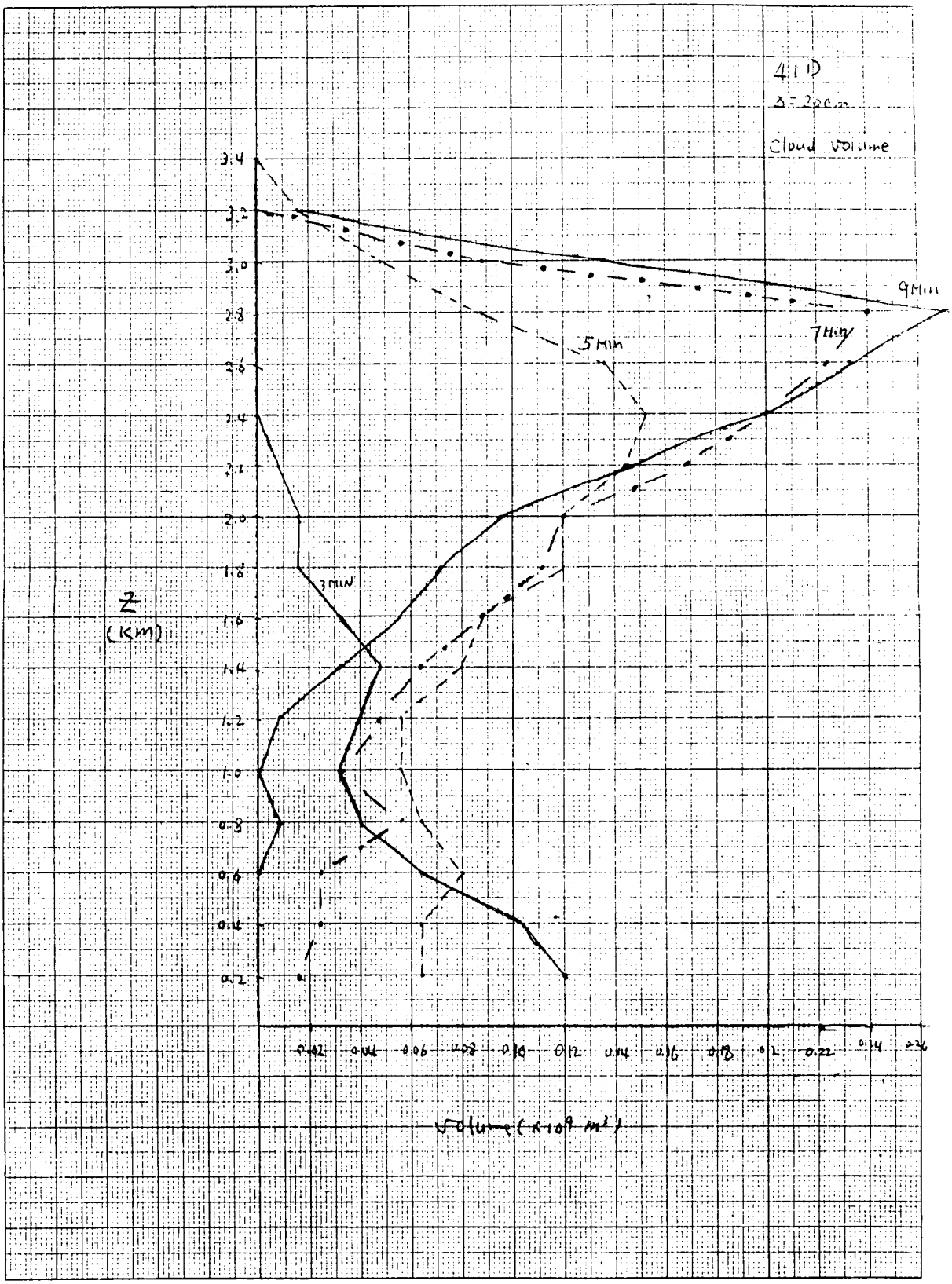

Figure 30.

ORIGINAL PAGE IS
OF POOR QUALITY

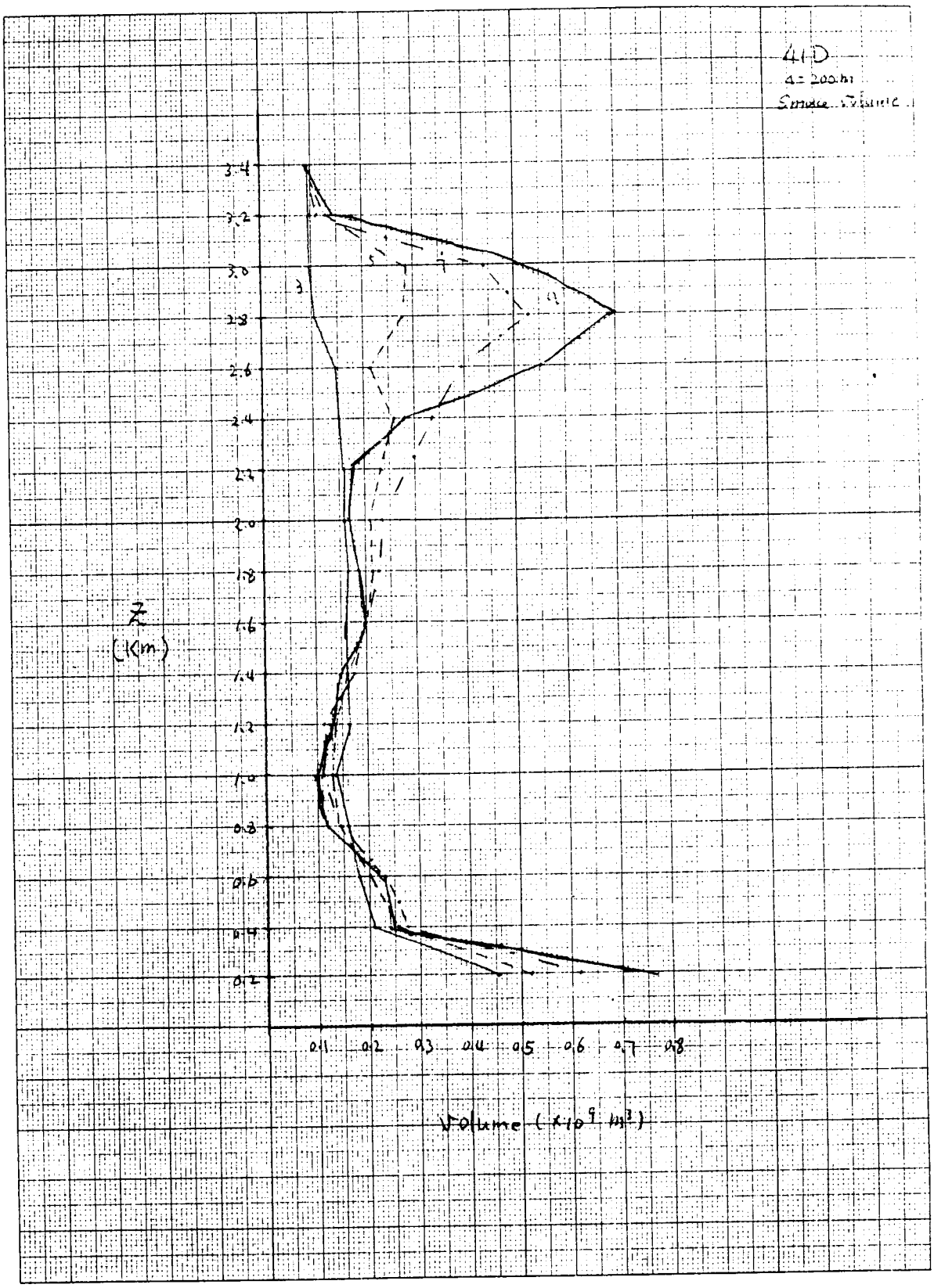

Figure 31.

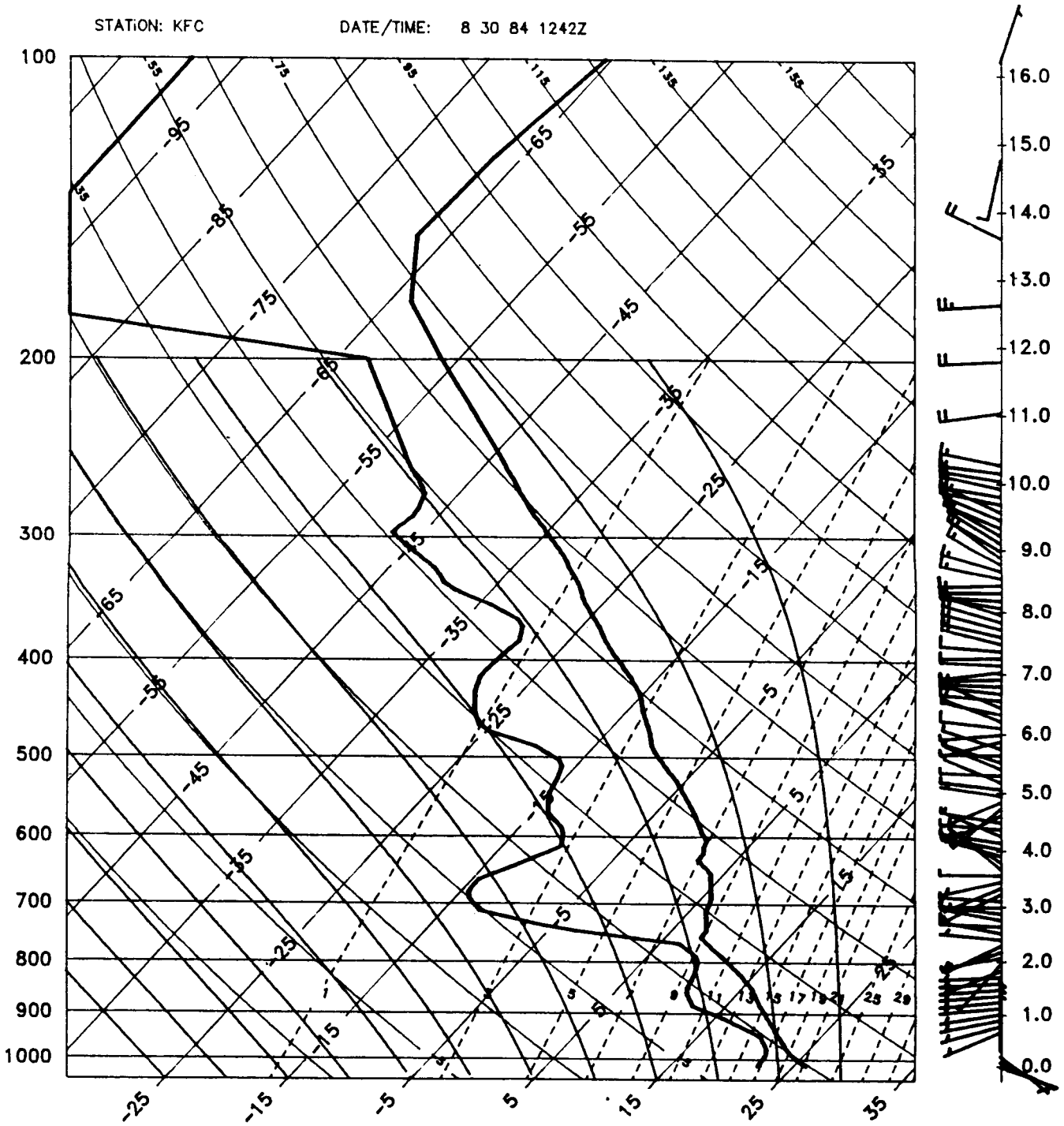

Figure 32. Upper air sounding for Mission 41D with modification of the vertical temperature distribution (called case 'UNS41D).

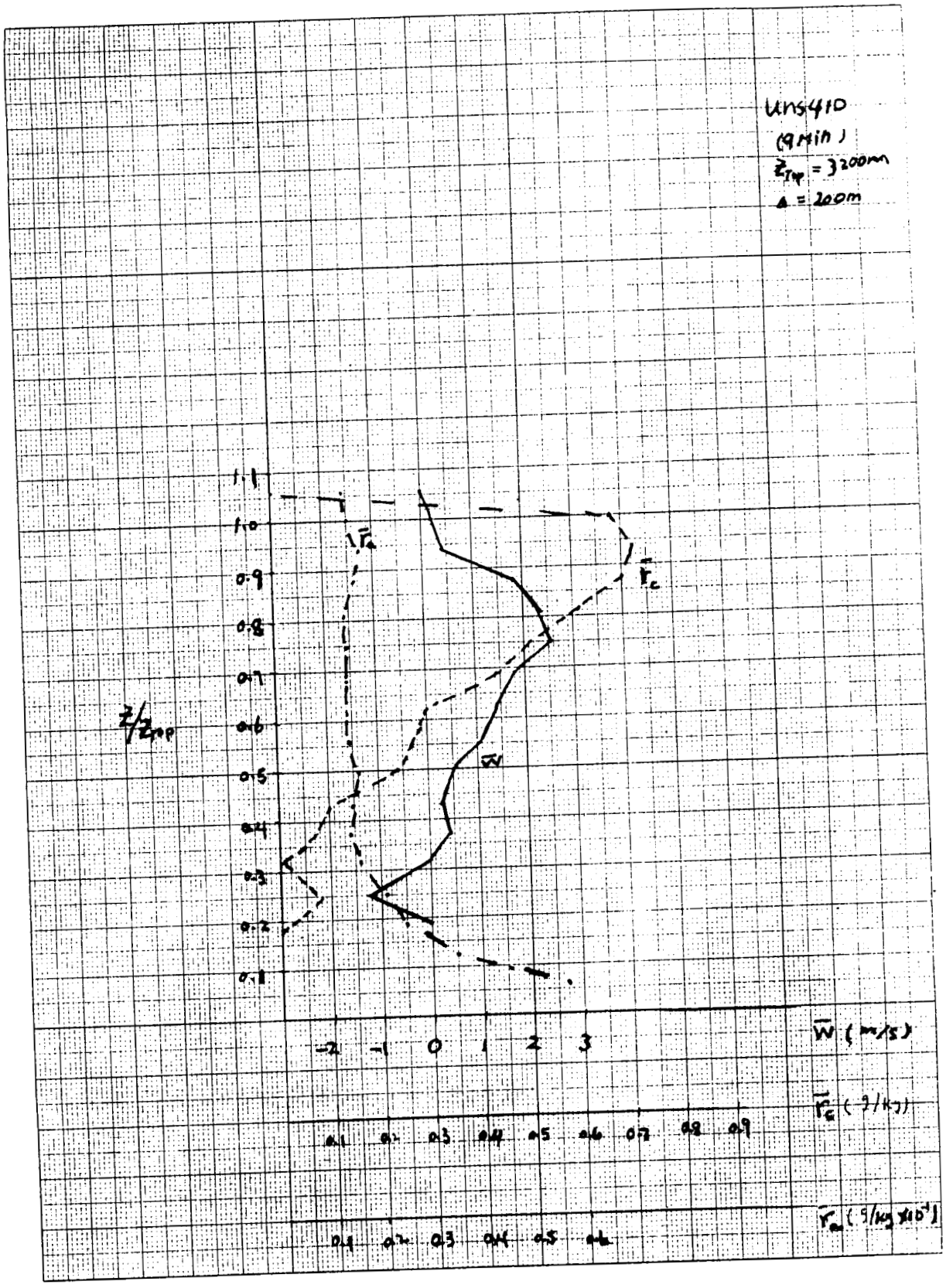

Figure 33.

cloud layer due to the weakening of the capping inversion. This process, which will dissipate the cloud more quickly, is similar to the entrainment process as reported by other investigators in the study of marine stratocumulus clouds [Chen and Cotton, 1983; Chen and Cotton, 1987; Deardorff, 1980; Randell, 1980]. Entrainment results from the evaporation of entrained dry air within the cloud layer, and its onset is determined by the jump in equivalent potential temperature (Θ_e) across the cloud top. When $\Delta\Theta_e$ $< 1^o$ K, across the inversion, rapid entrainment can occur at the cloud top. Θ_e is the equivalent potential temperature. Figure 34 represents the same plot except for 300 m resolution. It appears that the reduction in resolution can increase the intensity of the entrainment. Therefore, the cloud would be expected to dissipate faster in this coarse resolution case.

CASE MOS41D

This was a further modification of the 41D sounding where not only was the inversion weakened the same as UNS41D, but moisture was added near the base of the inversion (Fig. 35). Results of this simulation are presented in Figure 36. Note that there is more cloud water remaining but the average vertical velocity decreased from a few cm sec^{-1} upward to 1.0 m sec^{-1} downward at the top of the liquid water cloud. Maximum vertical velocity was also less reaching only 1.0 m sec^{-1} as opposed to 2.5 m sec^{-1} for UNS41D. The extra environmental moisture reduces the moisture gradient near the cloud top. Therefore, less intense entrainment should result. More liquid cloud water is a logical consequence. Furthermore, more rain was produced which could explain the slight reduction in vertical velocity.

Figures 37 and 38 are depictions of liquid cloud water for cases UNS41D and MOS41D respectively. The integration time for UNS41D was extended to 12

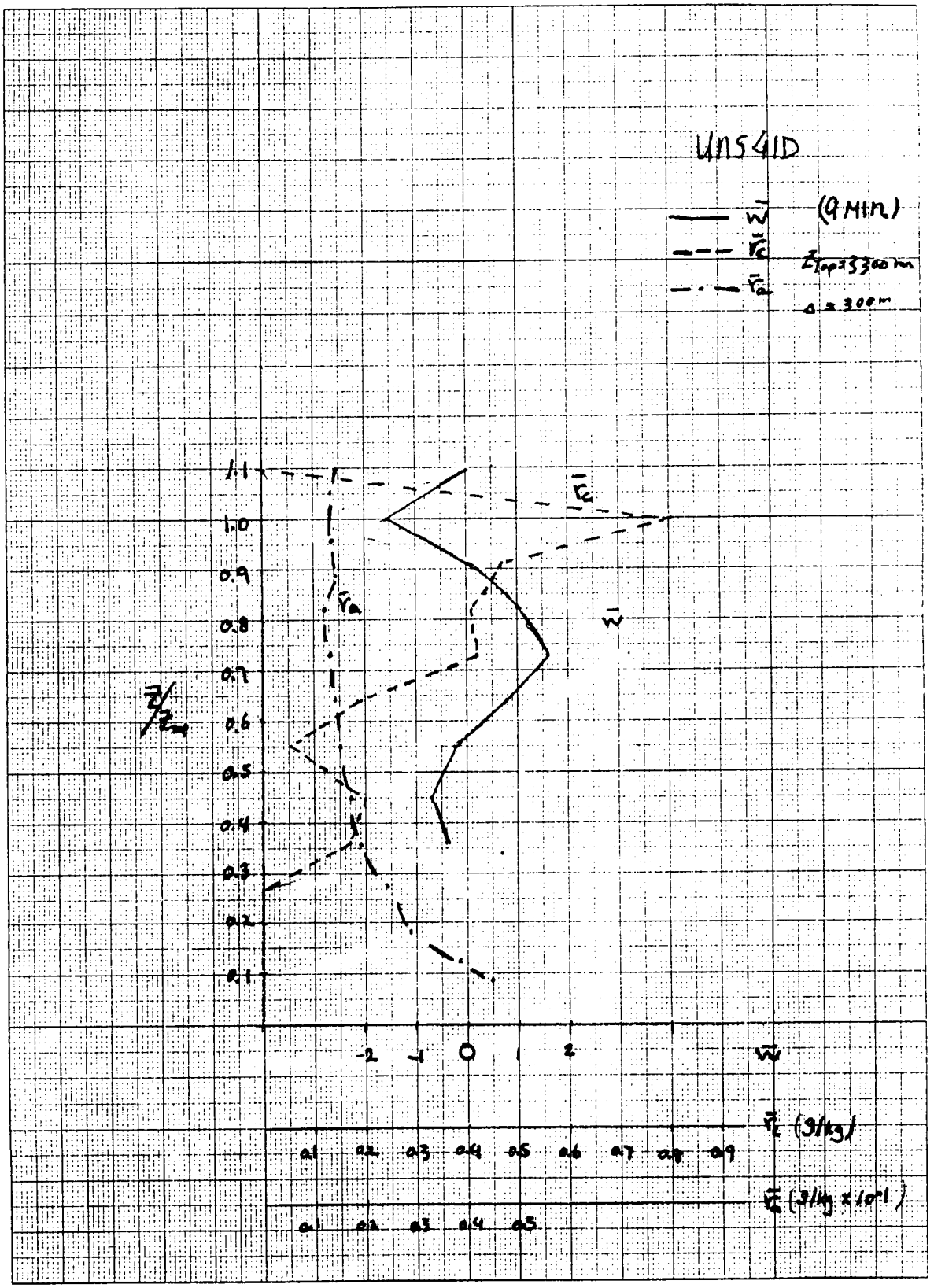

Figure 34.

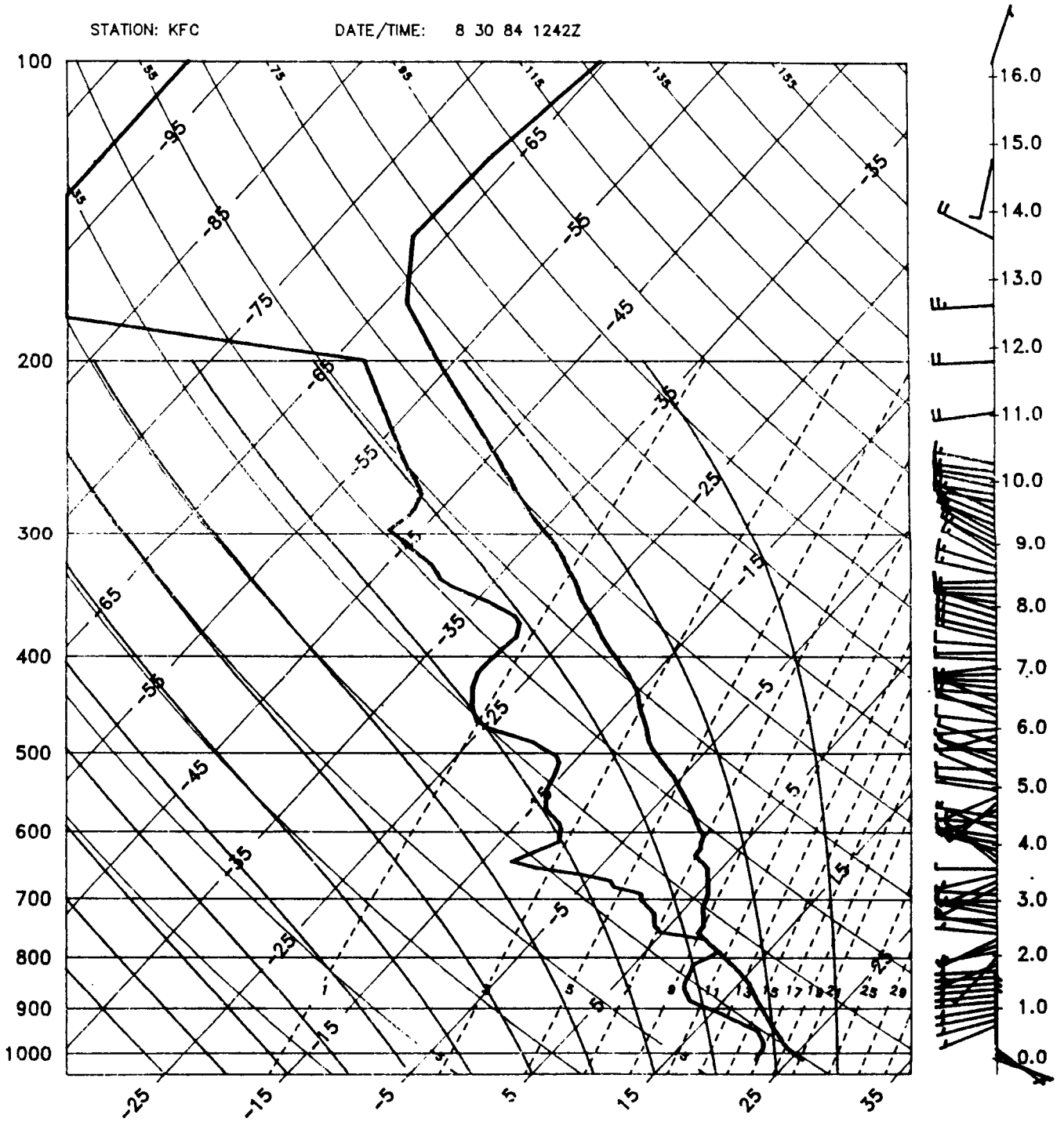

Figure 35. Upper air sounding for Mission 41D with modification of both vertical temperature and moisture distributions (case MOS41D).

Figure 36. Vertical distribution of average vertical motion, cloud water and smoke 9 minutes after initialization for case MOS41D.

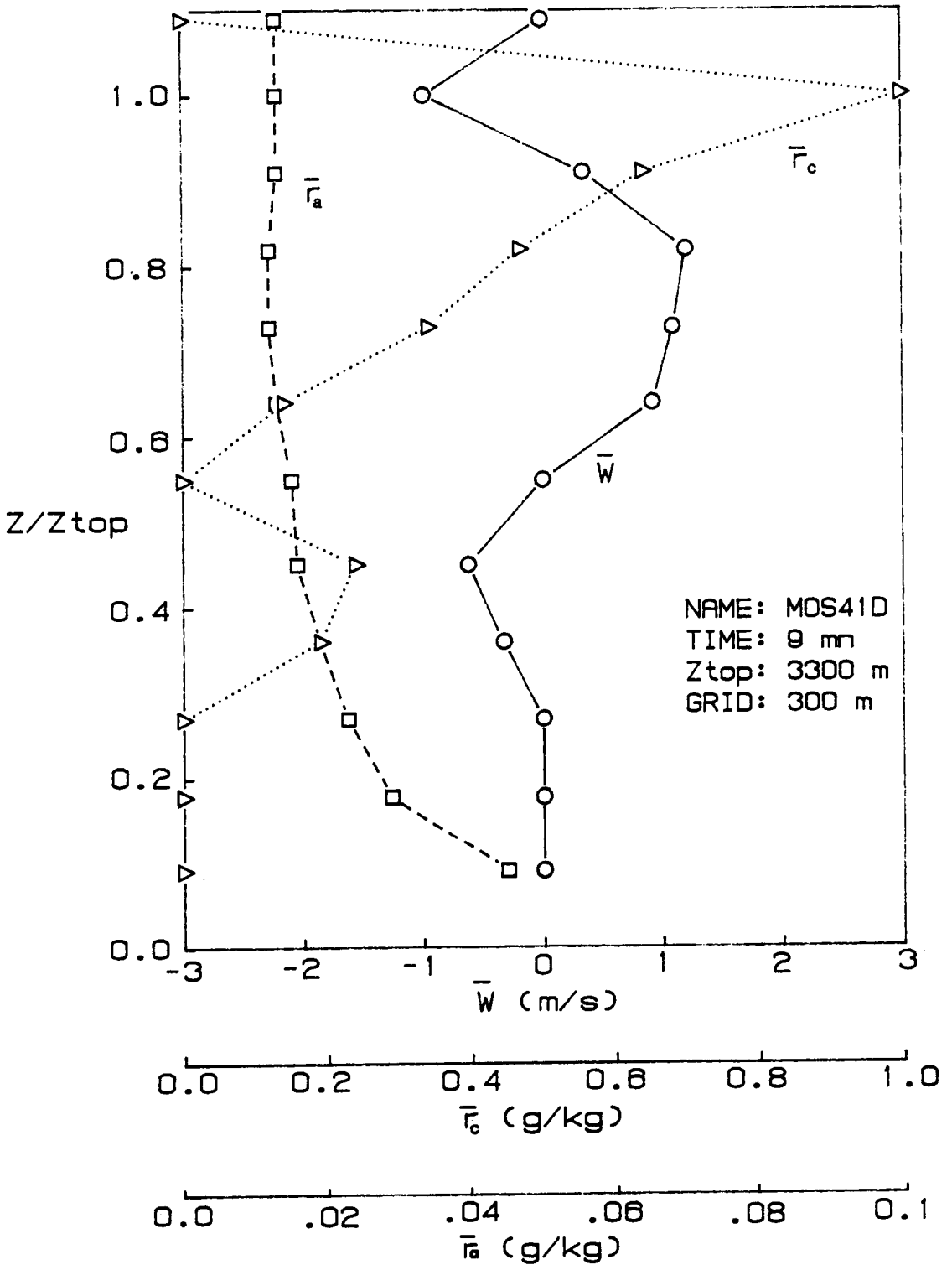

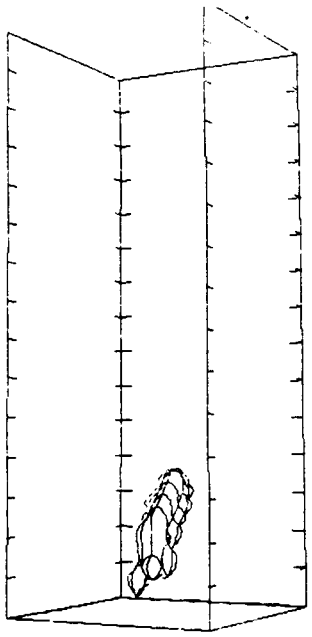

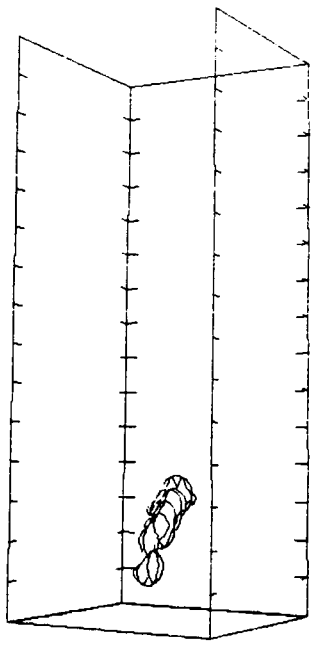

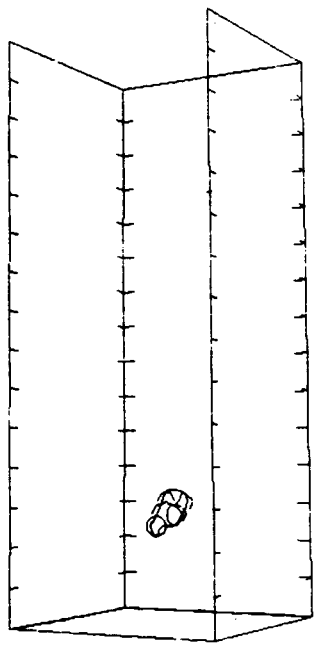

Figure 37. Model cloud water looking northeast at 7, 9 and 12 minutes after initialization for case UNS41D.

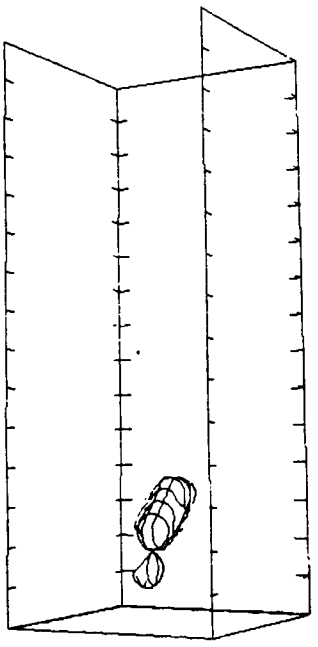

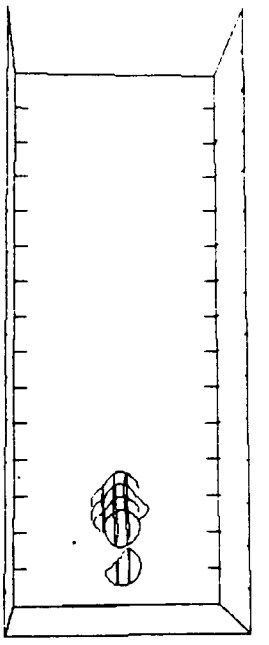

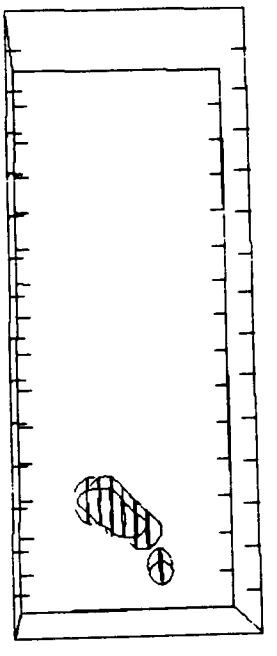

Figure 38. Model cloud water at 9 minutes looking northeast (top left) east (top right) and south (bottom) for case MOS41D.

minutes and Figure 37 shows the cloud evolution. This cloud begins to dissipate as early as 7 minutes into the simulation. For the case with added moisture and weaker inversion, we can see in Figure 38 that the cloud is slightly wider at the top at 9 minutes. Added environmental moisture adds to the cloud water content and slightly reduces the entrainment erosion, but this is compensated by the increase due to the reduced strength of the temperature inversion. The net result was a cloud which could not grow any higher than before.

CASES UNS AND MASS

These cases are for atmospheric conditions known to have produced thunderstorms. The former, UNS, is an actual sounding observed at Kennedy Space Center on August 30, 1982 at 0115 GMT. The MASS case is for a sounding predicted by a mesoscale model valid at 0300 GMT the same day [Kaplan, et al., 1982], the same time as an observed thunderstorm to the northeast of Kennedy Space Center. The UNS sounding is shown in Figure 39. There is no discernible capping inversion or dry layer as in the 41D sounding, but there is a wind direction change from predominately westerly winds about 5 to 10 m sec^{-1} below 2 km to easterly winds about the same magnitude above 2 km. There is a dew point depression (temperature minus dew point) of about 6k throughout the lower 4 km of the atmosphere. The MASS sounding (Figure 40) is nearer the time of observed thunderstorms and it has about a 4 degree dew point depression. The winds are westerly throughout the lower 5 km of the atmosphere and the temperature is about 3 degrees colder below 500 m than in the observed sounding.

Results of the simulations in the form of east-west (xz) and north-south (xz) cross sections are shown in Figures 41 and 42 for UNS and MASS

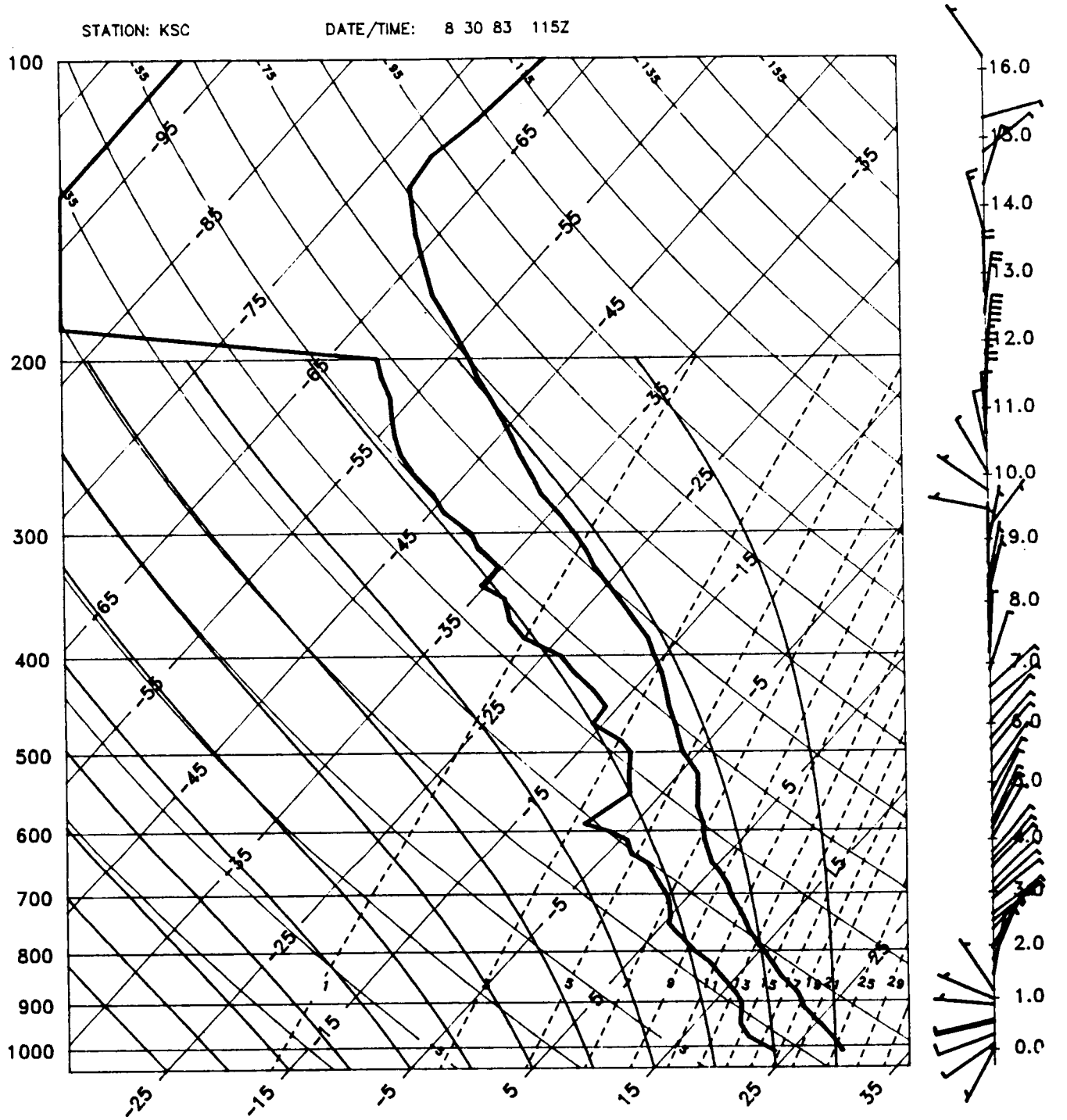

Figure 39. Observed upper-air sounding for Kennedy Space Center, FL August 30, 1982 01156Mt (case UNS).

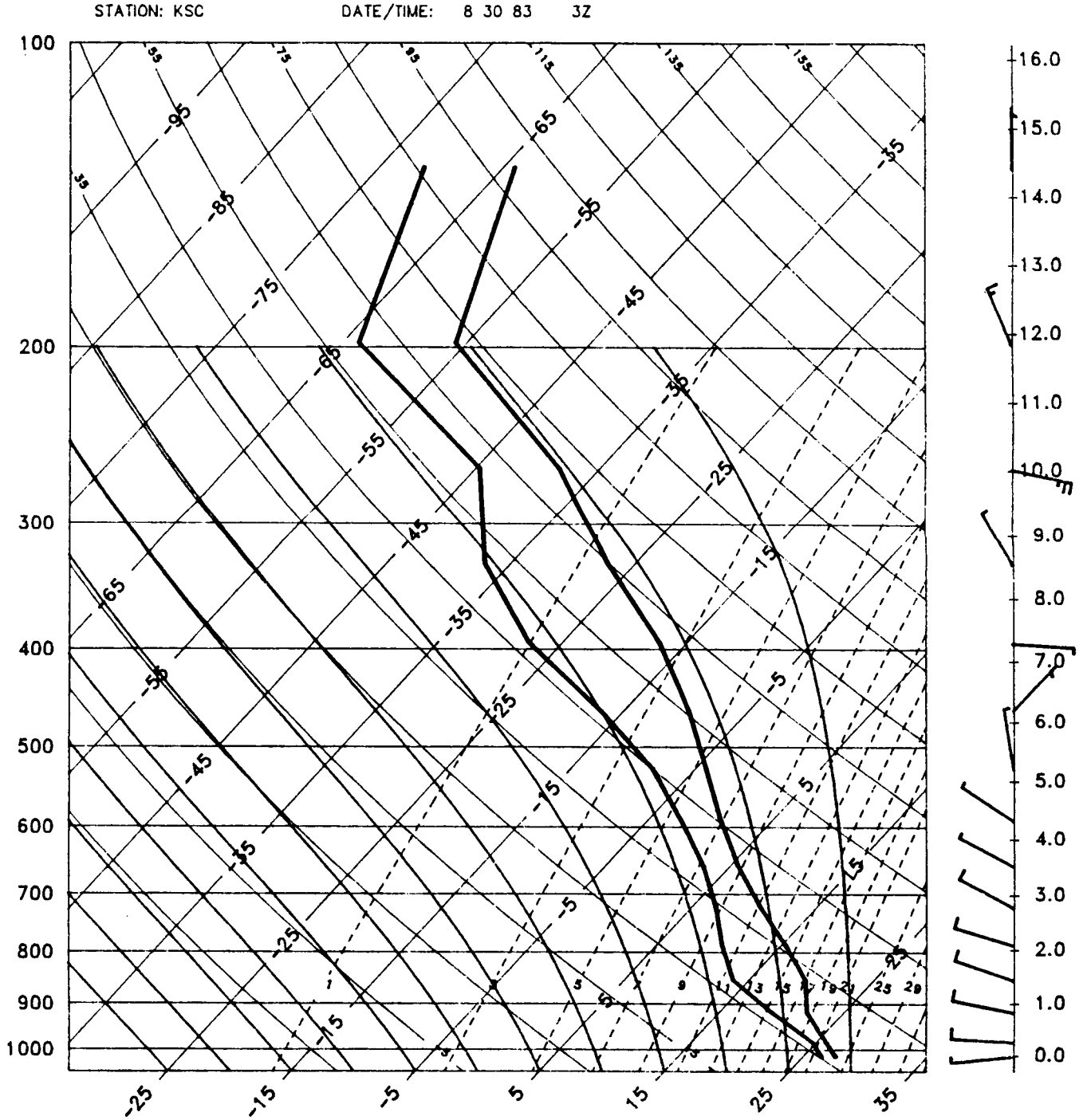

Figure 40. Upper-air sounding generated by a mesoscale model (case MASS).

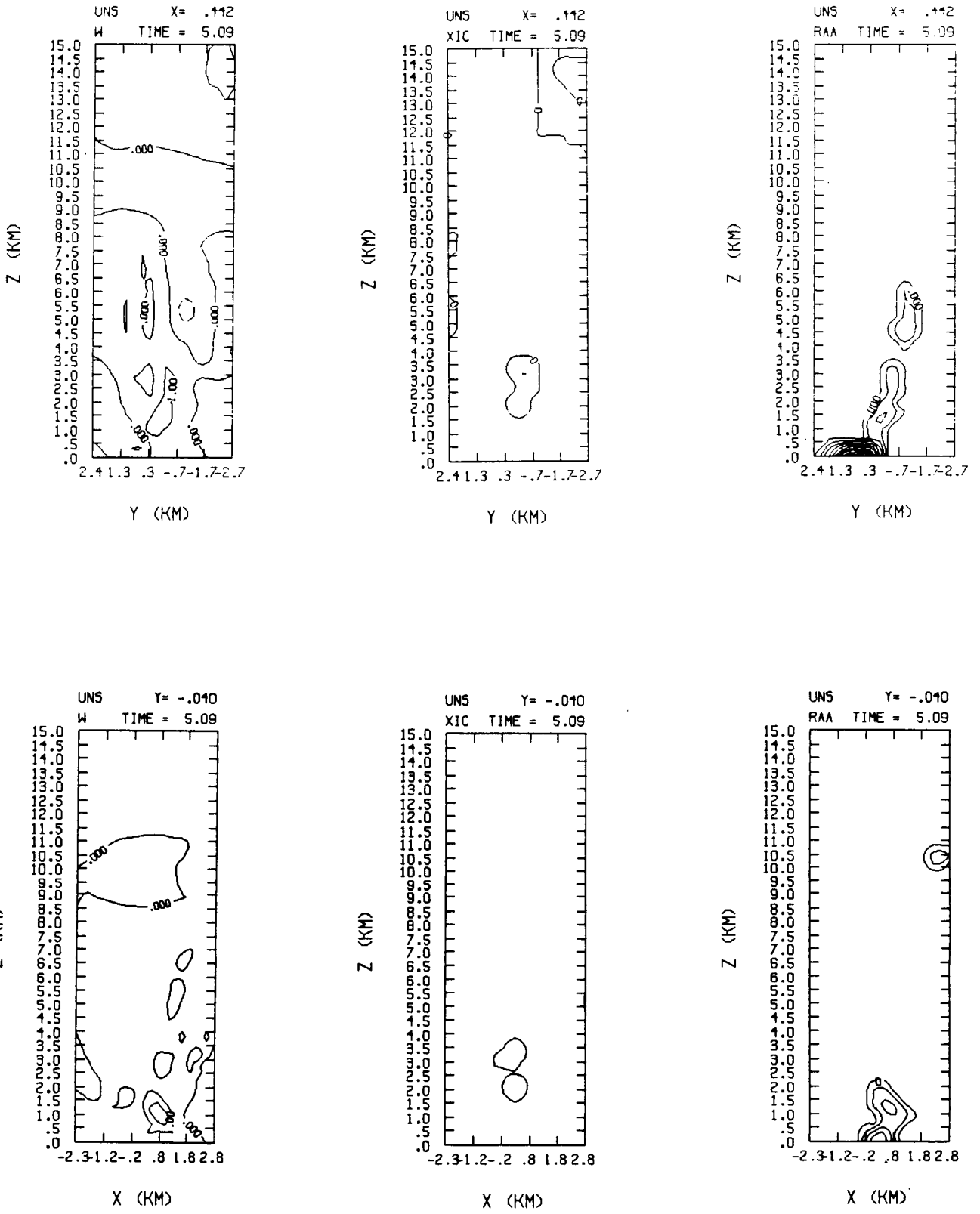

Figure 41. YZ (top) and XZ (bottom) cross sections for vertical motion, cloud water and smoke 5 minutes after initialization for the UNS sounding.

ORIGINAL PAGE IS
OF POOR QUALITY

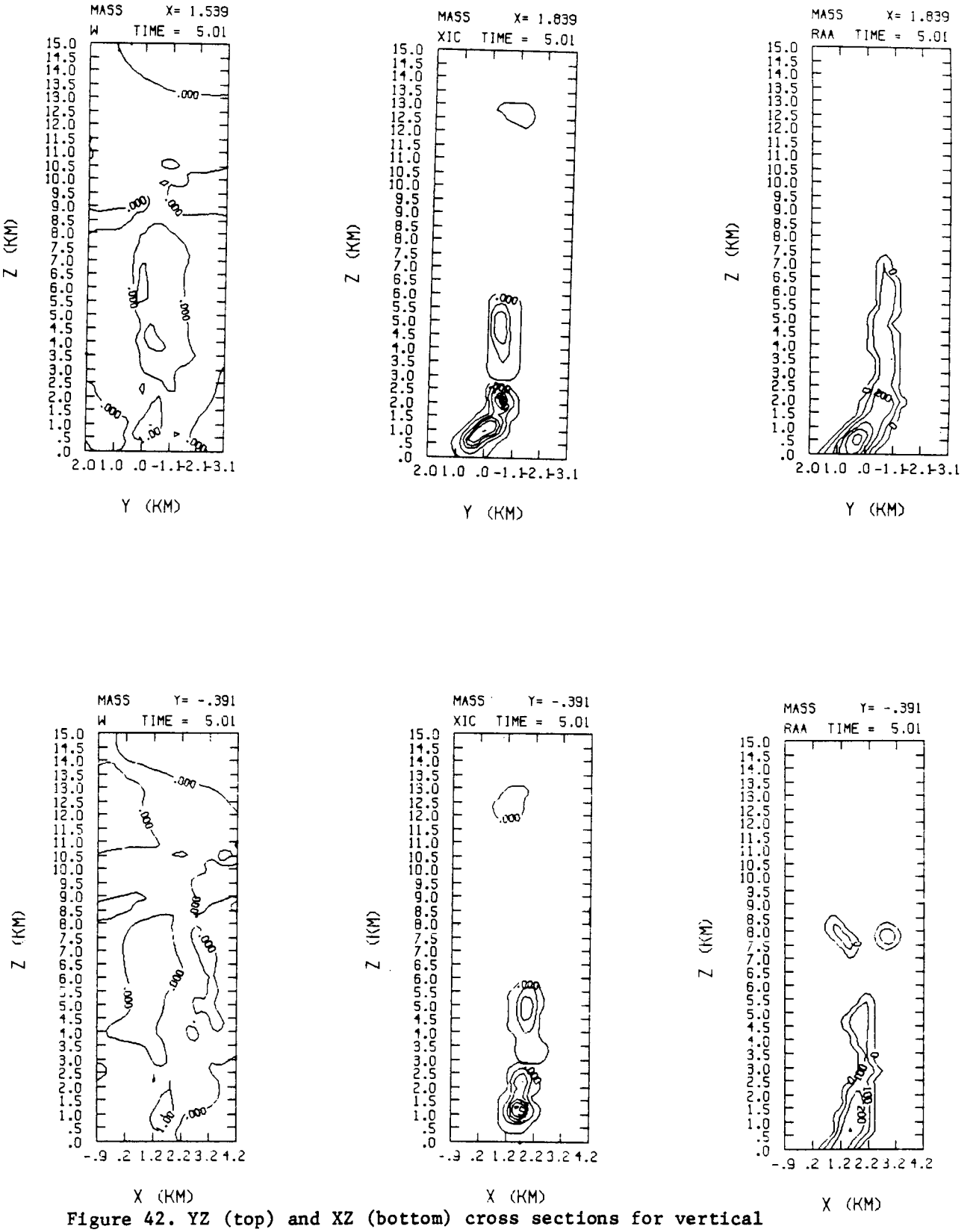

Figure 42. YZ (top) and XZ (bottom) cross sections for vertical motion, cloud water and smoke 5 minutes after initialization for the MASS sounding.

respectively. Both simulations show a very weak vertical velocity (1-2 m sec^{-1}) compared to the 41D case where 8 m sec^{-1} was indicated. Other evidence of weaker convection is the very low liquid water content for case UNS. There is not enough atmospheric moisture in the low levels to sustain a significant natural cloud at 5 minutes into the simulation. The perspective plots in Figure 43 for UNS show that the small liquid water cloud (left) has just about lost its low-level portion. The smoke field in the northeast perspective plot (right of Figure 43) shows the response to relatively stronger westerly winds at about 7 km.

On the other hand, the simulation for the MASS case with its greater amount of available environmental moisture indicates liquid cloud up to about 6.0 km, but the portion above 2.5 km appears to be the residual from a short-lived column cloud. The perspective plots in Figure 44 show the evolution of the cloud water between 5 and 9 min. The top (column) part of the cloud dissipates completely after 5 minutes. The entrainment process discussed earlier is again very active and effective in eroding the cloud. Plots of the vertical distribution of domain averaged quantities are shown in Figure 45 for UNS and Figure 46 for MASS. The former had an assumed top of the ground cloud at 3300 m while the latter had a top of 2400 m. Again, the added moisture in the MASS atmosphere produced more liquid but UNS had a stronger upward vertical motion field. It seems that this cloud is the more convective of the two because of the stronger vertical motion in the upper part of the UNS cloud. Given the addition of the same amount of low level heat and moisture from the rocket exhausts to the lower atmosphere, the UNS atmosphere has a steeper lapse rate therefore greater instability than the MASS case.

In no case did a cloud with organized thunderstorm-type convection develop. Although a very unstable low level atmosphere might produce a cloud

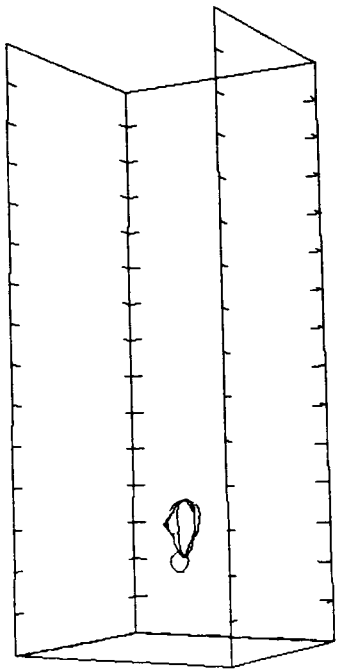

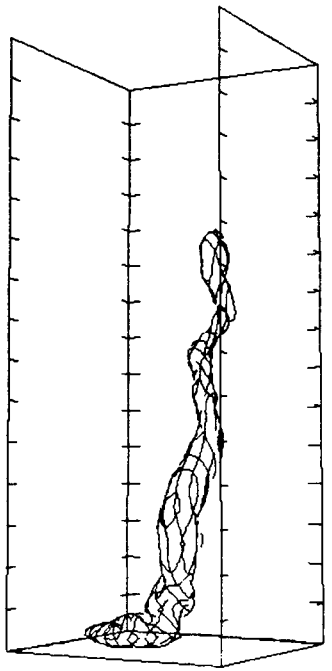

Figure 43. Model cloud water (left) and smoke (right) for the UNS sounding at 5 minutes after initialization looking northeast.

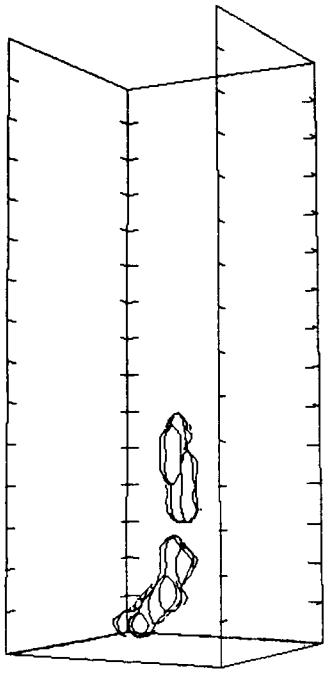

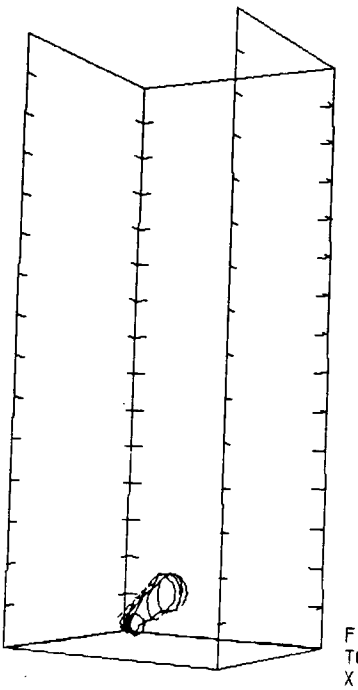

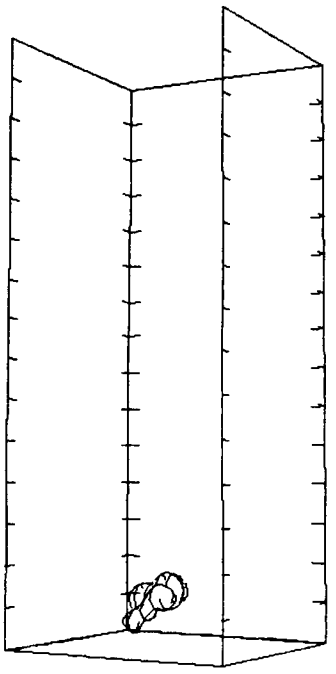

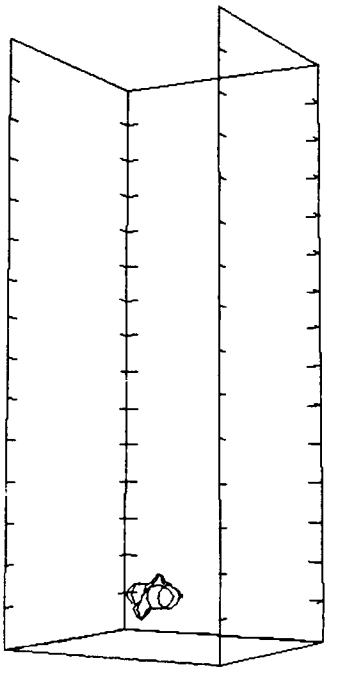

Figure 44. Model cloud water for the MASS sounding at 5, 7, 8 and 9 minutes after initialization looking northeast.

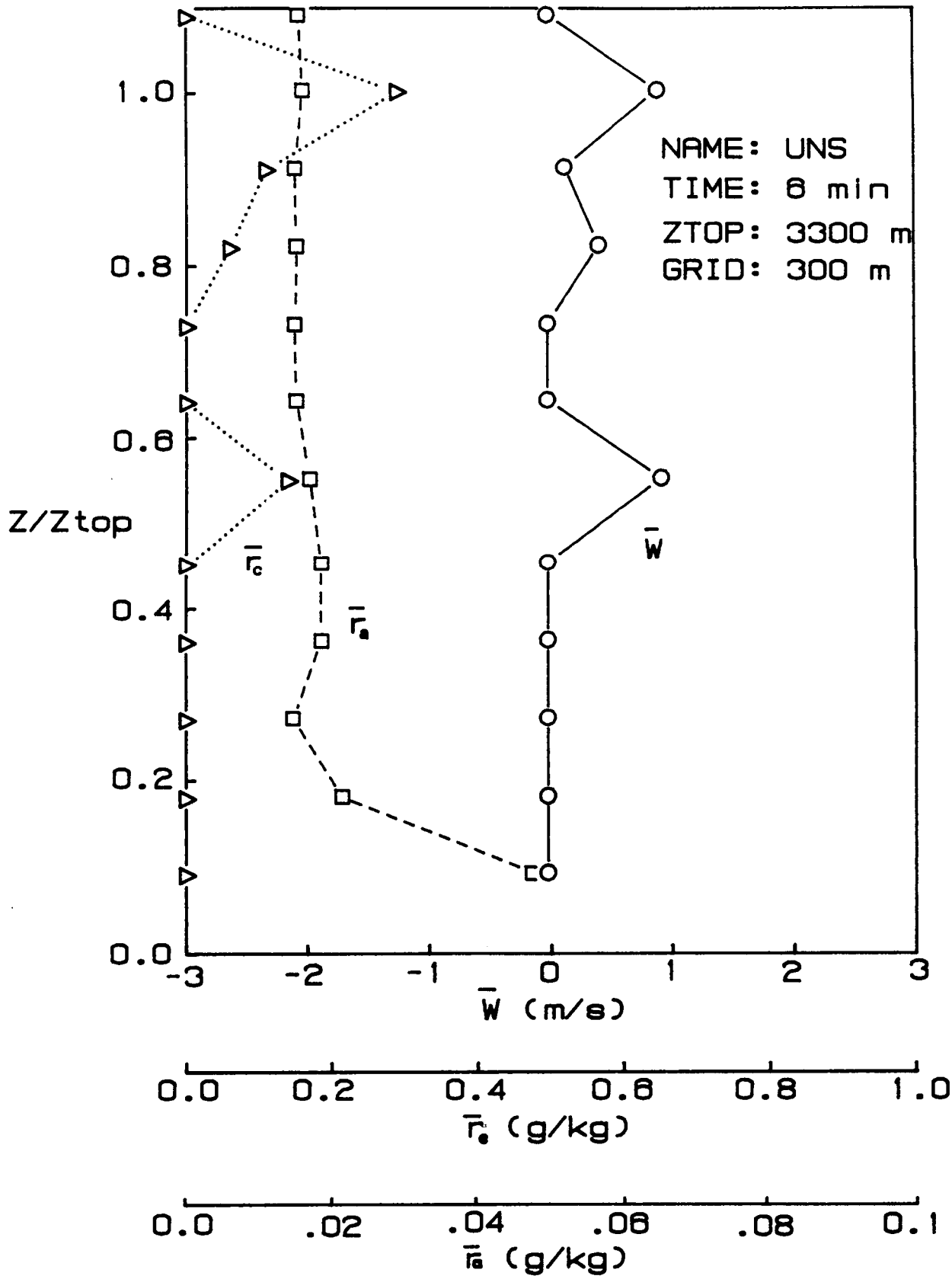

Figure 45. Vertical distribution of average vertical motion, cloud water and smoke 6 minutes after initialization for the UNS sounding.

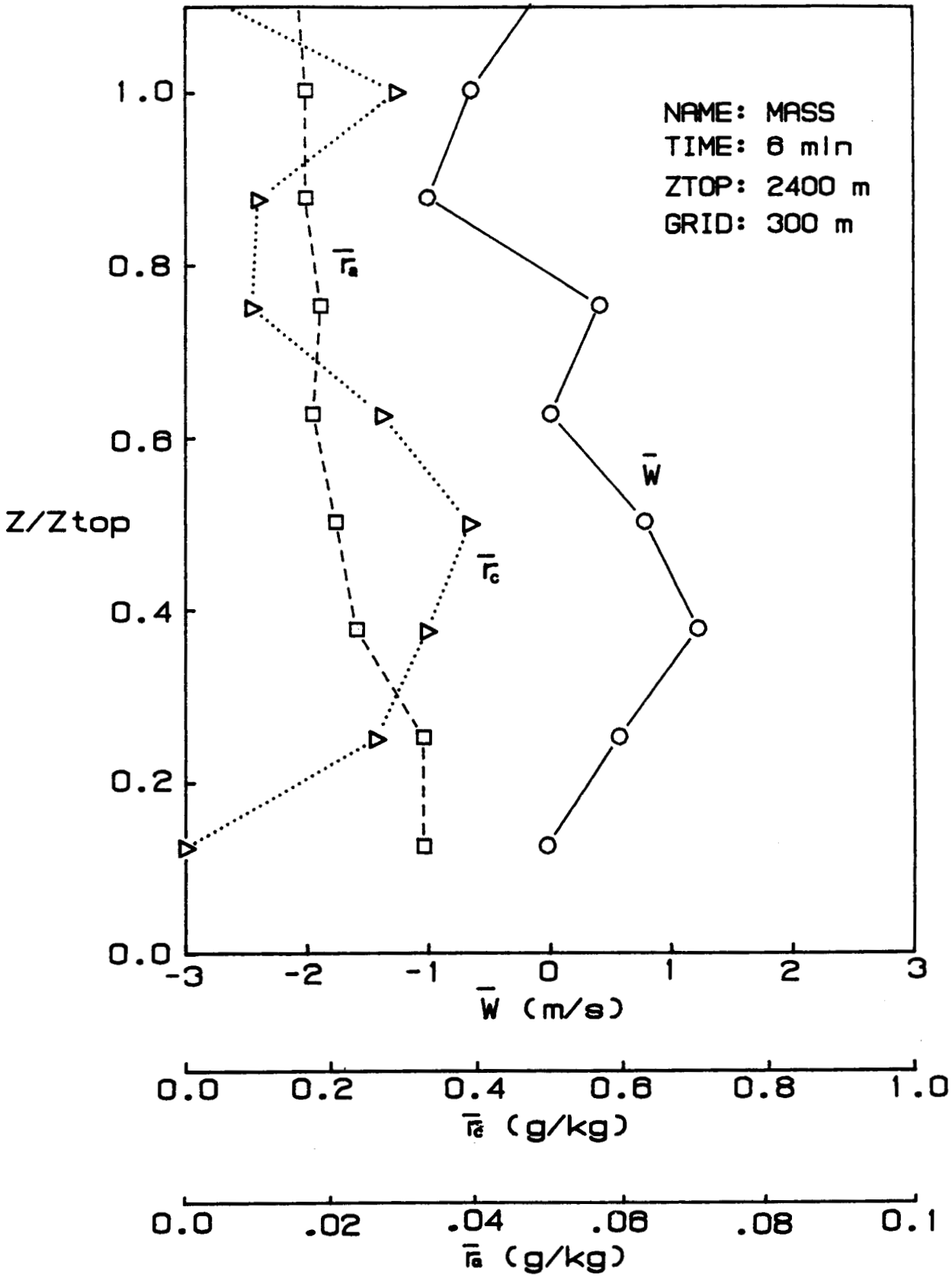

Figure 46. Vertical distributions of average vertical motion, cloud water and smoke 6 minutes after initialization for the MASS sounding.

which can exist for short periods up to 6 km, the entrainment process together with lack of organized larger-scale motion in the atmosphere precludes the development of significant convection.

Stable Atmospheres

In the previous section the model results in unstable atmospheres have been discussed. The next three cases represent stable atmospheres or those containing strong inversions.

CASE 51A

Like Case 41D, Case 51A has observed data that can be used to compare with model results. The atmosphere for Case 51A shown in Figure 47 has a stronger capping inversion than for 41D and the air near the surface is also drier. The inversion begins about 2.0 km above the surface and a layer of saturated air can be found at 1.5 km. From the surface to 1.5 km height the wind is from the northeast then shifts to northerly above 2 km. In general, Case 51A has stronger wind shear both in speed and direction.

Photographs of the 51A observed ground cloud are shown in Figure 48. The stratiform cloud in the background reflects the layer of saturated air as indicated in the sounding. The photogrammetry for this case indicates that the cloud base rises faster than that of Case 41D, however the calculation used an average base which did not count the very lowest part on the north side. The steeper (more adiabatic) lapse rate in the lower part of the atmosphere may have also played a role in Case 51A. In addition, because of stronger wind shear, the near-surface portion of the cloud for Case 51A diffuses faster. The core of convection for Case 41D appears well protected from the environment whereas for 51A the cloud reflects the strong wind shear

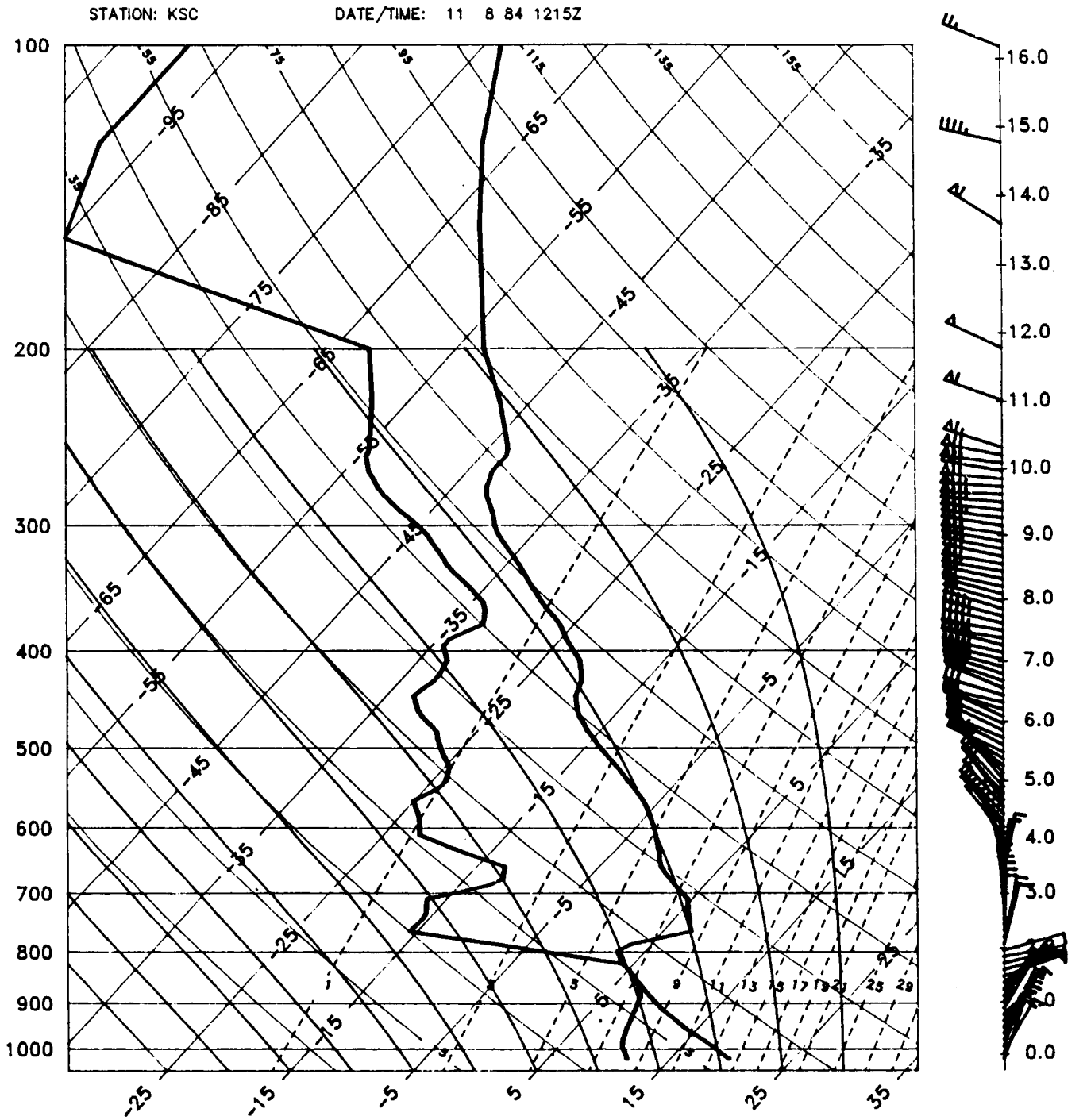

Figure 47. Observed upper-air sounding for Mission 51A, November 8, 1984, 1215 GMT.

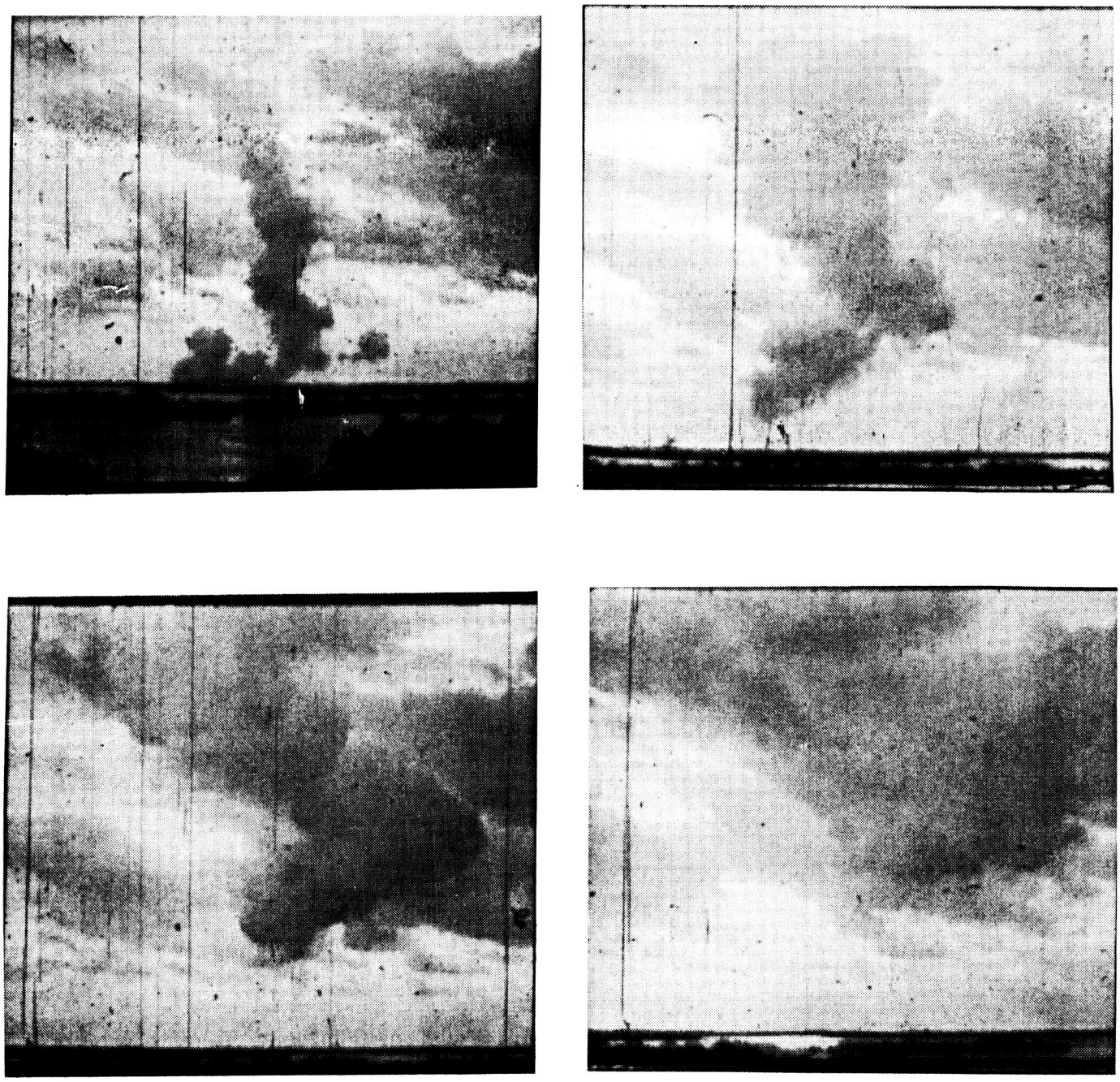

Figure 48. Photographs of digitization of 16mm film frames for the Shuttle Mission 51A ground cloud looking east a 1 minute (top left), 3 minutes (top right), 5 minutes (bottom left) and 7 minutes (bottom right) after launch.

in its appearance. Furthermore, 7 min. after launch, the cloud of Case 51A blends into the background cloud, and it becomes impossible to distinguish between the two in our photographs.

The next 4 Figures present the perspective plots of the modeled Shuttle cloud (liquid water) and smoke looking east and northeast. Comparing Figures 49 and 51, the cloud water in the model simulation, with Figure 48, one can see that the model predicted the cloud top height of about 2.4 km in good agreement with observations. However, the higher cloud base from the model indicates that the lower piece of observed cloud may be smoke as shown in Figures 50 and 52. Since Case 51A has dry air near the surface, any liquid water cloud will not last long.

The time history of cloud width is plotted in Figure 53 for both obsevations and model results. The differences between the NS and EW widths from model results compared to photogrammetry are due to the diagonal measurement of width from the photographs. Qualitatively, from Figure 48, one can see that for pure NS and EW measurements the model result of a wider NS dimension is correct. The model result also shows a larger cloud width than observed, but the model width is the maximum horizontal width in the vertical domain whereas the photogrammetry calculations (observations) represent the average cloud width throughout the total atmosphere below the cloud top measured perpendicular to the cloud walls.

The yz and xz cross sections of vertical velocity (W), cloud water (XIC) and smoke (RAA) are shown in Figures 54 to 59. The maximum W (Figs. 54 and 55) was found at 3 min with magnitude of 6 m/s. The maximum cloud water (Figs. 56 and 57) of 1.0 g/kg occurred at 6 minutes into the simulation. From Figure 58 one can see that the cloud convection transports smoke upward to the base of the inversion where it is dispersed laterally by the wind at the upper

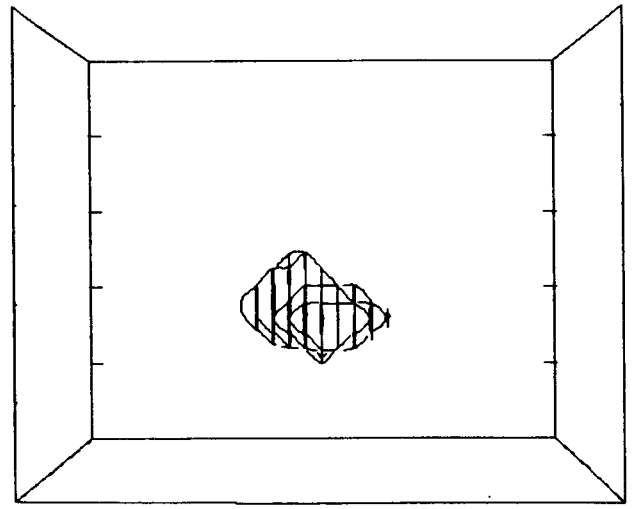

FILE NAME: 51A
TOP AT 5.0 KM
XIC AT 3.1 MIN
VIEW: LOOKING EAST

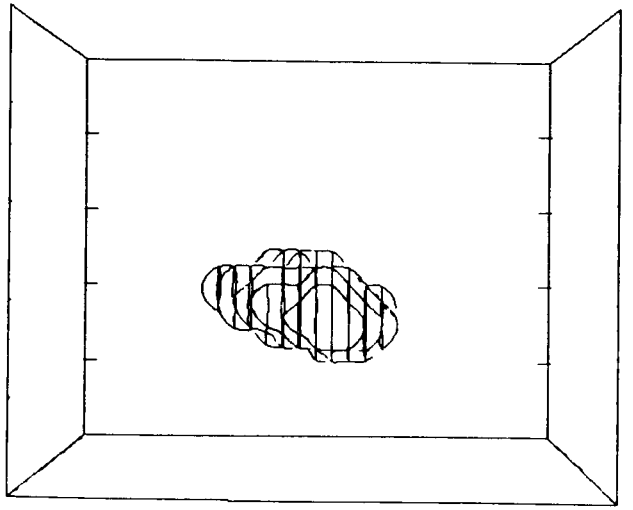

FILE NAME: 51A
TOP AT 5.0 KM
XIC AT 5. MIN
VIEW: LOOKING EAST

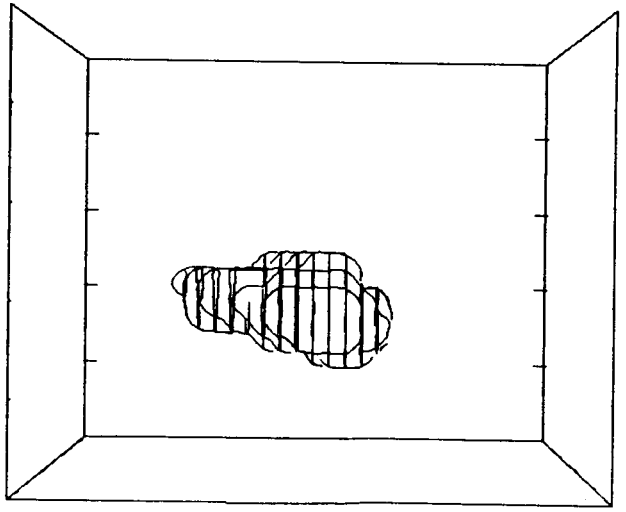

FILE NAME: 51A
TOP AT 5.0 KM
XIC AT 6.0 MIN
VIEW: LOOKING EAST

Figure 49. Model cloud water contours at 3, 5 and 6 minutes after initialization for the Mission 51A sounding looking east.

Figure 50. Model smoke contours at 3, 5 and 6 minutes after initialization for the Mission 51A sounding looking east.

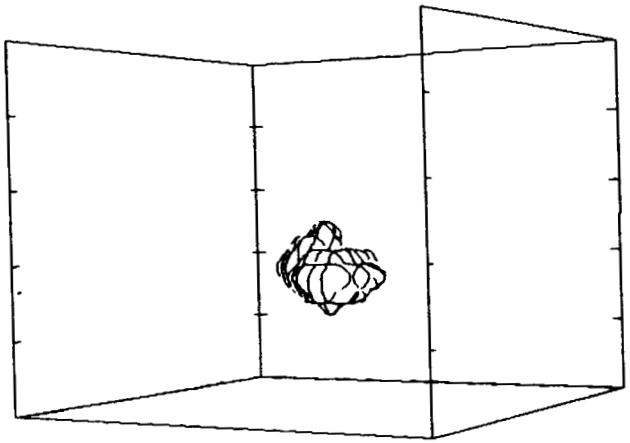

FILE NAME: 51A
TOP AT 5.0 KM
XIC AT 3.1 MIN
VIEW: LOOKING NORTHEAST

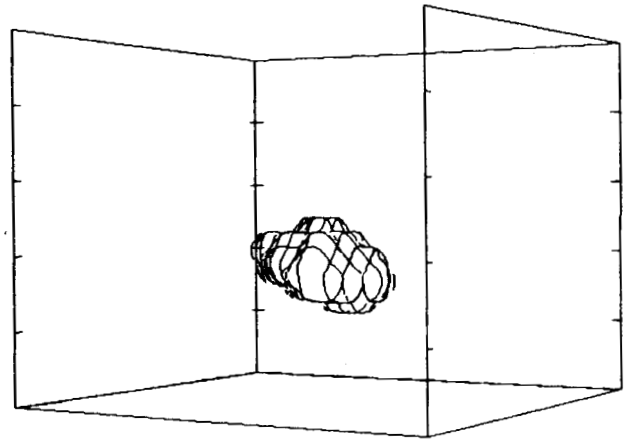

FILE NAME: 51A
TOP AT 5.0 KM
XIC AT 5.0 MIN
VIEW: LOOKING NORTHEAST

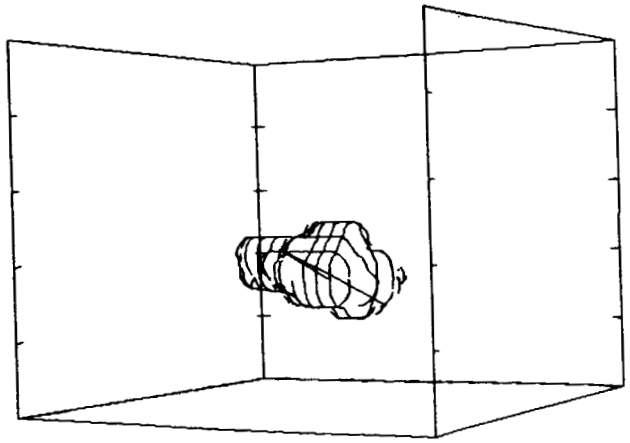

FILE NAME: 51A
TOP AT 5.0 KM
XIC AT 6.0 MIN
VIEW: LOOKING NORTHEAST

Figure 51. Model cloud water contours at 3, 5 and 6 minutes after initialization for the Mission 51A sounding looking northeast.

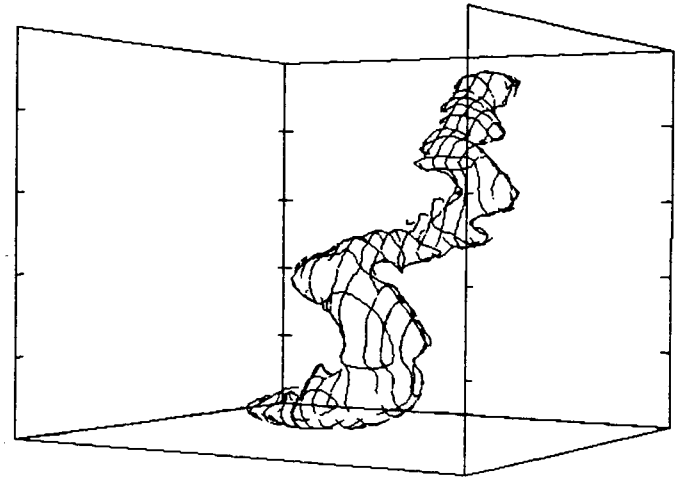

FILE NAME: 51A
TOP AT 5.0 KM
RAA AT 3.1 MIN
VIEW: LOOKING NORTHEAST

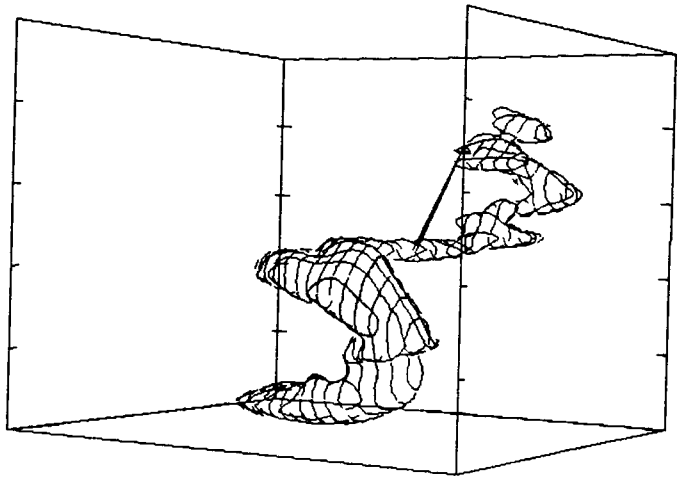

FILE NAME: 51A
TOP AT 5.0 KM
RAA AT 5.0 MIN
VIEW: LOOKING NORTHEAST

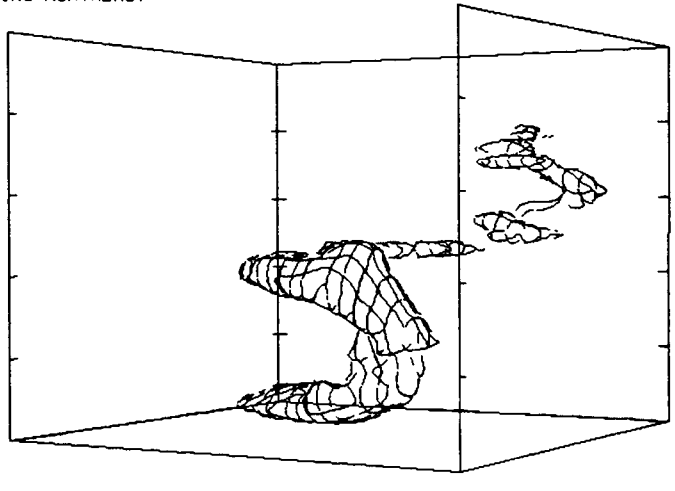

FILE NAME: 51A
TOP AT 5.0 KM
RAA AT 6.0 MIN
VIEW: LOOKING NORTHEAST

Figure 52. Model smoke contours at 3, 5 and 6 minutes after initialization for the Mission 51A sounding looking northeast.

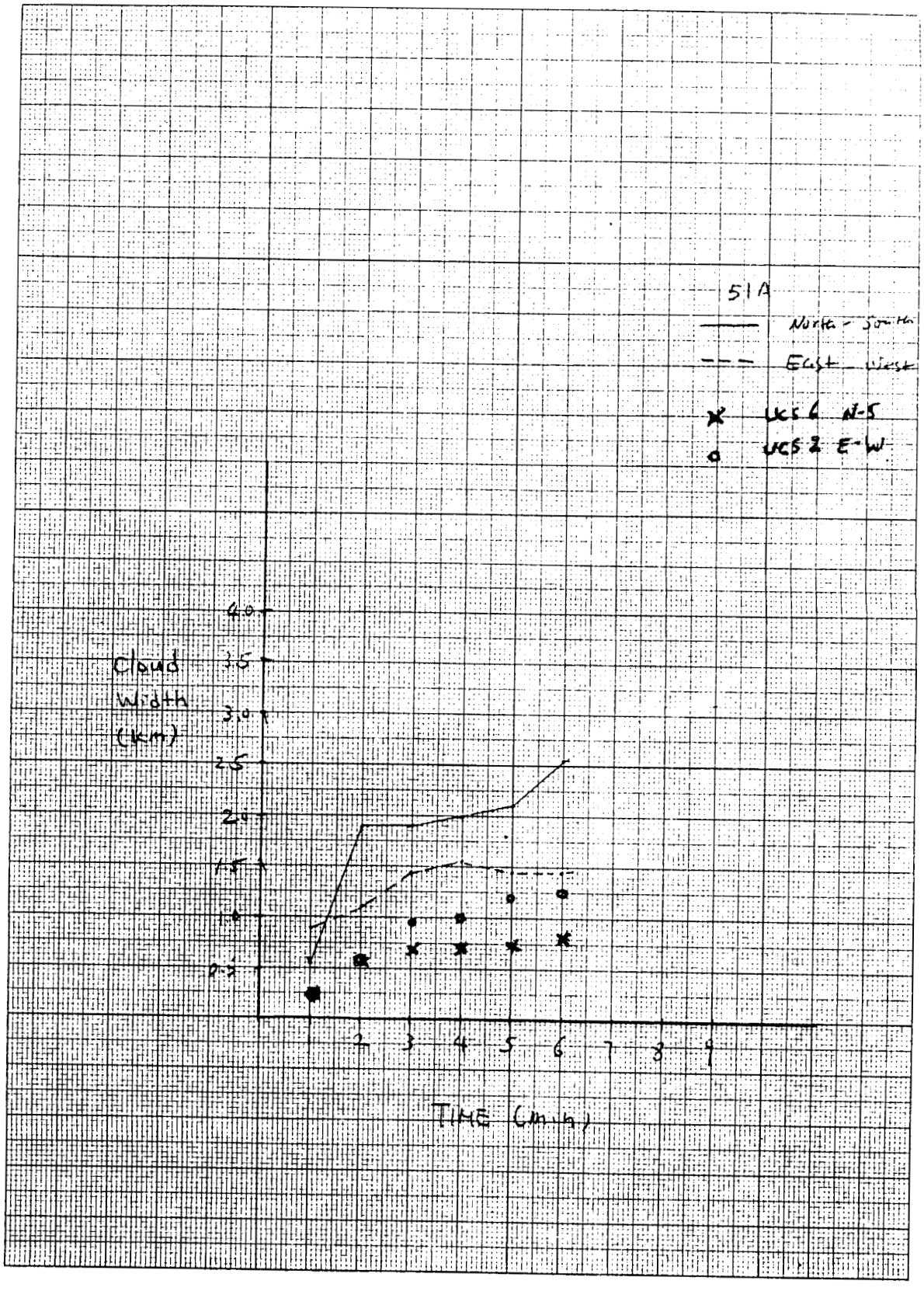

Figure 53.

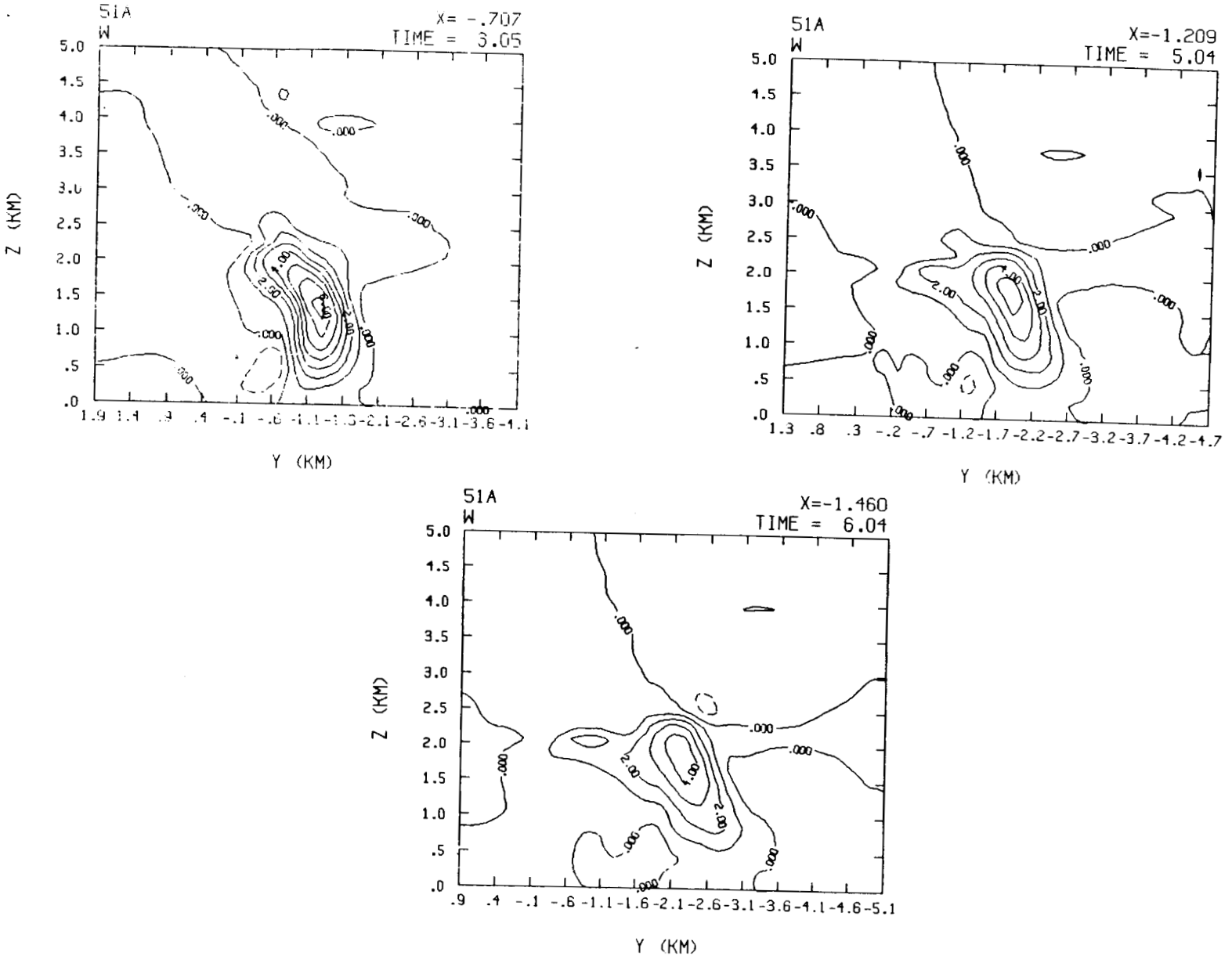

Figure 54. YZ cross section for vertical velocity at 3, 5 and 6 minutes after initialization for Mission 51A.

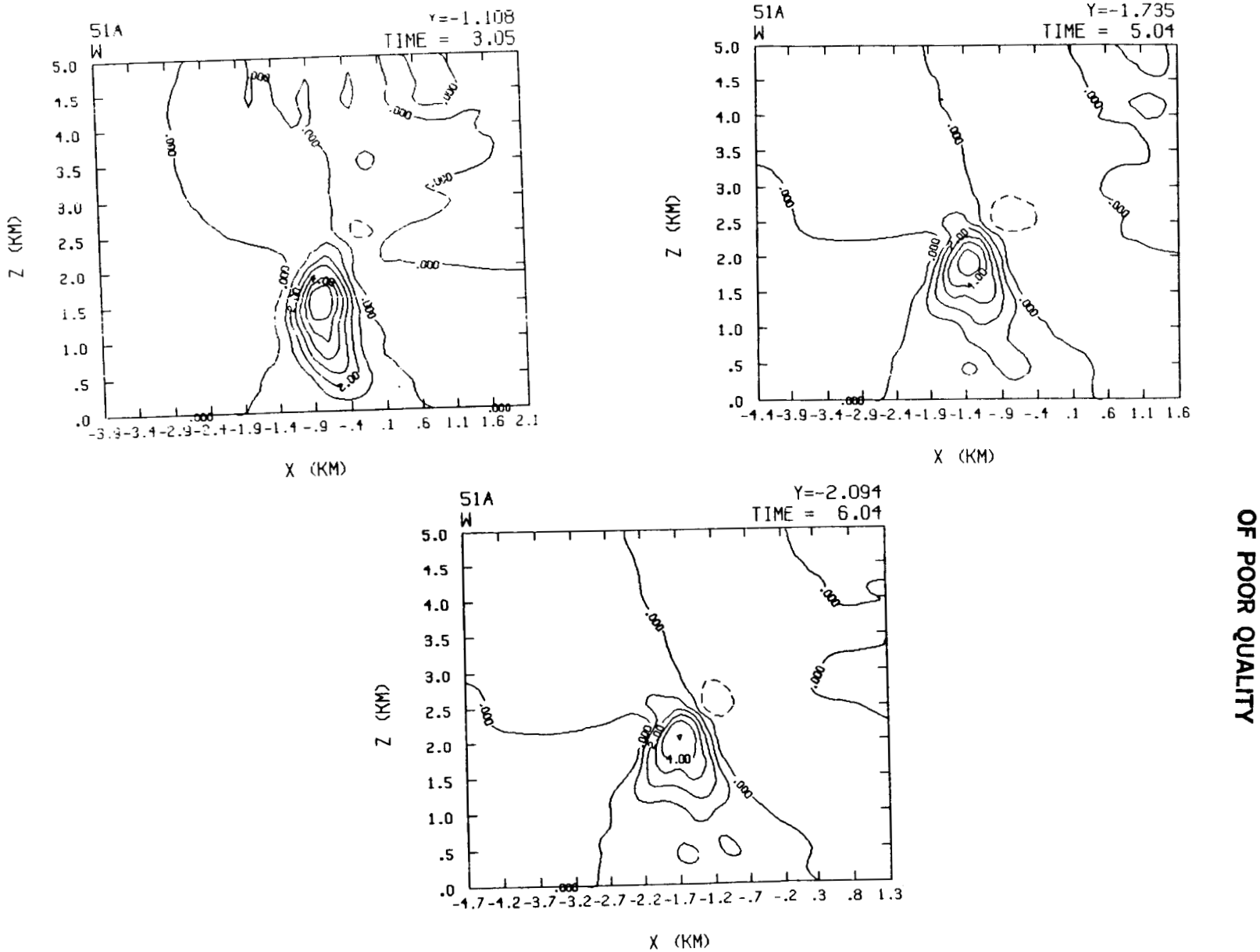

Figure 55. XZ cross section for vertical velocity at 3, 5 and 6 minutes after initialization for Mission 51A.

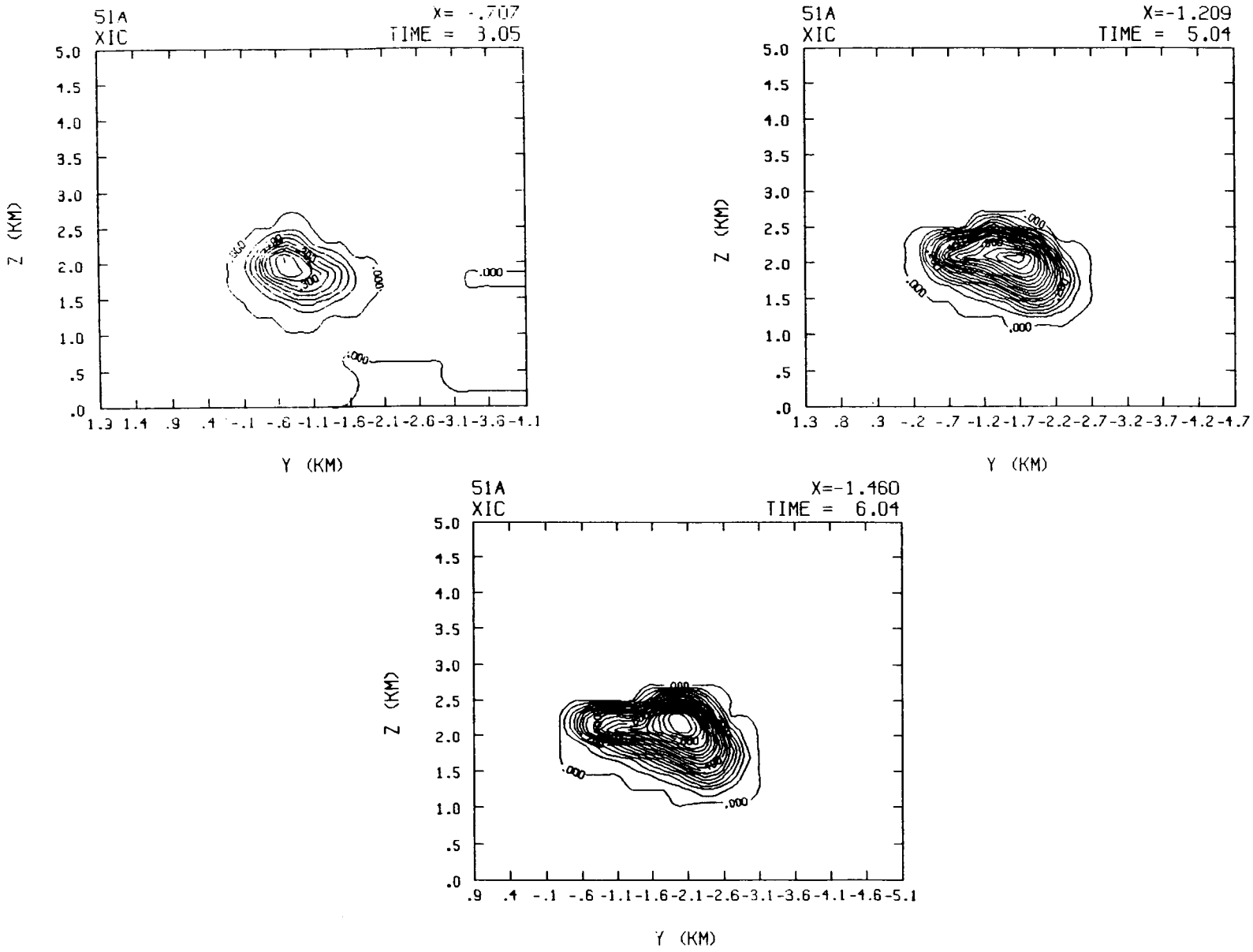

Figure 56. YZ cross section for liquid cloud water at 3, 5 and 6 minutes after initialization for Mission 51A.

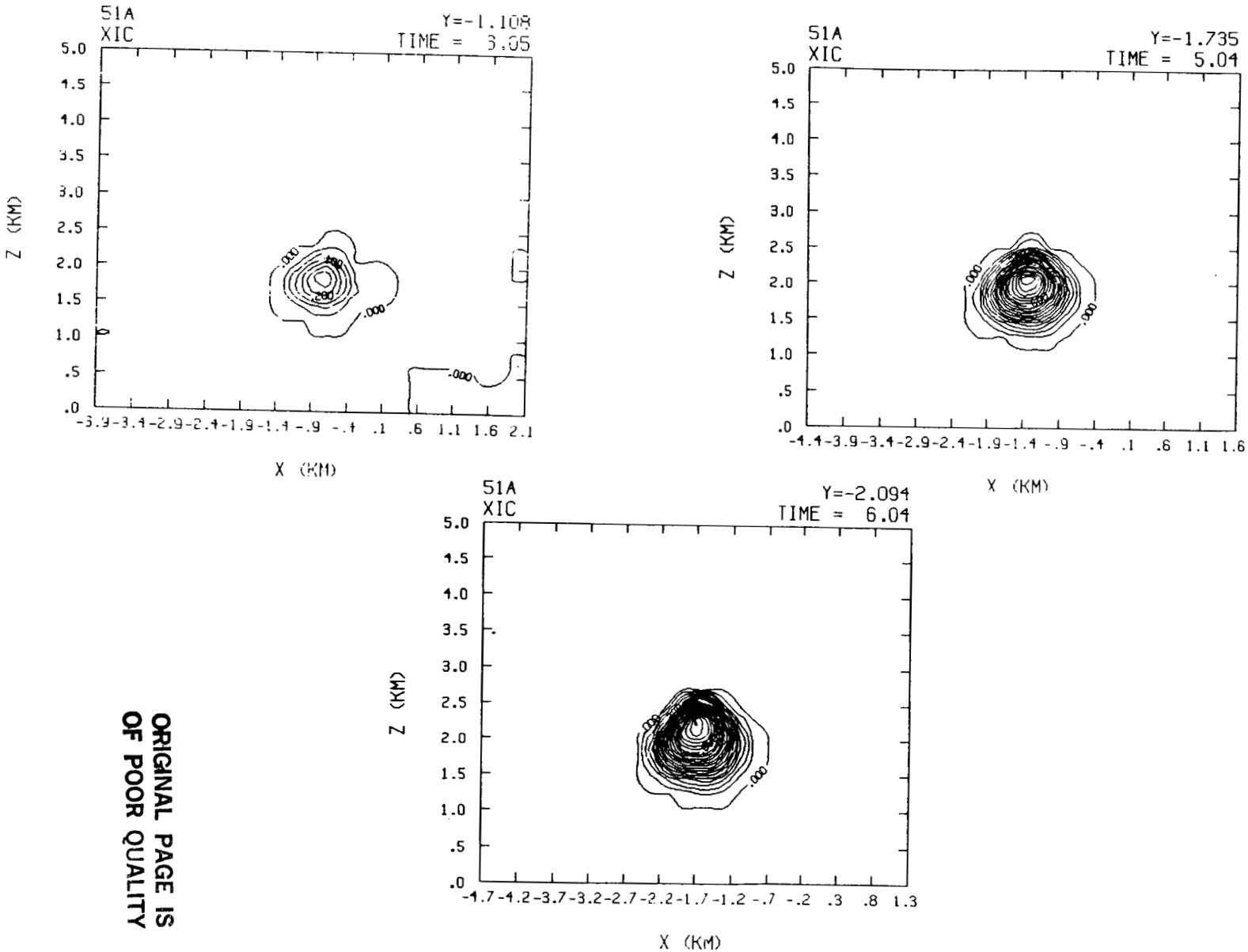

Figure 57. XZ cross section for liquid cloud water at 3, 5 and 6 minutes after initialization for Mission 51A.

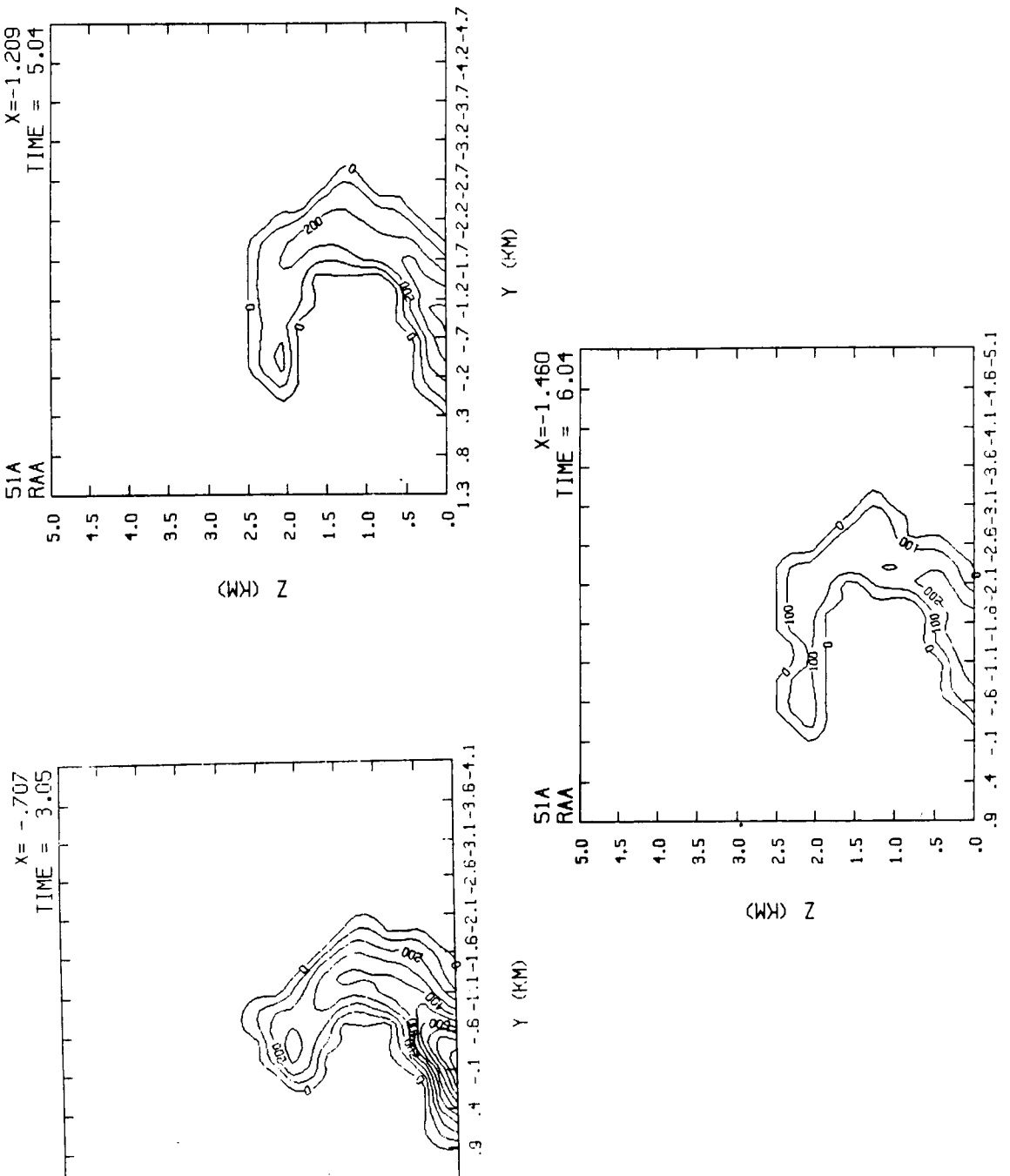

Figure 58. YZ cross section for smoke at 3, 5 and 6 minutes after initialization for Mission 51A.

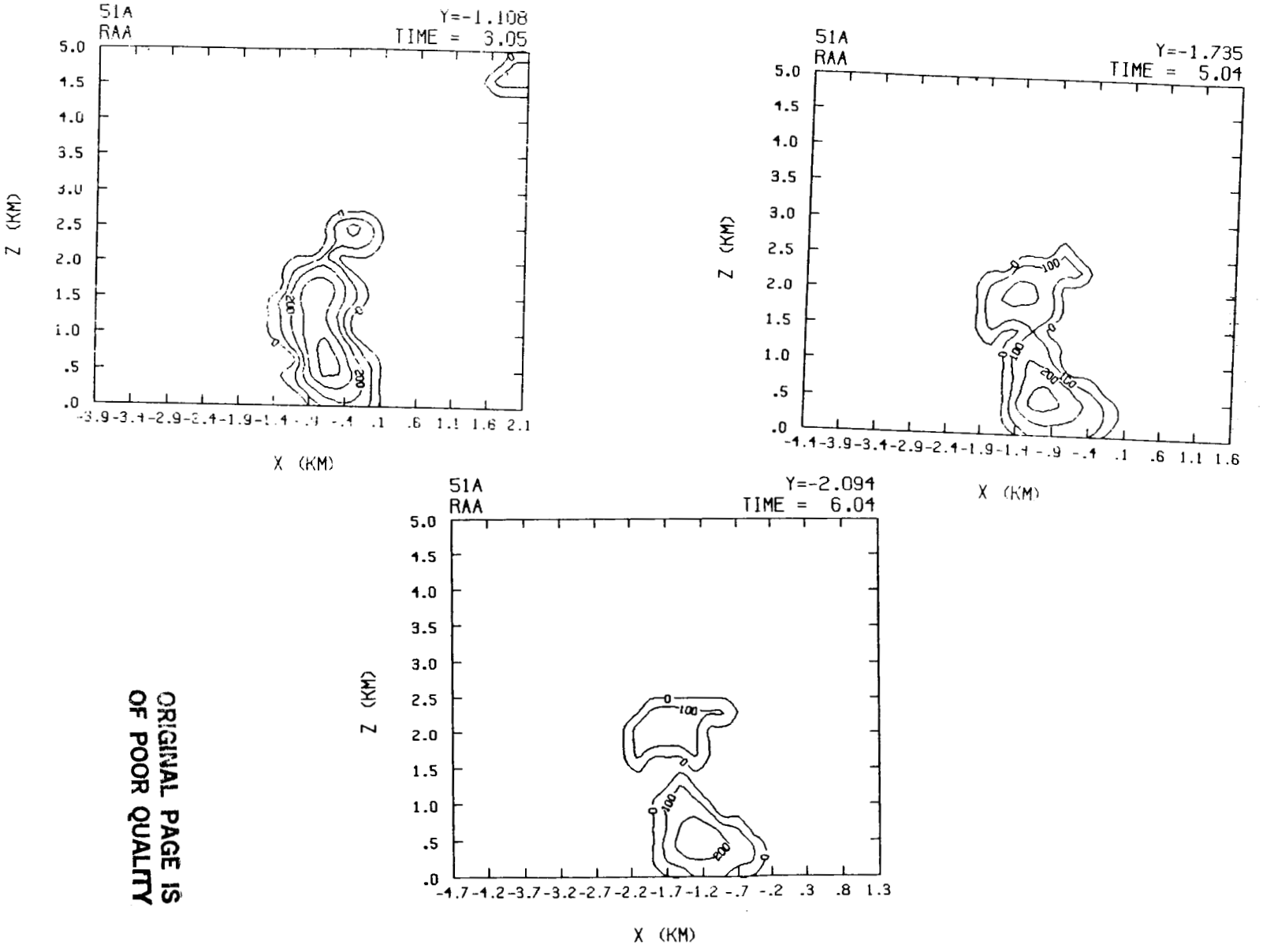

Figure 59. XZ cross section for smoke at 3, 5 and 6 minutes after initialization for Mission 51A.

part of the boundary as expected. The effects of the wind are not as apparent in the xz cross section of Figure 59.

The volume-time plot for 51A is shown in Figure 60. The smoke occupied considerably more volume than cloud. Compared with Case 41D (Fig. 28), both have similar smoke and cloud volumes. However the cloud volume continues to increase after six minutes for Case 51A most likely due to the effect of the wind. It is expected that the liquid cloud of 51A would last longer than that of Case 41D due to the strength of the inversion and environmental moisture although the simulations were not carried beyond 9 minutes.

CASE 41C

Although Case 41C also has a significant capping inversion, the sounding as shown in Figure 61 indicates that there is a very dry boundary layer. The perspective plots in Figure 62 looking northeast at 7 and 9 min show that the water cloud is very small compared to that of smoke. There is insufficient atmospheric moisture to support natural cloud growth for this day.

CASE INV

This case represents a very strong inversion typical of the California west coast. From Figure 63 the depth of the boundary layer is about 500 meters. There is a directional wind shear across the top of the boundary layer where the direction shifts from southeast to northeast. At the layer near the surface the wind is from the southwest.

The yz cross section of vertical velocity (W), cloud water (XIC) and smoke (RAA) is shown in Figure 64. The cloud water is effectively trapped below 500 m. The ground part of the smoke is also dispersed within the shallow boundary layer. The column part and ground part of the smoke appear

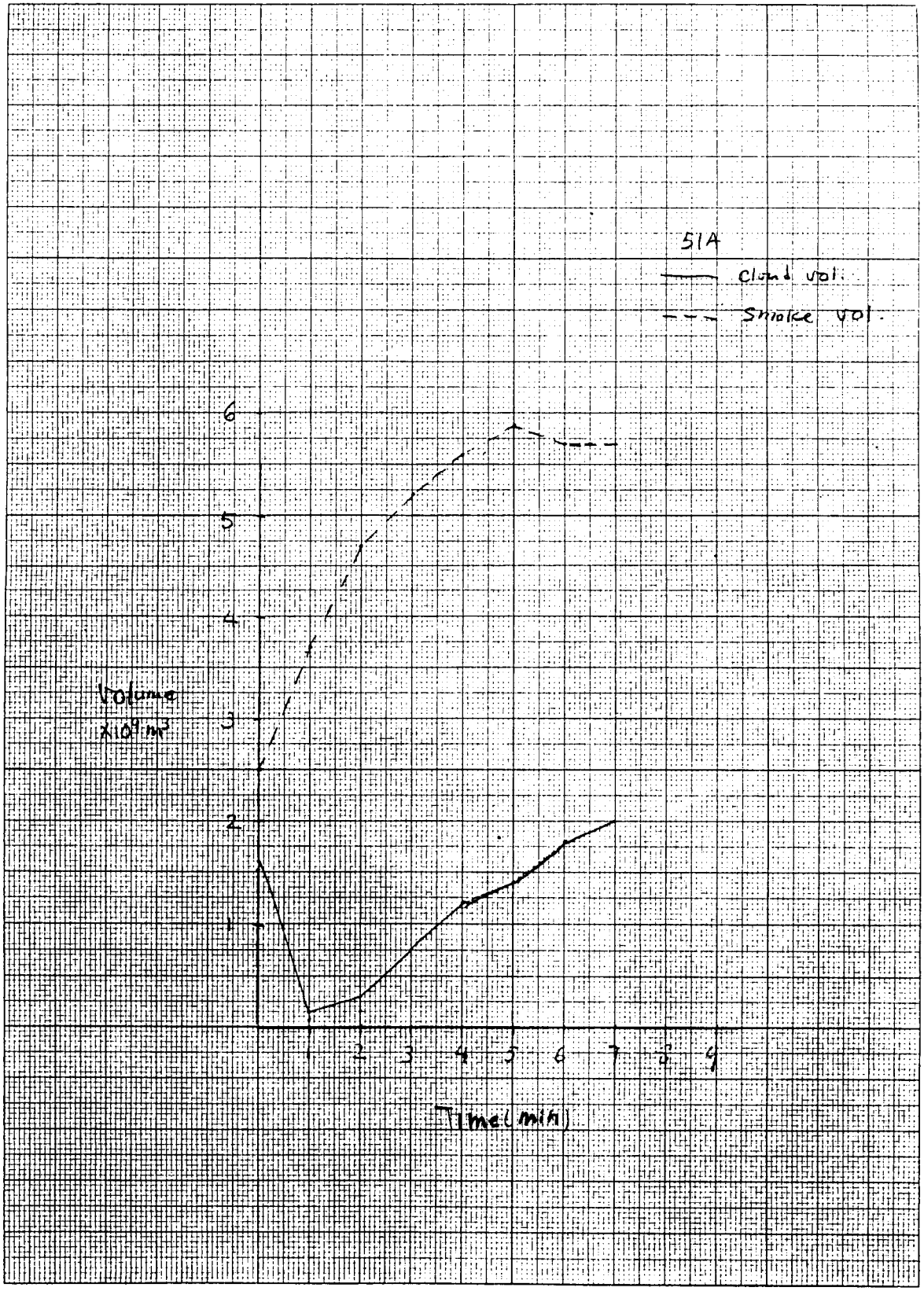

Figure 60.

ORIGINAL PAGE IS
OF POOR QUALITY

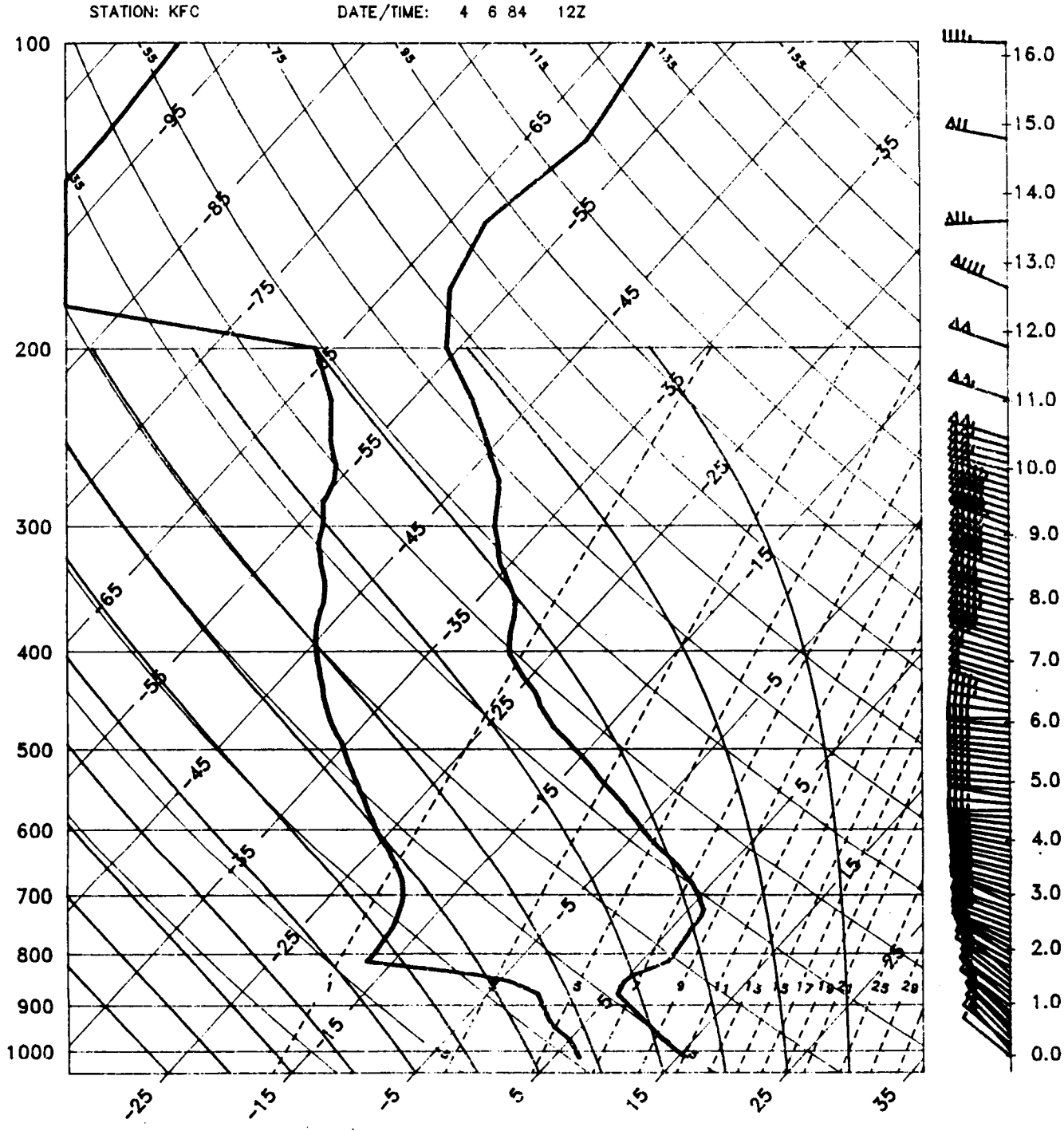

Figure 61. Observed upper-air sounding for Mission 41C, April 6, 1984, 1200 GMT.

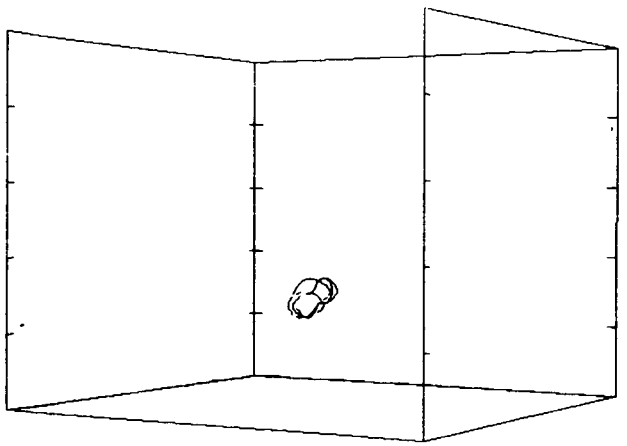

FILE NAME: 41C
TOP AT 5.0 KM
XIC AT 7.0 MIN
VIEW: LOOKING NORTHEAST

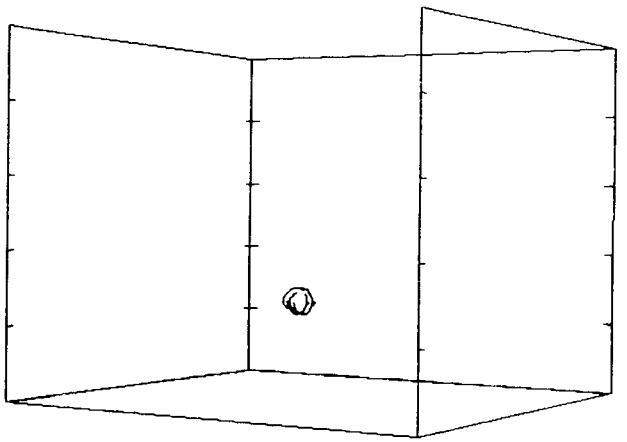

FILE NAME: 41C
TOP AT 5.0 KM
XIC AT 9.0 MIN
VIEW: LOOKING NORTHEAST

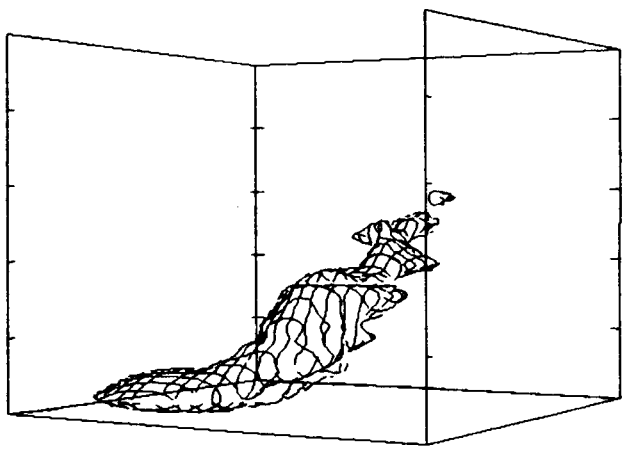

FILE NAME: 41C
TOP AT 5.0 KM
RAA AT 7.0 MIN
VIEW: LOOKING NORTHEAST

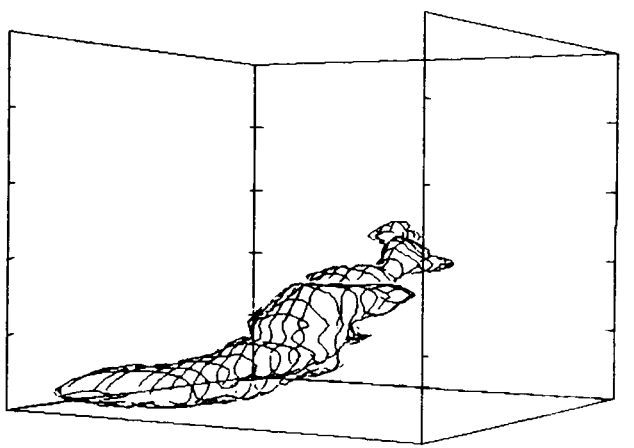

FILE NAME: 41C
TOP AT 5.0 KM
RAA AT 9.0 MIN
VIEW: LOOKING NORTHEAST

Figure 62. Liquid cloud water contours (top) and smoke contours (bottom) for 7 (left) and 9 (right) minutes after initialization for Mission 41C.

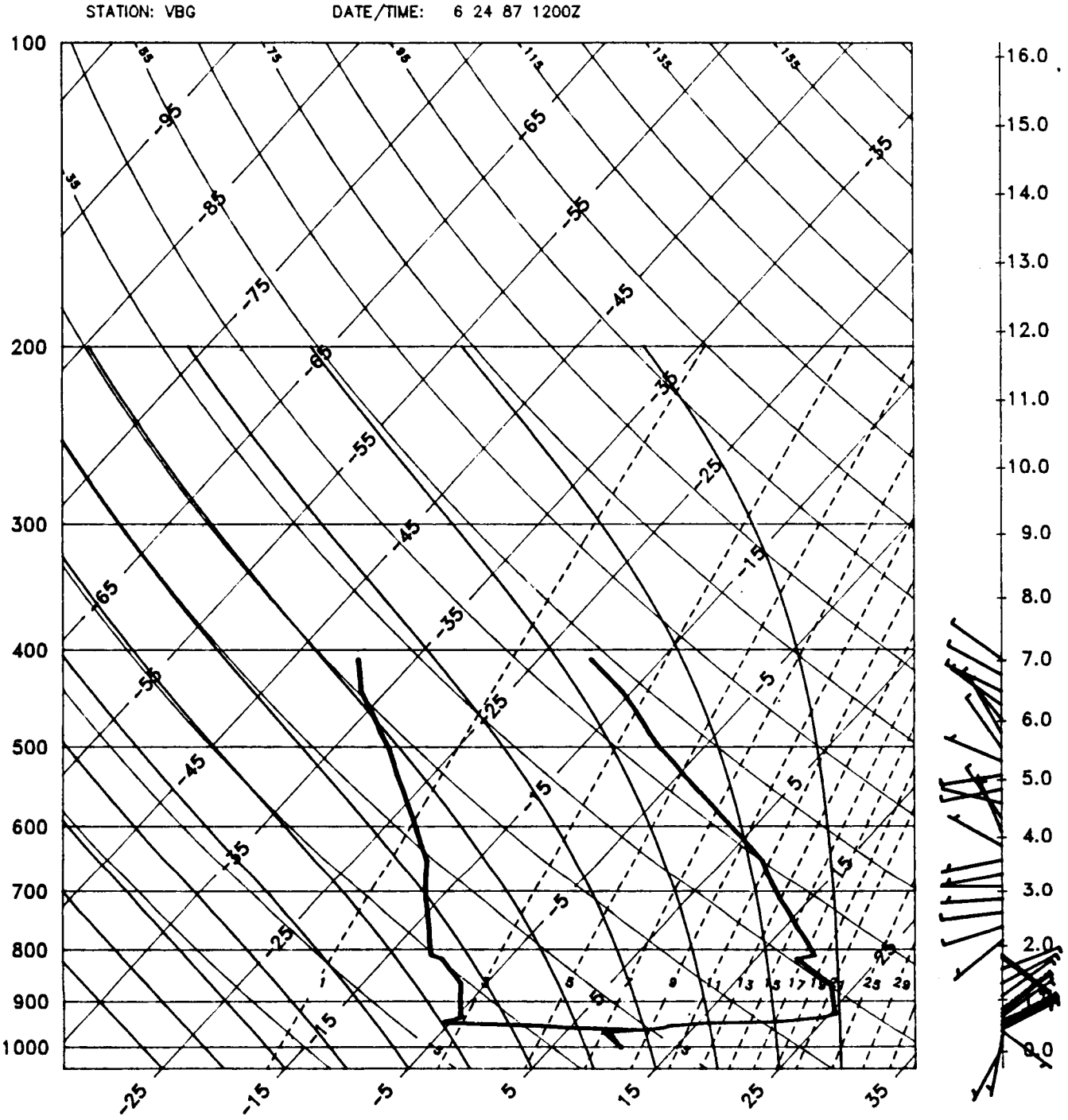

Figure 63. Observed upper-air sounding for Vandenberg AFB June 24, 1987, 1200 GMT (case INV).

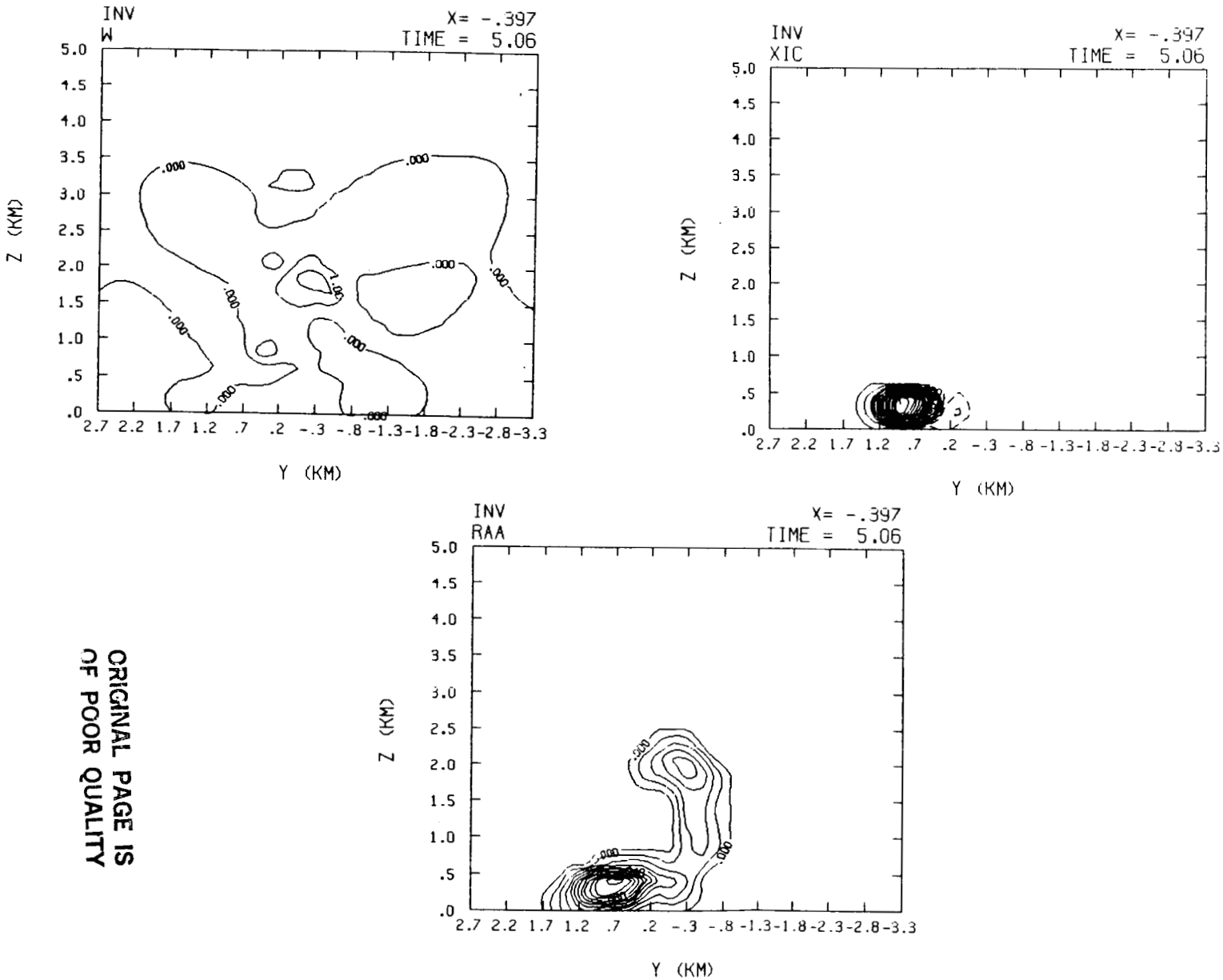

Figure 64. YZ cross section for vertical velocity, cloud water and smoke 5 minutes after initialization for the Vandenberg inversion (INV).

to be separated. Also note from Figure 53 that the max vertical motion is located at 2 km which is considerably above the boundary layer. This maximum reflects the column heat and a layer of thermal instability indicated in the sounding at 1.5 to 2.0 km.

Figure 65 shows the perspective plot of cloud water and smoke looking northeast at 5 min. Both cloud and smoke are dispersed laterally under 500 m. The smoke has a larger volume than the cloud in the simulation. At 2 km the smoke shows signs of convective bubbling also associated with the local instability at that level.

CASE Titan

In the Titan case, the model was initialized to represent an explosion. All heat, moisture and water vapor were added to the atmosphere 200 m above the surface. The perturbation was then decreased exponentially both in vertical and horizontal directions. The sounding for this experiment is shown in Figure 66. In general, this atmosphere was very dry with a series of shallow inversions below 800 m.

No cloud water was generated by the model. The 3D display of smoke for the model simulation of the Titan case is shown in Figure 67. There is not much structure. The cross section for vertical velocity and smoke is shown in Figure 68. The upward motion at 5 minutes is 3 m/s. The horizontal average smoke concentration is 0.015 g/kg. The grid resolution of 200 m was not sufficient in this case for the model to reflect the details in the low-level part of the sounding. The observed cloud for this actual explosion appeared to split into two pieces apparently in response to the weak low-level inversions.

Figure 65. Cloud water (left) and smoke contours (right) looking northeast at 5 minutes after initialization for the Vandenberg (INV) sounding.

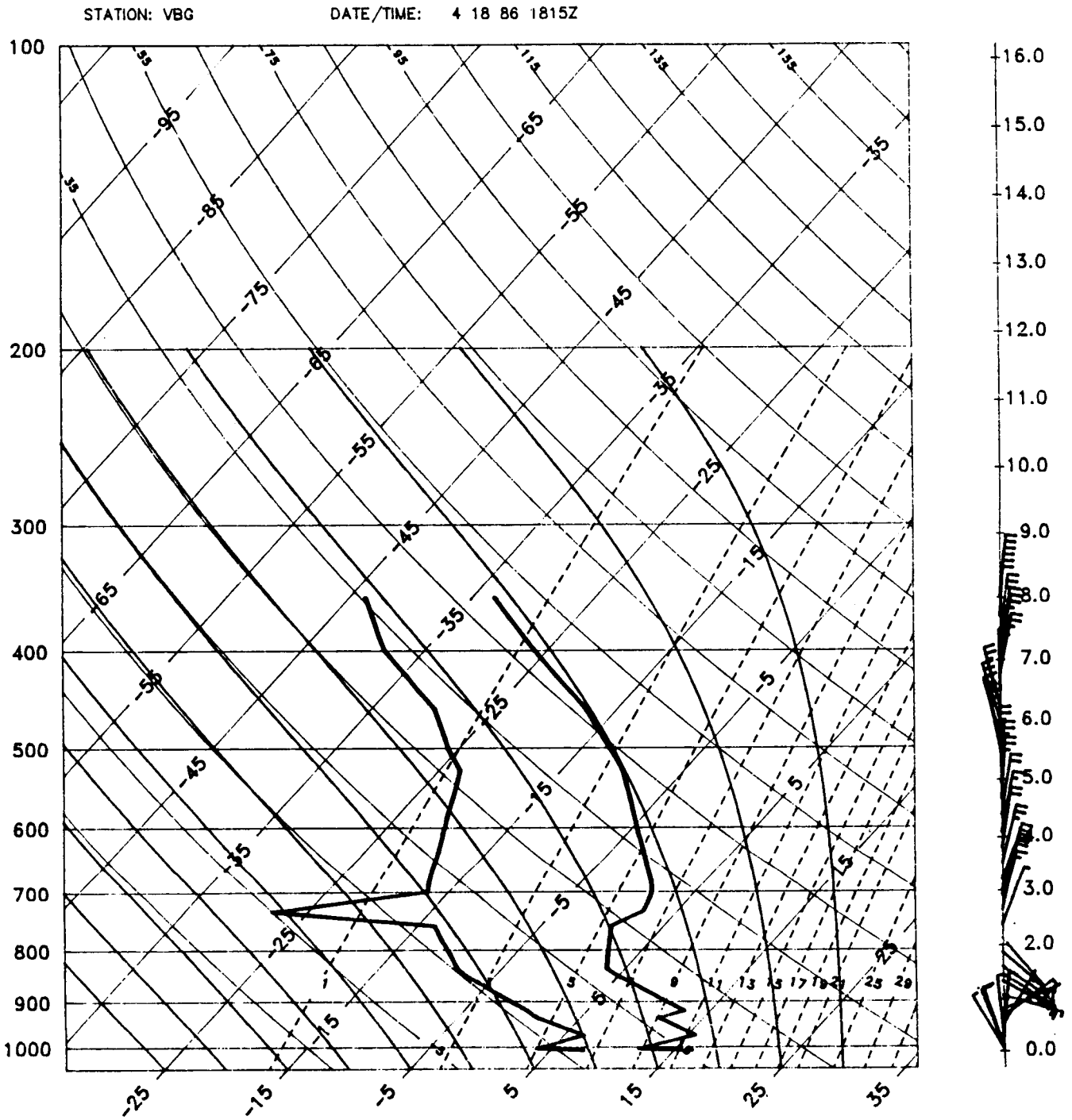

Figure 66. Upper-air sounding for Vandenberg AFB April 18, 1986, 1815 GMT (case TITAN).

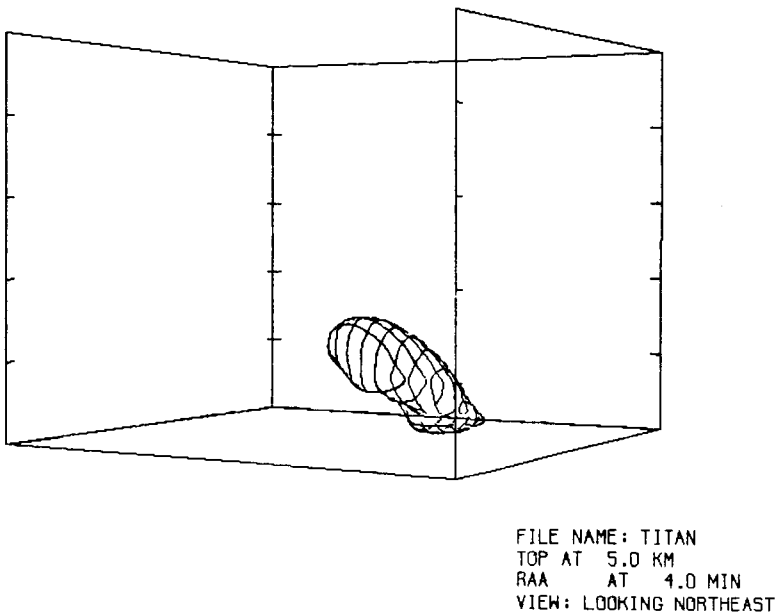

Figure 67. Simulated smoke contours for the TITAN case 4 minutes after initialization looking northeast.

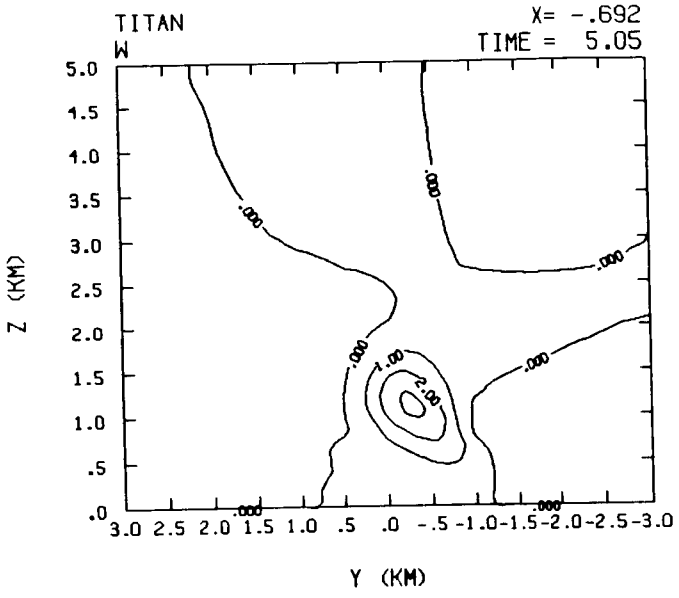

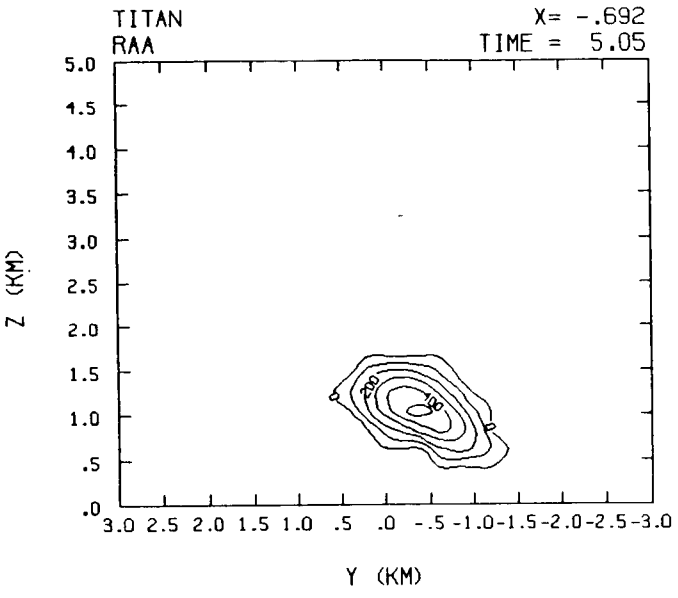

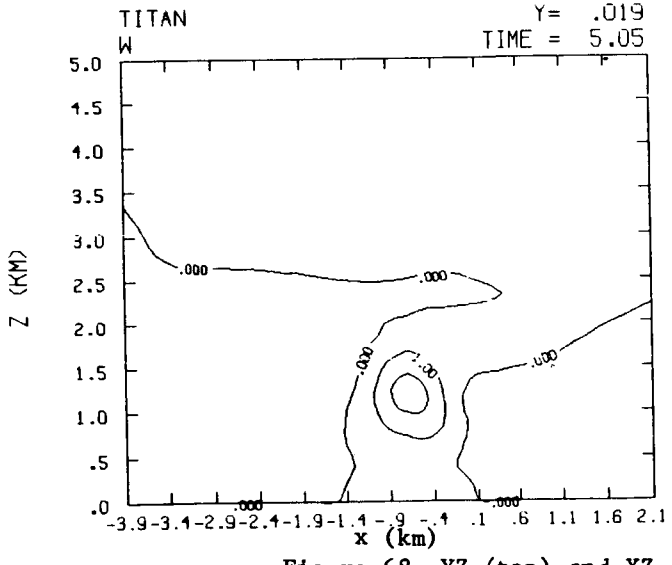

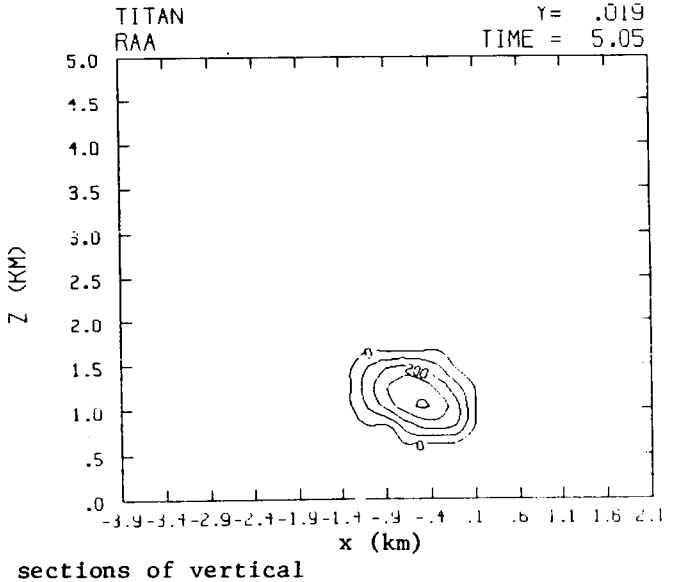

Figure 68. YZ (top) and XZ (bottom) cross sections of vertical motion (left) and smoke (right) for the TITAN explosion simulation 5 minutes after initialization.

CASE STS3

This is another case for which data are available from aircraft penetrations of the actual Shuttle ground cloud. The atmosphere for STS-3 launch at 1600 z, March 22, 1982 is shown in Figure 69. The region below 2 km is slightly moist and unstable; therefore, we would expect some enhancement to ground cloud growth. A moderately strong temperature inversion and significant drying began about 2 km with a weaker isothermal and dry layer at about 1.0 km. A shallow moist region near 600 m reflects scattered stratocumulus clouds. Surface winds were weak northeasterly from a sea breeze which just began a few minutes prior to launch. Above the shallow sea breeze were predominately westerly winds increasing with height. Directional shear existed near the top of the inversion.

The general structure and orientation of the simulated cloud in this environment is shown in the perspective plots of Figures 70 and 71. Figure 70 is cloud water looking south at 3, 5, 7 and 9 minutes. Notice that the cumulus nature of the ground cloud disappears by about 5 minutes and becomes more like a stratocumulus spreading eastward with the westerly flow. Figure 71 is identical to Figure 70 only the view is toward the northeast. The cloud appears to settle within the 500 to 1000 m altitude which ground photographs for this launch appear to confirm. Vertical motion contours in xz cross section are shown for the same time in Figure 72. After 5 minutes there is very little upward motion remaining in the simulation at this selected east-west slice. The maximum is at 3 minutes with magnitude of 6 m/s. The same cross section for cloud water is shown in Figure 73. The east-west asymmetry is again apparent. Maximum cloud water occurs at 7 minutes with a value of 0.2 g kg^{-1}. Because of the dry layer between 600 and 1000 m significant erosion of the cloud through entrainment is occurring. The simulated cloud

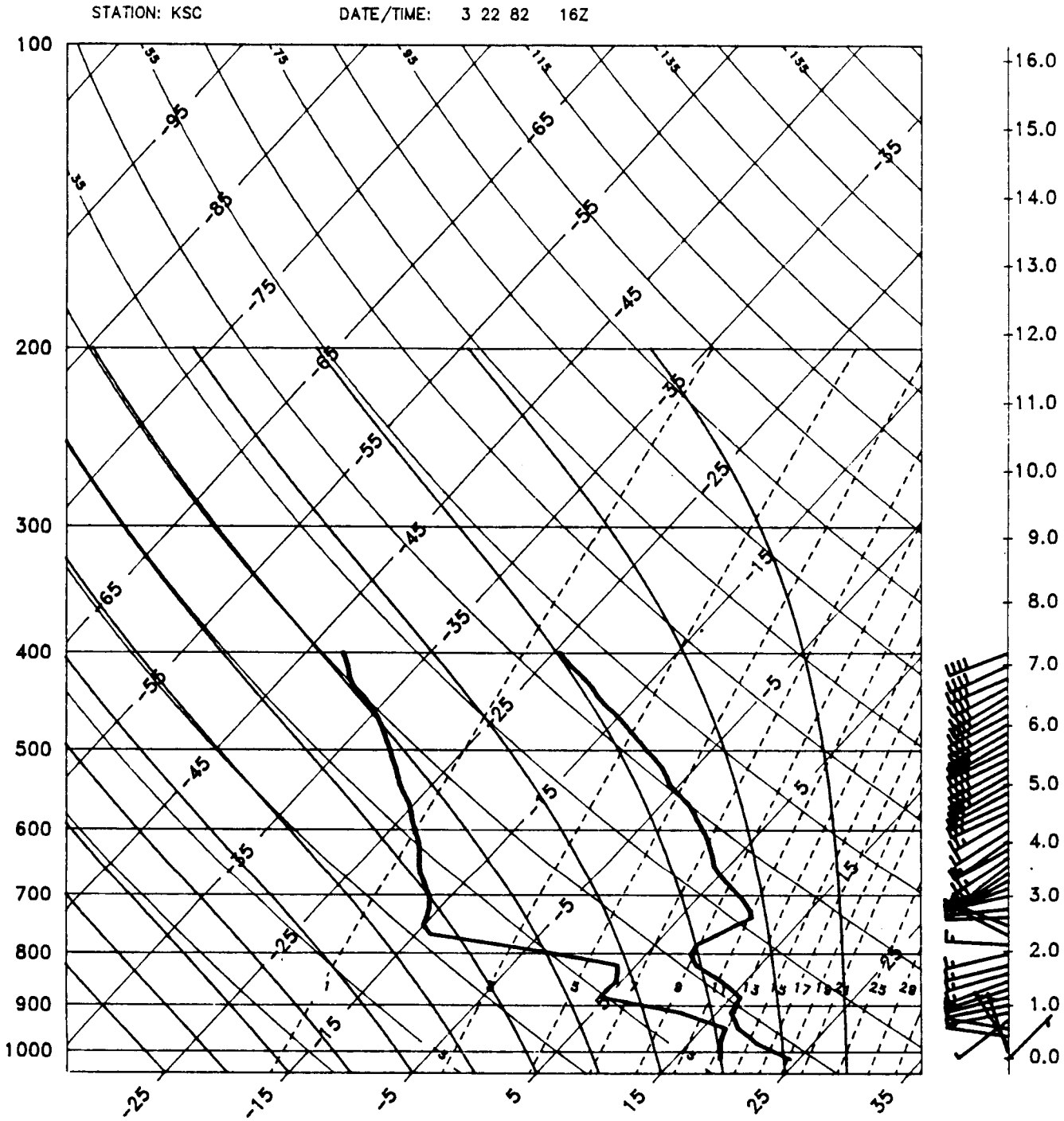

Figure 69. Upper-air sounding for STS-3 Shuttle launch March 22, 1982, 1600 GMT.

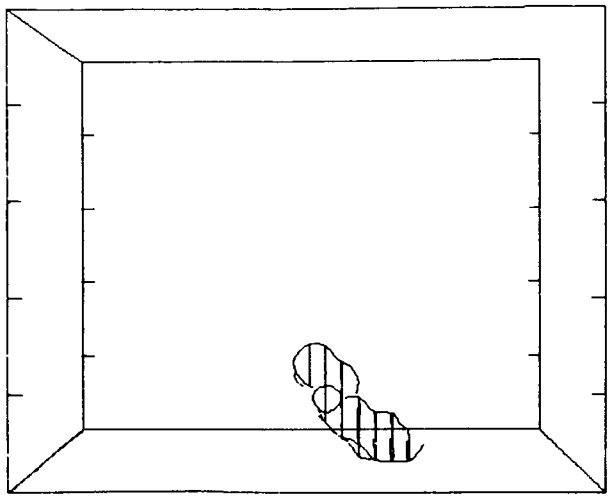

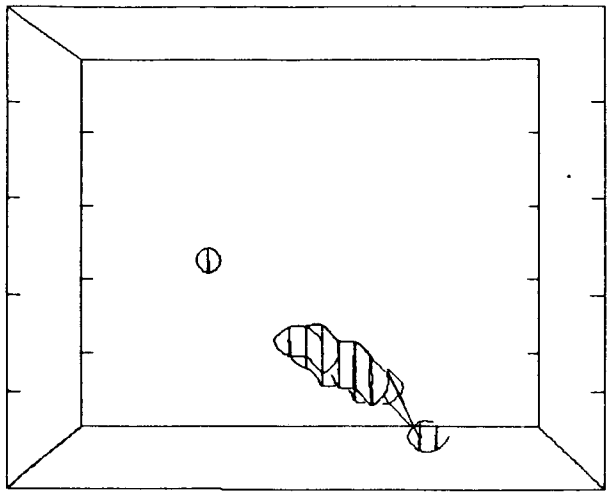

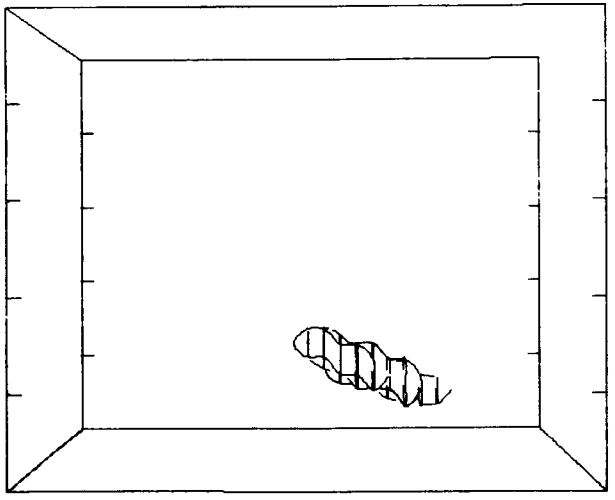

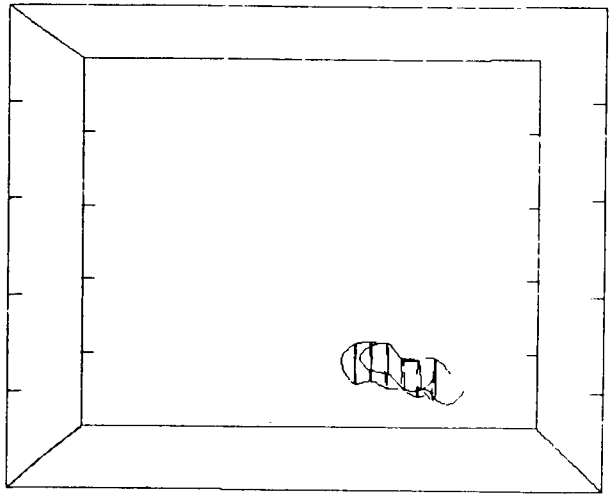

Figure 70. Cloud water contours looking south at 3, 5, 7 and 9 minutes after initialization for the STS-3 atmosphere.

Figure 71. Cloud water contours looking northeast at 3, 5, 7 and 9 minutes after initialization for the STS-3 atmosphere.

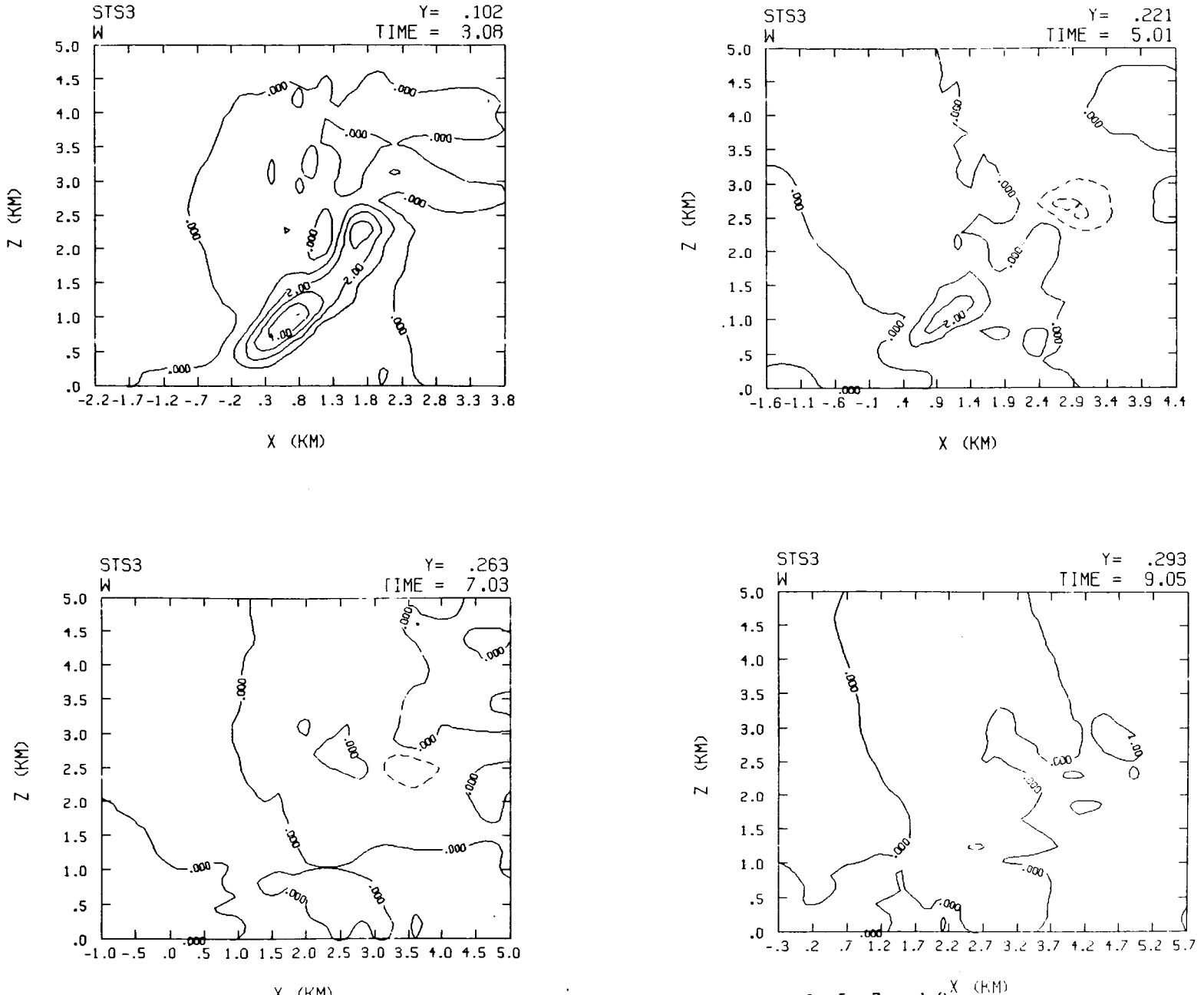

Figure 72. XZ cross section of vertical motion at 3, 5, 7 and 9 minutes after initialization for STS-3.

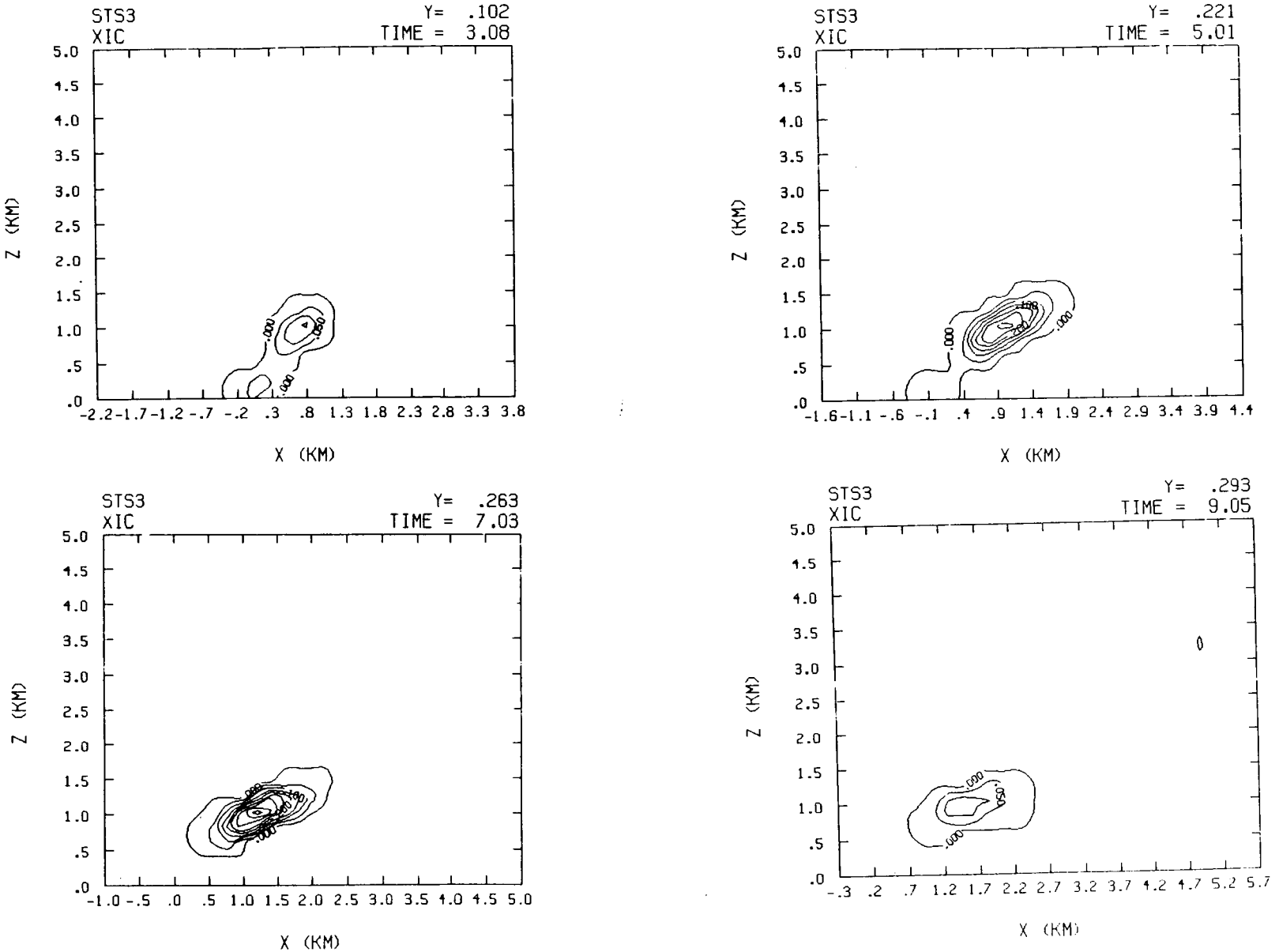

Figure 73. XZ cross section of cloud water and 3, 5, 7 and 9 minutes after initialization for STS-3.

after 7 minutes is losing volume.

Figure 74 is the 3D smoke field and it shows the response to the windshear between 2 and 2.5 km. There is an overall west to east tilt with the turn into the paper (south) being a response to the NW winds at the inversion. This response is shown more dramatically in the perspective viewed toward the east in Figure 75.

The time-height plot of simulated cloud top and base is shown in Figure 76. The maximum cloud top height is 1.4 km while the average cloud base is about 600 m. The cloud width as shown in Figure 64 averages about 1700 m in the east-west direction and 800 m in the north-south direction. The model in this case was not able to produce the 4 m/s upward motion observed by aircraft at 7 and 9 minutes. Some of this difference could result from horizontal averaging within the cloud domain and the 200 m resolution as discussed earlier.

CASE UNSDB

In one experiment we doubled the amount of heat and moisture available from the rocket-launch system in the same atmosphere as case UNS. As shown in Figure 77 the volume of cloud water increased significantly and the ground cloud grows to 4 - 5 km at 6 minutes compared to about 3.3 km for standard initialization. Vertical velocity at 6 minutes had a peak of 5 m/s compared to a peak of 2.5 m/s for case UNS. Also there is a small region of water cloud originating from the rocket exhaust column between 9 and 12 km similar to case MASS. This is most likely due to condensation from upward motion and cooling in the relatively moist upper troposphere. Despite the increased size and vertical motion, this cloud appears to be in its dissipating stages already in the simulation and further growth would not be expected.

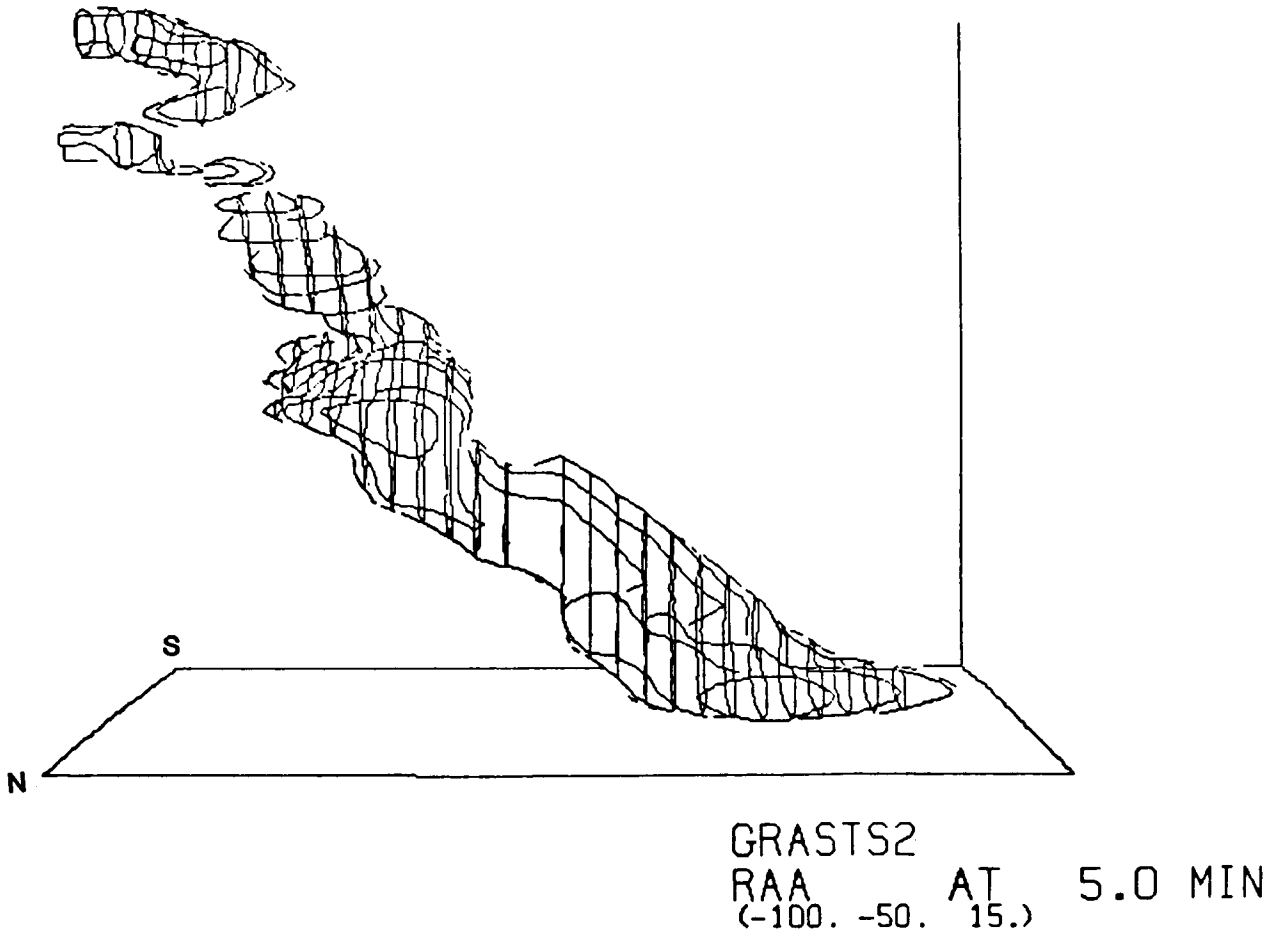

Figure 74. Smoke contours looking south at 5 minutes after initialization for STS-3.

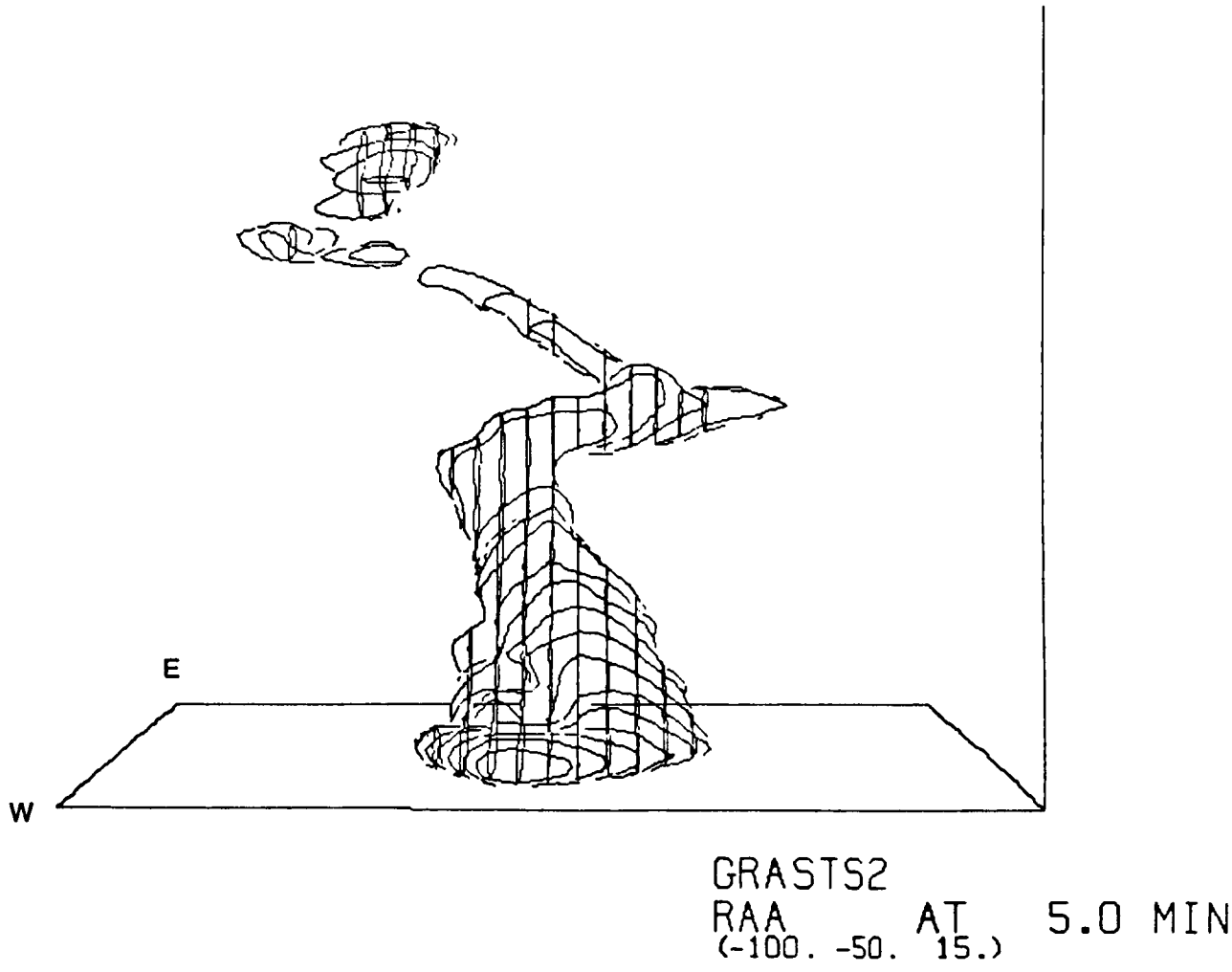

Figure 75. Smoke contours looking east at 5 minutes after initialization for STS-3.

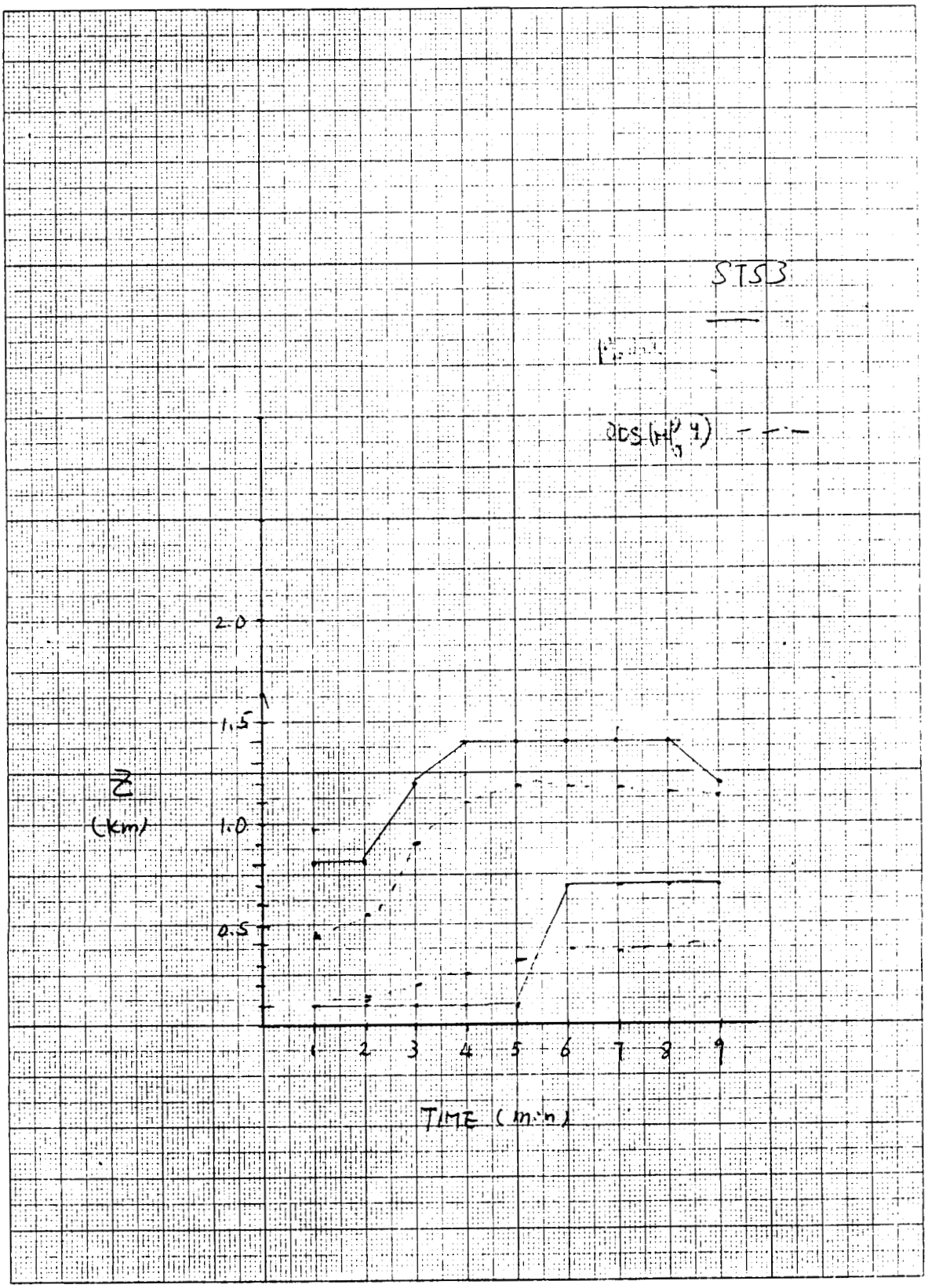

Figure 76.

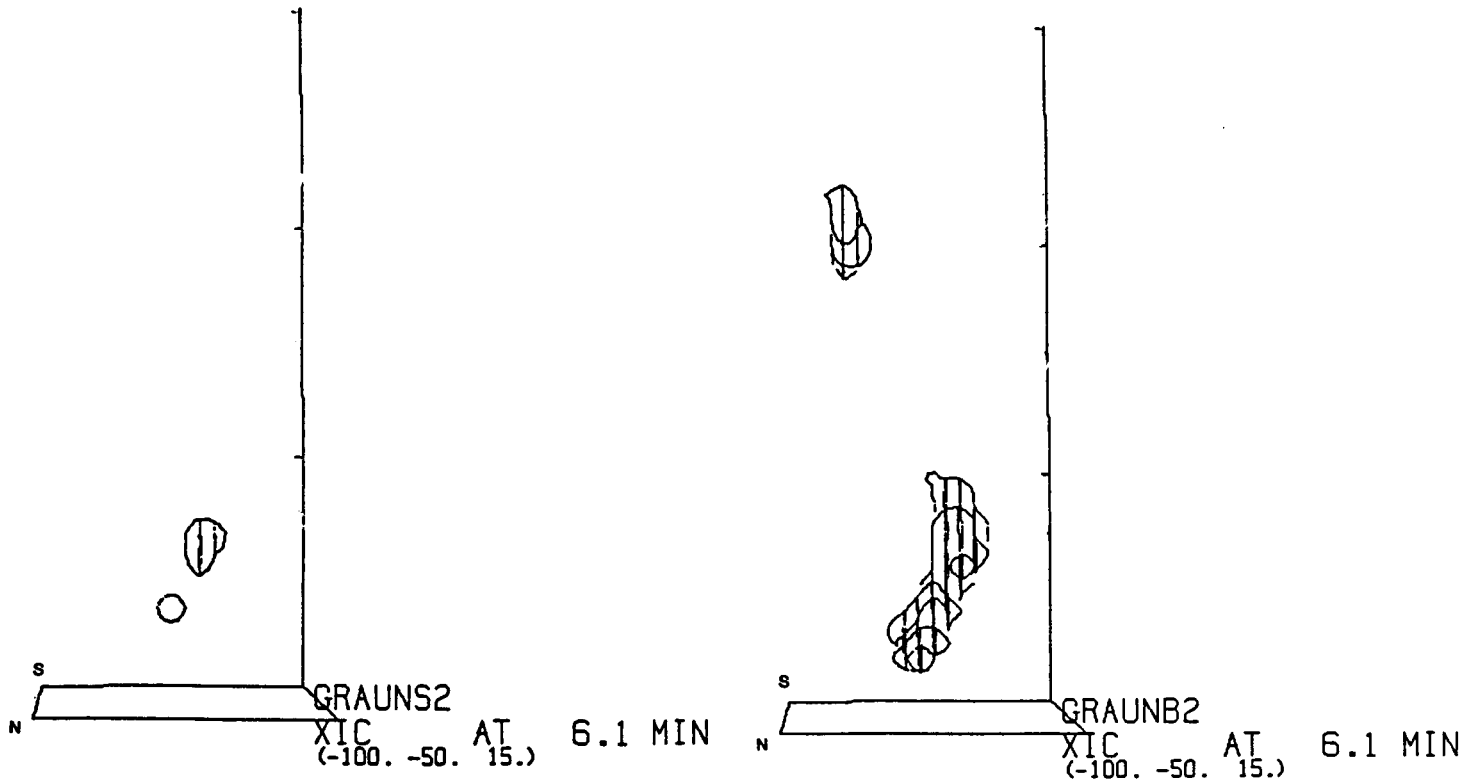

Figure 77. Cloud water contours for case UNS (left) and UNSDB (right) at 6 minutes after initialization looking south.

SECTION 6 - SUMMARY AND CONCLUSIONS

The TASS cloud model produced clouds which resemble the Sapce Shuttle ground cloud in size, volume, maximum tops, vertical motion, liquid water content, movement, growth and decay for the cases where measurements existed. The bubble motion of different convective elements was also reproduced in the model but the rise time was about a minute slower in the model than for observed clouds.

The combined effects of ambient atmospheric temperature, moisture content and wind are dominant factors in the shape, maximum cloud top, liquid water contents, vertical velocity and longevity of simulated ground clouds. Model clouds show relatively high degrees of asymmetry in all runs. Maximum asymmetry occurs with maximum low level wind shear. The initial partioning of heat and moisture from the launch system as well as the separation or location of the input (eg., surface grid points affected) is important in the initial shape of the lower ground cloud, but not important to max cloud top in model results. Wind shear in the column smoke field dramatically altered the appearance of the column. There were sections of the vertical column which were tilted nearly 90 degrees in response to wind direction and speed changes.

Different amounts of low level moisture and heat in the environment controlled the production of liquid cloud water in the model. The amount of cloud water produced in the model ground cloud was very sensitive to the amount of available moisture and degree of saturation in the lower 3 km of the atmosphere. Some atmospheres (TITAN), which were very dry in the low levels (less than 3 km), failed to generate any natural cloud liquid water in the model.

Maximum cloud tops can exceed 3 km in unstable, moist atmospheres; but

the maximum observed top in any simulation with realistic initial conditions was about 4.0 km. The most unstable atmosphere presented to the model did not produce a sustaining precipitation-generating cloud even though this atmosphere supported significant natural convection. When the size of the initial heat and moisture was doubled for the unstable atmosphere, a significantly larger (liquid water content) cloud developed. It continued to rise to about 12 minutes, but the cloud top reached stabilization at only 4.5 km.

The presence of a temperature inversion helped to prevent erosion of the cloud top through entrainment. When the inversion was eliminated the cloud decayed more quickly. A strong low level inversion trapped the ground cloud below it. Max tops were only about 500 m in one case.

SECTION 7 - REFERENCES

Anderson, B. J., and V. W. Keller: Space Shuttle Exhaust Cloud Properties. NASA TP 2258, December, 1983, 116 pp.

Bowman, C. R., Bjorklund, J. R. and Rafferty, J. C.: Users Manual for the REEDM (Rocket Exhaust Effluent Diffusion Model) Computer Program for Launches at Kennedy Space Center. USAF contract F08606-83-C-0014, Vol. 1, December, 1985, 112 pp.

Chen, C., and W. R. Cotton, 1983: A One-dimensional Simulation of the Stratocumulus-Capped Mixed Layer. Boundary-Layer Meteorology, Vol. 25, pp. 289-321.

Chen, C. and W. R. Cotton, 1987: The Physics of the Marine Stratocumulus-Capped Mixed Layer. Journal of Atmospheric Science, Vol. 44, pp. 2951-2977.

Cohen, Nathaniel B.: The Effects of Space Shuttle Launch Propulsion Systems on the Atmosphere. 1973 JANAF Propulsion Meeting, November 6-8, 1973, Las Vegas, NV, CPIA Pub 242 Vol. III, January, 1974, pp. 309-327.

Deardorff, J. W.: Cloud Top Entrainment Instability. Journal of Atmospheric Science, Vol. 31, pp. 131-147.

Hass, W. R. and S. Prince; Atmospheric Dispersion of Hypergolic Liquid Rocket Fuels (Vol. I of II). November, 1984, ESL-TR-84-18, Engineering and Service Laboratory (ESL), Air Force Engineering and Services Center, Tyndall AFB, FL.

Hwang, Bao Chuan and Harold S. Pergament: Environmental Effects of Space Shuttle Solid Rocket Motor Exhaust Plumes. NASA CR-145079, July , 1976.

Hwang, Bao Chuan, and Joseph J. Mathis Jr.: A Comparative Study of Tropospheric Ground Cloud Diffusion Models. Reprints, Joint Conference on Applications on Air Pollution Meteorology, November 29 - December 2, 1977, American Meteorological Society, pp. 261-268.

Kaplan, M. L., J. W. Zack, V. C. Wong, and J. J. Tuccillo, 1982: Initial Results from a Mesoscale Atmospheric Simulation System and Comparison with the AVE-SESAME I Data Set. Monthly Weather Review, Vol. 110, pp. 1564-1590.

Koller, Albert M. Jr.: A Summary of the Characteristics of the Shuttle Launch Exhaust Ground Cloud. In Ybanez, 1985, pp. 79-80.

Pellet, G. L., et al.: HCL in Rocket Exhaust Clouds: Atmospheric Dispersion, Acid Aerosol Characteristics, and Acid Rain Deposition. Journal of the Air Pollution Control Association, Vol. 33, No. 4, April, 1983, pp. 304-310.

Potter, Andrew E.: Environmental Effects of the Space Shuttle. Journal of Environmental Sciences, Vol. XXI, No. 2, March/April, 1978, pp. 15-21.

Proctor, Fred H.: The Terminal Area Simulation System. Vol. I: Theoretical Formulation, NASA CR 4046, April 1987, 123 pp.

Proctor, Fred H.: The Terminal Area Simulation System, Vol. II: Verification Cases, NASA CR 4047, April 1987, 97 pp.

Stephens, J. Briscoe, and Roger B. Stewart: Rocket Exhaust Effluent Modelling for Tropospheric Air Quality and Environmental Assessments. NASA TR 4-473, June 1977.

Ybanez, A., editor: Atmospheric Transport and Diffusion Modelling (S&EPS Workshop), Chemical Propulsion Information Agency (CPIA) Publication 433, June 1985, 423 pp.

Zak, Robert A.: The Determination of Exhaust Cloud Dimensions from Films of Space Shuttle Launches, NASA CR 4103, December, 1987, 53 pp.

1. REPORT NO.	2. GOVERNMENT ACCESSION NO.	3. RECIPIENT'S CATALOG NO.
NASA CR-4223		

4. TITLE AND SUBTITLE	5. REPORT DATE
A Cloud Model Simulation of Space Shuttle Exhaust Clouds in Different Atmospheric Conditions	March 1989
	6. PERFORMING ORGANIZATION CODE

7. AUTHOR(S)	8. PERFORMING ORGANIZATION REPORT #
C. Chen and J. A. Zak	

9. PERFORMING ORGANIZATION NAME AND ADDRESS	10. WORK UNIT NO.
ST Systems Corporation (STX) 28 Research Drive Hampton, VA 23666	M-610
	11. CONTRACT OR GRANT NO. NAS8-36715
	13. TYPE OF REPORT & PERIOD COVERED
12. SPONSORING AGENCY NAME AND ADDRESS	Contractor Final Report
National Aeronautics and Space Administration Washington, DC 20546	14. SPONSORING AGENCY CODE

15. SUPPLEMENTARY NOTES

Some of the work performed by Meso Incorporated, 28 Research Drive, Hampton, VA 23666-1325 under subcontract No. 85-6000-A1603, task order No. 3 (6206)

16. ABSTRACT

A three-dimensional cloud model was used to characterize the dominant influence of the environment on the Space Shuttle exhaust cloud. The model was mofified to accept the actual heat and moisture from rocket exhausts and deluge water as initial conditions. An upper-air sounding determined the ambient atmosphere in which the cloud could grow. The model was validated by comparing simulated clouds with observed clouds from four actual Shuttle launches. The model successfully produced clouds with dimensions, rise, decay, liquid water contents and vertical motion fields very similar to observed clouds whose demensions were calculated from 16 mm film frames. Once validated, the model was used in a number of different atmospheric conditions ranging from very unstable to very stable. In moist, unstable atmospheres simulated clouds rose to about 3.5 km in the first 4 to 8 minutes then decayed. Liquid water contents ranged from 0.3 to 1.0 g kg^{-1} mixing ratios and vertical motions were from 2 to 10 ms^{-1}. An inversion served both to reduce entrainment (and erosion) at the top and to prevent continued cloud rise. Even in the most unstable atmospheres, the ground cloud did not rise beyond 4 km and in stable atmospheres with strong low level inversions the cloud could be trapped below 500 m. Wind shear strongly affected the appearance of both the ground cloud and vertical column cloud. The ambient low-level atmospheric moisture governed the amount of cloud water in model clouds. Some dry atmospheres produced little or no cloud water. One case of a simulated TITAN rocket explosion is also discussed.

17. KEY WORDS		18. DISTRIBUTION STATEMENT
Space Shuttle	Cloud Model	Unclassified - Unlimited
Exhaust Cloud	Cloud Rise	
Environmental Impacts	Cloud Dimensions	Subject Category: 45
Atmospheric Effects	Cloud Simulation	
Kennedy Space Center		

19. SECURITY CLASSIF. (of this report)	20. SECURITY CLASSIF. (of this page)	21. NO. OF PAGES	22. PRICE
Unclassified	Unclassified	136	A07

For sale by National Technical Information Service, Springfield, Virginia 22161